O KE KAHUA MA MUA, MA HOPE O KE KŪKULU: IMPACTS OF A DECADE OF BIOCULTURAL RESTORATION ON AQUATIC BIOGEOCHEMISTRY AND DIATOM COMMUNITY ABUNDANCE IN HE‘EIA FISHPOND

A THESIS SUBMITTED TO THE GRADUATE DIVISION OF THE UNIVERSITY OF HAWAI‘I AT MĀNOA IN PARTIAL FULFILLMENT OF THE REQUIREMENTS THE DEGREE OF

MASTER OF SCIENCE

IN

OCEANOGRAPHY

November 2023

By
Charles Albert Kaiaka Beebe

Thesis Committee:

Rosanna Alegado, Chairperson
Craig Nelson
Kyle Edwards
Yoshimi Rii

Keywords: He‘eia Fishpond, biogeochemistry, biocultural restoration, loko i‘a, diatoms, seasonality

ACKNOWLEDGEMENTS

This research was supported by the University of Hawaiʻi Sea Grant College Program, the Hauʻoli Mau Loa Foundation, the Hawaiʻi State Department of Health and Heʻeia National Estuarine Research Reserve.

This work was made possible by so many people and communities who contributed their time, expertise, skills and resources, creativity, perseverance and faith. I would like to thank the faculty and staff of the Oceanography department who helped facilitate my growth in research, and the people of C-MORE Hale who graciously shared resources and equipment for my work when needed as well as camaraderie. The joint lab meetings of members from the Nelson, Steward, and Alegado lab always provided valuable discussion and feedback. My lab mates Hoaka, Becca, Kuʻi, and Nalani were dependable and resourceful colleagues and friends. Craig Nelson, Kyle Edwards, and Shimi Rii who also advised this work through the end. Completion of this thesis would not have been possible without kokua from Keanu Rochette-Yu Tsuen, Sara Kahanamoku-Meyer and Becca Lensing. My advisor Rosie Alegado who encouraged and supported me through the end. Nā Kiaʻi Loko of Paepae ʻo Heʻeia, thank you for allowing me to be a part of the process of learning about traditional Hawaiian fishponds.

ABSTRACT

Biocultural restoration and Indigenous resource management that benefit coupled natural-human ecosystems has recently gained attention as an alternative to nature-only based approaches. In Hawaiʻi, Native Hawaiian stewardship of ʻāina has also regained traction; yet, few large-scale efforts have evaluated the ecosystem shifts that result from biocultural restoration. In this contribution, we assess shifts in physical and biogeochemical conditions concomitant with over a decade of biocultural restoration at Heʻeia Fishpond, a traditional Hawaiian mariculture system built in an estuary of Koʻolaupoko, Oʻahu. Using discrete sampling of nutrients and quantification of diatom abundance, we further link customary management practices with potential for primary production in this estuarine system. We hypothesized that biocultural restoration, including but not limited to the removal of invasive vegetation and rebuilding of traditional fishpond structures, engendered environmental conditions that increased the potential ecological capacity for efficient food web dynamics required for production of target fish species. We found that restoration increased freshwater input, particularly during the wet season, associated with increased diatom abundance. Furthermore, these infrastructure changes increased the horizontal spatial homogeneity of water quality conditions, allowing increased access to freshwater and nutrients throughout the fishpond with positive implications for resource management. These data parameterize the results of biocultural restoration into metrics that can be applied to other coastal ecosystems undergoing restoration, providing a model for increasing ecosystem resilience in the face of climate change.

TABLE OF CONTENTS

LIST OF ABBREVIATIONS

IRM: Indigenous resource management

HFP: Heʻeia Fishpond

POH: Paepae o Heʻeia

NERR: National Estuarine Research Reserve

NKHoH: Na Kilo Honua o Heʻeia

HPLC: High Performance Liquid Chromatography

FACS: fluorescence activated cell sorting

qPCR: quantitative polymerase chain reaction

CHAPTER 1. INTRODUCTION

1.1 Estuarine ecosystems

Coastal regions encompass one-fifth of the total land area on Earth and estuaries play a key role in mediating the flux of material between terrestrial and marine realms (Burke & Institute, 2001). As the interface of land and sea, estuaries are where streams and rivers bring nutrients into the coastal oceans, supporting high species biodiversity (Cardoso, 2020). Recycling of nutrients and particulate matter within the estuary varies strikingly in response to diurnal, tidal, seasonal and climatic forcing. Estuaries are key ecotones that support a number of ecosystem services including transport and transformation of nutrients and organic matter, sedimentation of terrestrial particulates and flocculates, and high phytoplankton biomass. Nutrients entering estuaries are often modified as a result of particle-water interactions and primary production. Specifically, coastal zones can function as major sinks for nitrogen (N), phosphorus (P), and carbon (C) (Jickells, 1998). During storm events, increases in stream flow and erosion mobilizes material transported to the coast. Indeed these stochastic events can constitute up to 80% of nutrient and sediment inputs to coastal environments (Milliman & Meade, 1983). Kāneʻohe Bay is a subtropical embayment on the eastern coast of Oʻahu, Hawaiʻi that is known for high biodiversity of tropical species. There, pulses of nutrients have dramatic effects on the microbial community structure, most apparent in phytoplankton blooms (D. J. Hoover & Mackenzie, 2009; R. S. Hoover et al., 2006; Ringuet & Mackenzie, 2005), which in turn can significantly impact trophic linkages and transfer of carbon and energy to higher order trophic levels.

1.2 Loko iʻa: Constructed estuaries

In ancient Hawaiʻi, management of resources to support the hunting-fishing-gathering mode of life predicated the maintenance of water resources throughout the watersheds. Native Hawaiians converted wetlands into loʻi kalo (flooded agroecosystems for cultivating taro) that were engineered to effectively trap nutrients and sediment for growth of the staple crop of kalo (*Colacasia esculenta*) and limit coastal nitrification (Bremer et al., 2018). Coastal marine habitats are directly affected by the quality of freshwater entrained from rivers and streams.

Typically situated in coastal estuaries at the convergence of terrestrial freshwater and marine environments, loko iʻa (fishponds) constitute a unique form of mariculture innovated by Hawaiians in the 12-13th centuries (Kikuchi, 1976). Loko iʻa practitioners target lower trophic level fish species for cultivation, such as ʻamaʻama or striped mullet, *Mugil cephalus* (Figure 1). These juvenile species graze on eukaryotic phytoplankton including diatoms, microphytobenthos, and detritus (Hiatt, 1947; Julius, 2007; Schemmel et al., 2019). Therefore, a functional loko iʻa environment must be suitable for the growth of these primary producers to efficiently maximize the production of herbivorous fish (Keala et al., 2007). A certain degree of environmental control within loko iʻa is achieved by the management of water exchange via mākāhā (sluice gates) built into the kuapā (basalt perimeter walls). Historically, these highly productive estuarine systems had the capacity to produce ~1 million kg fish annually but this potential currently is eroded to less than 1% of historical production (Apple & Kikuchi, 1975; Cobb, 1901; Keala et al., 2007).

The physical structure of the kuapā and mākāhā create an enclosed embayment constraining flow of freshwater and marine sources, in effect, functioning as an estuarine mesocosm embedded within the natural coastal environment. The configuration of loko iʻa embedded within the estuary provides a unique and natural system to study and quantitate the interaction of physical, geochemical and biological processes in tropical environments under constrained conditions.

1.3 Biocultural restoration of Heʻeia Fishpond: 2007 - 2019

Land use changes in Hawaiʻi have severely impacted loko iʻa. Many were destroyed or left unmanaged and derelict, overtaken by invasive species and damaged by the elements. Recently, local communities have begun restoring loko iʻa as cornerstones of sustainable food production within Indigenous Resource Management (IRM). IRM aims to increase ecosystem services through an Indigenous lens of resource management, as a holistic approach to managing from mauka to makai (ridge to reef), from loʻi kalo to loko iʻa. Through this process, Native Hawaiians maintained high biodiversity, low sediment and stream runoff, and good water quality to ensure a healthy coral reef. Indeed, historical documents of at least 30 fishponds in Kāneʻohe Bay are evidence of the thriving nature of this system (Figure 2A). However, the links between environmental conditions and its target ecosystem service, such as optimizing the growth of desirable phytoplankton and microphytobenthos species that sustain target stocks, are unknown and require investigation for success of biocultural restoration.

Located downstream of the Heʻeia wetlands that were cultivated as loʻi, Heʻeia Fishpond (HFP, also known as Pihi Loko Iʻa) was built atop the Malaukaʻa fringing coral reef on the windward side of Oʻahu, Hawaiʻi (Figure 2B). In the mid-1800s, loʻi were converted to plantation style agriculture for cultivation of rice and sugar. These agricultural practices led to deterioration of the watershed and confluent riparian areas along with sedimentation of the loko iʻa and nearshore environments. In order to stem further damage to the reef, non-native red mangrove (*Rhizophora mangle*) was planted in the Heʻeia estuary in 1922 (Allen, 1998; Walsh, 1963). *R. mangle* subsequently proved to be an invasive species, establishing itself in Heʻeia, spreading unchecked and drastically changing the landscape and biodiversity within the Heʻeia estuary (Demopoulos et al., 2007), and further damaging the loko iʻa infrastructure to the point of dysfunction.The circulation and water volume flux patterns within Heʻeia Fishpond were compromised during the Keapuka Flood, when the highest discharge rate on record from Haʻikū and ʻIolekaʻa streams occurred (Banner, 1968) on May 2, 1965. Flood waters first broke the kuapā in the northwestern sector adjacent to Heʻeia Stream, creating a 183 m opening in the loko iʻa. Historical tidal data (*Water Levels - NOAA Tides & Currents*, 2018) indicate that the flood likely occurred during a perigean spring tide, thus the 56 m break in the kuapā on eastern seaward side as well ("Ocean Break") likely resulted from build-up of internal pressure within the loko iʻa coupled with an extremely low tide outside the loko iʻa.

Intentional biocultural restoration by Paepae o Heʻeia (POH), the current kiaʻi loko (stewards) of HFP, has been ongoing and improving both the skills of the kiaʻi and the abundance of ʻāina (natural resources that provide the requirements to sustain and edify the human system) since the early 2000s (Figure 3). With removal of mangroves and reconstruction of the kuapā beginning on the southeast section of HFP in 2001 and continuing along the 1 mile long makai kuapā (wall facing the ocean), the work has been a community effort. Thousands of volunteers work with Paepae O Heʻeia, revitalizing Native Hawaiian culture and sustainable indigenous food systems, as was seen in the 2015 public event “Pani ka puka,” with the closure of the 200-foot “Ocean Break” and installation of a new mākāhā (sluice gate), Kahoʻokele. This effort received statewide attention from local media spotlighting the ongoing work of POH, the kiaʻi of HFP. In 2017-2019, half an acre of invasive mangrove was removed from “Egret Island" within HFP, resulting in the loss of habitat for approximately 2,000 non-native cattle egrets, a major contributor to fecal and nutrient contamination. This work is part of a larger movement that does not and cannot stop at where the land meets the ocean.

Currently the restoration of the mauka land (in the wetlands, towards the mountains) involves removal of *R. mangle*, implementing integrated agroforestry in reforestation, and revitalizing the practice of mahiʻai (farming) with loʻi kalo and diversified agriculture. Construction of loʻi kalo in strategic configurations to natural water flow are being monitored and assessed for ecosystem services and ecological impact to Heʻeia water sources. Six acres of monotypic mangrove forest has been removed from the wetland and riparian areas of the Heʻeia stream immediately confluent with the fresh water flow and flux into inland mākāhā of HFP. Taken together, these restoration works have and will be a vital impetus of ecological change that must be considered when taking up a study of any natural phenomena in the Heʻeia estuary and HFP.

1.4 Previous and current Research: Nā Kilo Honua o Heʻeia

Initiated in 2007, Nā Kilo Honua o Heʻeia (NKHoH) has conducted monthly (or more frequent) sampling and maintained *in situ* instruments to record physical and biogeochemical variability in Heʻeia Fishpond and the adjacent coastal ocean, Table 1. Previous studies at HFP have revealed complex dynamics shown through spatial and temporal environmental gradients in circulation, temperature and salinity, dissolved nutrients, and chlorophyll and phytoplankton biomass (Briggs et al., 2013; Dulai et al., 2016; Hull, 2010; D. McCoy et al., 2017; Moehlenkamp, 2018; Young, 2011).

Kāneʻohe Bay is the largest semi-enclosed body of water in Hawaiʻi and receives runoff from several perennial streams from the Koʻolau Mountains, including Heʻeia Stream. Previous studies have shown the reliance and sensitivity of Kāneʻohe Bay to terrigenous input from perennial streams and episodic storm events, highlighting geochemical dynamics (Ringuet and MacKenzie 2005, De Carlo et al. 2007) and ecological dynamics at pico- and micro-plankton scales (Cox et al., 2006; Laws, 1985; Selph et al., 2018; Yeo et al., 2013). Phytoplankton community distribution and relative abundances within Kāneʻohe Bay are heterogeneous along the estuarine gradient of multiple geochemical parameters (Cox et al., 2006; Laws, 1985; Selph et al., 2018; Yeo et al., 2013). Temporal succession of phytoplankton is initiated following storm events as the dominant taxa of the community shifts from cyanobacteria to larger phytoplankton eukaryotes like diatoms, then back to cyanobacteria. This reactivity of the mode of primary producers in Kāneʻohe bay is of special interest in the context of loko iʻa.

Similar to Kāneʻohe Bay, HFP is sensitive to episodic weather events - stormwater runoff alters nutrient inventories, resulting in changes in the planktonic community structure. During previous storm events, defined as rainfall exceeding 5 cm (R. S. Hoover et al., 2006), NKHoH investigators (K. Ruttenberg, UH Manoa and M. McManus, UH Mānoa) deployed instruments to collect physical data at high frequency in addition to collecting repeated biogeochemical measurements at high resolution. NKHoH time series data show that following storm events, nitrogen inventories in HFP rapidly increase (Young, 2011). Concomitant with the pulse of nutrients into the estuary, chlorophyll *a*, a proxy for phytoplankton biomass, increases, indicating a phytoplankton bloom. Additional pigment analysis to derive the composition of the phytoplankton revealed a pattern of phytoplankton succession post-storm. The relative abundance of constituent phytoplankton measured by HPLC of diagnostic pigments revealed that diatoms are the dominant phytoplankton present with relative abundance of 21% during non-storm conditions increasing to 61% during storm events (Young, 2011). Persistence of storm event effects vary with respect to wind characteristics and timing with tidal phase which are the two main forces driving circulation and residence times. It is assumed that as N:P ratios decrease, the estuary returns to a nutrient-limited state as the relative ratios of cyanobacteria rise. Pilot nutrient addition experimentsrecapitulating a 2007 storm event (D. Hull, unpublished) showed that the growth of heterotrophic bacteria was much greater than *Synechococcus* associated with freshwater environments in response to increased nutrients. Recent work by Mohlenkamp et al. (2019) has demonstrated that biocultural restoration altered circulation patterns and pond water residence times, salinity and microbial biogeography of significant bioindicators. While the NKHoH chronosequence efforts have provided data informing research into environmental response of large magnitude physical forcing such as storms, the focus on improvement of ecological services due to biocultural restoration has not been specifically investigated.

The goal of this research is to understand the dynamics of He‘eia Fishpond’s diatom abundance and distribution in relation to geochemical gradients and assess whether biocultural restoration from 2007-2019 has changed the gradients of measured dissolved nutrients and other geochemical measurements within HFP. We partnered with Paepae o He‘eia and the He‘eia National Estuarine Research Reserve (NERR) to monitor water quality and phytoplankton community dynamics during continuous removal of invasive species and fishpond restoration. To capture the changes over this period of restoration, we selected periods of time from three different field sampling campaigns (Figure 3): 1) **2007-2008:** The southern edge of the kuapā had been restored prior to this period, and specifically during 2007-08, restoration involved mangrove removal and ~25% of kuapā reconstruction along southern and eastern sides of HFP. 2) **2014-2015:** Reconstruction of the remaining seaward kuapā occurred from 2008-2014, with installation of two ocean-facing mākāhā. During 2014-15, repair of the “ocean break” and installation of the southeastern mākāhā Kaho‘okele occurred. 3) **2017-2019**: From 2015-2017, kuapā restoration from the stream mouth to Wai 2 occurred, with installation of Wai 1. During the sampling period of 2017-2019, removal of mangroves including egret island, and the repair of kuapā and mākāhā Wai 2 and Wai 3 from the north region moving inland westward along He‘eia Stream occurred (Table 1). This period marked the completion of mākāhā restoration. While all three periods measured temperature, salinity, dissolved oxygen, and pH using a YSI multiparameter sonde, and collected discrete bottle samples for measurement of nitrogen, phosphorus, and silicate, we were challenged by differences in sample site locations, sampling effort, and methods. During 2014-2015 and 2017-2019, we also collected genomic DNA which enabled correlation between environmental parameters and the abundance of a significant primary producer of the planktonic community, diatoms, using quantitative polymerase chain reaction (qPCR) of a diatom-specific *rbcL* gene marker (Li et al., 2013).

1.5 Hypotheses

1.5.1 Hypothesis 1: Spatial structure of water column geochemistry across HFP between 2017-2019

H1.1: Environmental parameters (e.g. salinity, temperature, dissolved nutrients) vary spatially across HFP.

Null: Environmental parameters are uniform across HFP.

H1.2: The spatial heterogeneity of HFP environmental parameters will be predominantly explained by salinity.

Rationale: He‘eia Fishpond is influenced by terrestrial input on the northern and western sides, and marine inputs mainly on the ocean-facing eastern and southern walls running from north to south. With low stream flow into HFP through the stream mākāhā and poor circulation due to shallow depth and silty substrate, HFP is likely to display heterogeneous biogeochemical hotspots, likely influenced by salinity.

1.5.2 Hypothesis 2: Correlations between aquatic geochemistry and diatom abundance of HFP between 2017-2019

H2.1: Diatom abundance is not spatially uniform across HFP.

Null: Diatom abundance is spatially uniform across HFP.

H2.2: Average diatom abundance will be higher in the fishpond than fluvial and marine source environments external to HFP.

Null: Diatom abundances in and out of the fishpond will be equal.

H2.3: Diatom abundance is correlated with environmental parameters such as salinity and dissolved macronutrients (nitrate + nitrite, ammonium, phosphate, and silicic acid).

Null: Diatom abundance and environmental parameters exhibit inconsistent correlations.

Rationale: Diatoms are an important diet source of juvenile ‘ama‘ama, the native striped mullet (*M. cephalus*). Diatom growth and population structure is greatly influenced by nitrate and silicic acid concentrations, and thus, we hypothesize diatom abundances to be heterogeneous in HFP due to spatial differences in circulation and geochemical parameters.

1.5.3 Hypothesis 3: Comparison of Restoration Time Periods (2007-08, 2014-15, 2017-19)

H3.1: Aquatic environmental parameters measured within geographical regions vary significantly between the different phases of biocultural restoration.

Null: The aquatic environmental parameters within geographic regions of HFP remain the same over distinct restoration periods.

H3.2: Salinity is a strong predictor of the most current HFP aquatic environment during Phase III: 2017-19, in comparison to preceding restoration states observed (Phases I and II).

Null: The effect of salinity on other aquatic environmental parameters is the same across the three restoration phases.

Rationale*:* Activities conducted during biocultural restoration alters physical and biogeochemical parameters and dynamics. The ecological influence of biocultural restoration at HFP stems from two main management practices implemented by POH: mangrove removal and kuapā restoration. Mangrove removal decreases the carbon subsidy in the form of leaf litter and root sloughage delivered to the system in the form of refractory detritus and recalcitrant organic matter in sediment. These changes are quite drastic and a different dynamic of nutrient cycling, metabolic efficiencies and trophic linkages will emerge. Kuapā and mākāhā restoration influences water volume flux, residence times, and circulation. The balance of allochthonous material input and autochthonous biogeochemical processes are influenced. This may bring about a more stable system with less extreme variability in the aquatic environment, hence environmental parameters during each phase of restoration are likely highly dependent on changes in salinity as greater exchange of fresh and salt water occurs within the fishpond.

CHAPTER 2. RESEARCH DESIGN AND METHODS

2.1 Kanaka ʻōiwi research paradigm and methodology

Indigenous researchers typically approach scientific inquiry and questions differently from conventional scientists (Tuhiwai, 1999; Wilson, 2001, 2008). The development, implementation and analysis of this project incorporates approaches and processes guided by kanaka ʻōiwi values and epistemologies. When conducting research in Indigenous communities, the history, people and place must be respected; the relationship between the researcher and community should be reciprocal; the researcher should be aware of their position, intentions, power and value to the community they are working with; and all research should be transparent and inclusive (Kulana Noiʻi Working Group, 2018). Over the course of this project, I, as a kanaka ʻōiwi student researcher, met regularly with loko iʻa stewards to identify their research needs, share findings, and implement their suggestions and feedback, while including them as co-authors on all products arising from this work. I participated in community work days to strengthen my connection with the people and place of Heʻeia, demonstrate my commitment to place outside of the research, and to give back in tangible ways to my community partners. All raw data and figures are made accessible to POH on a private shared drive maintained by NKHoH and Heʻeia NERR. Therefore this project is grounded in personal connections to place and community, to Heʻeia and its kupaʻāina (residents and lineal descendants). All fieldwork was conducted with the permission of Paepae o Heʻeia and the private landowner, Kamehameha Schools (Joey Char, Land Asset Manager, Kamehameha Schools Community Engagement and Resources Division).

2.2 Site Description

HFP is a ~ 0.356 km^2 loko iʻa kuapā built ~800 years ago at the confluence of Heʻeia Stream and Kāneʻohe Bay (21.436° N, 157.808° W) within the moku of Koʻolaupoko Oʻahu, Figure 2B (Kelly, 1975). Heʻeia Stream drains the approximately 11.45 km^2 of socio-ecological landscape of Heʻeia ahupuaʻa with ʻIolekaʻa Stream and Haʻikū Stream tributaries joining to flow through concrete drainages serving the residential developments before entering the Hoi Wetland. Some of the water of Hoi is diverted into ʻauwai (water course) irrigating loʻi kalo and diversified agricultural crops. HFP is bordered by Kāneʻohe Bay on the southern and eastern edges and Heʻeia Stream to the north.

The interior of HFP is enclosed by ~1.67 km of restored kuapā, made of dry stack pohaku (basalt rock) and in-filled by koʻa (coral rubble). Unrestored sections of the kuapā are covered by mixed vegetation of mainly hau (*Hibiscus tilaceus*) and red mangrove (*R. mangle*) on the western side adjacent to a residential development. The configuration of HFP includes mākāhā interspersed along the kuapā allowing for controlled discharge of freshwater from the terminus of Heʻeia Steam and tidally driven exchange of ocean water from Kāneʻohe Bay (Figure 3). Hereafter, names of mākāhā follow the convention used by POH in 2018. Water geochemistry within Heʻeia fishpond is characterized by influx of distinct water masses: freshwater from Heʻeia Stream that varies depending on the amount of precipitation, submarine groundwater discharge (Kleven, 2014), and seawater from Kāneʻohe Bay that fluctuates with the tidal cycle.

2.2 Sampling campaigns and effort: 2007-2008, 2014-2015, 2017-2019

To assess changes in the aquatic environment of HFP concomitant with a decade of biocultural restoration, we analyzed biogeochemical parameters from three NKHoH sampling campaigns: 2007-2008 (Young, 2011), 2014-2015, and 2017-2019. The 2007-2008 campaign spanned a period of restoration when about 25% of mangrove had been removed and ~600 m kuapā had been repaired on the southern side of HFP to (Moehlenkamp, 2018). During this campaign, samples were collected monthly at 10 sites within HFP. Data from 2014-2015 reflects conditions during the period when the ocean-ward kuapā and mākāhā were rebuilt. During this field campaign, samples were collected every two weeks from 10 locations within the boundaries of HFP kuapā. The 2017-2019 campaign spanned the clearing of Heʻeia Stream, which increased freshwater flow into HFP and complete removal of mangrove on "Egret Island", a source of nutrients and fecal bacteria. During this campaign, samples were collected from 19 sites: 11 within HFP, 6 mākāhā, and 2 end members from Heʻeia stream and the edge of the reef outside of Kahoalāhui (Figure 3).

To inform selection of sample dates unaffected by large magnitude rain events, stream discharge data from Heʻeia Stream was used (*USGS Current Conditions for USGS 16275000 Heeia Stream at Haiku Valley Nr Kaneohe, Oahu, HI*, n.d.). A recursive digital filter was applied to Heʻeia Stream discharge data (Fuka et al., 2018; Nathan & McMahon, 1990) to separate the components of streamflow as baseflow and quick flow, representing discharge of the aquifer, and high frequency events representing increased discharge from precipitation that does not contribute to aquifer recharge.

2.4. Water sample analytical methods

Each campaign measured salinity, pH, dissolved oxygen, and temperature using a multiparameter sonde (YSI Pro Plus for 2017-19, YSI 6600 v2 for 2014-15 and 2007-08; YSI Incorporated, Yellow Springs, OH) at each site (Table 1). The YSI multi-parameter water quality sonde was held in place for 2-3 minutes to ensure stabilization of all parameters before reading. All sampling efforts involved discrete sampling for dissolved macronutrients: phosphate (TDP, PO_4^{3-}), nitrogen (TDN = (NO_2^-+ NO_3^-) + NH_3), and silicic acid (H_4SiO_4). At each site, 1 L was collected from surface waters (10-30 cm) in acid-washed Nalgene bottles after a triple rinse with ambient surface water. All samples were stored on ice until further processing. Processing for nutrient analysis was carried out with the following differences (Figure 4): in 2007-2008, samples were filtered through Pall GHP filters 47 mm diameter with a pore size of 0.2 µm membrane and stored at -20 °C ; in 2014-2015, nutrient concentrations were measured from unfiltered water samples using a DR900 Multiparameter Portable Colorimeter (Hach, Loveland, CO); in 2017-2019 samples were filtered through 47 mm diameter, 0.45 µm pore size Pall membrane (GH Polypro, Pall Gelman Inc., Ann Arbor, MI) and stored at -20 °C. The 2007-2008 and 2017-2019 samples were processed at the SOEST Laboratory for Analytical Biogeochemistry (Honolulu, HI).

2.5 Multivariate analysis of 2017-2019 biogeochemistry

To visualize the spatial structure of biogeochemical parameters, the overall or aggregated mean was calculated for each site across all baseline sampling dates for each environmental parameter. An Inverse Distance Weighted (IDW) raster was calculated to interpolate an estimated value for each parameter over a continuous spatial field and was applied using Quantum Geospatial

Information System (QGIS) software (version 3.24.2 - Tisler; (Flenniken et al., 2020; le Roux et al., 2023). Statistical analyses were conducted using several packages in R, as described below. Normality of biogeochemical parameters was investigated using a Shapiro-Wilks test (Appendix Table 1) and distributions were examined using histograms (Appendix Figure 1). Environmental parameters were $\log_{10}$-tranformed and Euclidean distances were used for distance-based multivariate analyses. A non-parametric Kruskal-Wallis test followed by posthoc Dunn's multiple comparisons tests with a single pooled variance were computed using GraphPad Prism 10.0 to determine whether environmental parameters varied by regions. To test whether multivariate biogeochemistry varied between regions or over time, and whether spatiotemporal variation could be explained by salinity, Permutational Multivariate Analysis of Variance Using Distance Matrices (PERMANOVA) test was performed using "adonis2" (vegan 2.5-7; (Oksanen et al., 2020). To visualize multivariate environmental gradients, non-metric multidimensional scaling (nMDS) ordinations were generated with "metaMDS" and plotted with "ordiplot" in two-dimensions, including the variables temperature (°C), salinity (ppt), pH, DO (%), nitrate (µM), nitrite (µM), ammonium (µM), total reactive phosphate (µM), orthosilicic acid (µM). Significant environmental variable responses were extracted for plotting vectors with "envfit" and plotted with the corresponding biogeochemical ordinations. To evaluate goodness of fit for nMDS ordinations, goodness of fit Shepard diagrams and nonmetric fit were evaluated for each ordination with function "stressplot".

2.6 Diatom abundance

2.6.1 Quantification of diatoms

Samples for genomic analysis were also collected from the 2014-2015 and 2017-2019 field seasons (Figure 4). One liter (L) of surface water was filtered through 47-mm, 0.45-µm pore size

Pall filter membranes (GH Polypro, Pall Gelman Inc., Ann Arbor, MI) and stored at -80°C. Total genomic DNA was isolated from filters using Power Water DNA extraction kit (MoBio Labs, Carlsbad CA) following the manufacturer's instructions. Quantitative PCR was used to determine the abundance of the diatom-specific rubisco *rbcL* gene (Ribulose-1,5- Bisphosphate Carboxylase/Oxygenase) with primers developed by Li et.al (2013; Table 2). We used a targeted synthetic oligonucleotide gBlocks© Fragment (Integrated DNA Technologies, IA, USA) as a standard for quantification of *rbcL*. A 508 bp gBlocks fragment was designed based off of the *Nitzschia inconspicua* partial *rbcL* gene fragment (Genbank HF675093.1). The synthetic standard was quantified using a Qubit (Thermo Fisher Scientific) and known concentrations of the oligonucleotide were used in subsequent reactions (Figure 9). Total volume per reaction was 20 µL which consisted of 5 µL sample template, 0.5 µL for each forward and reverse primer, 10 µL KAPA Master Mix, and 4 µL PCR grade water. Cycling parameters were as follows: 15 minutes at 94° C, followed by 45 cycles of 15 seconds at 94° C, 30 seconds at 53° C, and 35 seconds at 72° C, and a final step of 7 minutes at 72° C. Sample aliquots were diluted with PCR grade water at a rate of 1:5 and run in triplicate. Standards were run in triplicate using an 8-point series targeting 10^7 to 5 x 10^3 *rbcL* gene copies. Quantification with a KAPA SYBR FAST qPCR Master Mix Kit (KAPA BIOSYSTEMS, Cape Town, South Africa) and a fluorescence threshold of detection was set to determine baseline and drift correction for the Mastercycler ep realplex Real Time System (Eppendorf Hamburg, Germany). Cycle threshold (C_t) values were converted to diatom cells mL^{-1} using a conversion factor of 200 copies *rbcL* $cell^{-1}$ which is a conservative estimate based on literature, Appendix Figure 2 (Cox et al., 2006; Li et al., 2013; Lim & Lee, 2017; Pierce, 2014).

2.6.2 Correlation between 2017-2019 biogeochemistry and diatom abundance

Diatom abundance was calculated as mean diatom cells mL^{-1} from qPCR data, and to normalize the data for statistical analysis, abundance was log-transformed and normality was assessed by plotting model residuals using "plotResiduals" (Appendix Figure 3). The influence of salinity on diatom abundance was tested using a generalized additive model. To determine which nutrient parameters best predict diatom abundance (using AIC as the criterion), we used the model selection tool "dredge" to create all possible linear models with each nutrient parameter as the predictors. We retained all predictors with summed Akaike weights > 0.6, and then used interactions to test whether the effects of nutrients differed between the Wet (November through March) and Dry (April through October) seasons.

2.7 Multivariate analysis of biogeochemistry across biocultural restoration phases / sampling campaigns

Sampling campaigns had few sites in common between all 3 periods (Table 1). Mākāhā and endmembers were not regularly sampled and the spatial distribution of sites differed, with some areas of the fishpond densely sampled and others very sparse. In order to standardize spatial sampling effort, endmember sites were excluded, and the sites were grouped into 6 regions based on geographical coordinates (Figure 5, Table 1). Sites from all three of the campaigns are represented in each of the 6 regions by at least one site.

To evaluate in-pond variation across sampling campaigns, a series of sequential PERMANOVA were applied using the function "adonis2" (vegan 2.5-7; (Oksanen et al., 2020). The sequential tests were performed on Euclidean distance matrices constructed from the aggregate means of biogeochemical parameters collected from each sampling campaign as the response matrix, to test the influence of region (representing spatial heterogeneity) and salinity (representing circulation). Due to the large sets collected and asnon-parametric tests have no assumptions about normality, parameters were not log transformed. The PERMANOVA model included a term for sample date in order to reduce unexplained variation when testing effects of salinity and region.

Non-metric multidimensional scaling (nMDS) ordinations of temperature, salinity, pH and DO were generated with “ordiplot” in two-dimensions. To evaluate goodness of fit for points in nMDS ordinations, goodness of fit Shepard diagrams and nonmetric fit were evaluated for each ordination with function “stressplot”. Analysis of multivariate homogeneity of group dispersions (variances) was conducted using the function “betadisper” from the “vegan” package. Distances-to-centroid were extracted and tested for pairwise statistical differences between dates using Dunn's Pairwise Test For Multiple Comparisons Of Mean Rank Sums with Bonferroni p-value adjustment with the function “posthoc.kruskal.dunn.test()” from package “PMCMRplus”. To determine whether parameters varied significantly between field campaigns, univariate nonparametric Analysis of Variance Using Distance Matrices (ANOVA) tests were performed in GraphPad Prism v.9. For metrics that varied significantly by date, pairwise differences between parameters were tested using the post-hoc Dunn's Pairwise Test For Multiple Comparisons Of Mean Rank Sums with Bonferroni p-value adjustment amongst regions and across HFP.

CHAPTER 3. RESULTS

3.1 Establishing a baseline for characterizing restoration

Large magnitude rain events are not uncommon in Hawaiian watersheds, presenting a departure from day-to-day conditions with increased transport of terrigenous materials from the watershed to the estuary. To examine the impact of Indigenous management practices on loko iʻa functioning, we focused specifically on background steady state conditions. The loko iʻa is heavily influenced by freshwater and marine inputs, therefore we excluded large rain events. Rain event sample dates were delineated using an operational criterion of stream discharge greater than 30% contribution of quick flow at any time within a period of 102 h, the window based on maximum HFP residence time (Moehlenkamp, 2018) preceding 08:00 of each sampling date. This operationally defined criterion is based on the empirical distribution of log-transformed quick flow calculated from Heʻeia Stream discharge data spanning August 2007 - June 2019 and the maximum (Figure 6). Examination of data without extreme rain events is crucial for comparison of baseline values within each sampling campaign. A total of 11 sampling dates were removed from the data set based on the rain event criteria and 59 sampling dates were removed based on the extreme tidal event criteria. Subsequent statistical analysis was performed using 60 dates encompassing 761 individual observations (Table 3). A second criteria was applied to remove spring tide sample dates as geochemical conditions were not distinguishable from end member values. Previous work by ourselves and others (D. McCoy et al., 2017; D. E. McCoy, 2011; Moehlenkamp, 2018) established sampling during neap tides as an ideal window for capturing steady state water chemistry, thus we excluded observations taken during spring tides (Table 3). Sample dates occurring on spring tides were determined based on moon phase (*Phases of the Moon*, n.d.).

3.2 2017-2019 Loko iʻa biogeochemistry is spatially heterogeneous

The 2017-2019 sampling campaign occurred concomitant with significant biocultural restoration milestones at HFP: the entire sea and stream facing perimeter, 4,800 feet of the 7,000 foot long kuapā, had been rehabilitated; removal of Egret Island (Figure 7), an internal stand of *Rhizophora mangle* housing between 2,000-3,000 cattle egrets; and the construction of a new mākāhā that allowed consistent freshwater input into the loko iʻa. As this time period reflects the most re-established intact wall infrastructure and the achievement of thousands of community members and tens of thousands of labor hours over a decade, the loko iʻa biogeochemistry during this period of time served as the reference point for this study.

To better understand spatial distribution patterns of these environmental parameters as well as nutrient inventories across HFP, we calculated the mean value for each parameter at each sample site (Table 4). The mean surface temperature from 2017-2019 was 24.73 ± 2.56 ℃, salinity was approximately 22.19 ± 1.42 ppt, mean pH was 7.83 ± 0.30, and mean dissolved oxygen was 80.08 ± 22.38, typical of brackish ecosystems. Surface salinity, pH, dissolved oxygen, nitrogen and phosphate species as well silicic acid distributions displayed a strong spatial gradient (Figure 8) indicative of mixing of surface water from Heʻeia Stream and seawater from Kāneʻohe Bay that fluctuates with tidal pumping. Heʻeia Stream passes through the Hoi wetland, comprised of invasive grasses and mangrove. The loko iʻa also receives input from submarine groundwater discharge that is a mixture of freshwater from an underground aquifer and recirculated seawater (Dulai et al., 2016). Indeed dissolved salinity, dissolved oxygen, pH, DIN, nitrate + nitrate, phosphate and silicilic acid varied significantly by site (Kruskal Wallis, $p<0.05$).

Salinity exhibited an isohaline distribution, indicative of a vertically homogeneous estuary. Temperature, pH and dissolved oxygen distribution patterns correlated positively with salinity with high ranges in the seaward sites and the lowest values nearest to the freshwater mākāhā (Figure 8). Sites L06, L07, L08, L09 were significantly lower in salinity (13.53 ± 8.83 ppt, 6.276 ± 6.40 ppt, 20.82 ± 6.21 ppt, and 14.67 ± 8.56 ppt respectively), dissolved oxygen (72.79 ± 6.19%, 59.05 ± 8.42%, 80.23 ± 11.47%, and 68.32 ± 21.11% respectively) and pH (7.698 ± 0.21, 7.358 ± 0.25, 7.847 ± 0.15, 7.808 ± 0.15 respectively) and higher in H_4SiO_4 (180.3 ± 106.1 μM, 222.7 ± 117.8 μM, 119.4 ± 82.66 μM, and 139.5 ± 99.16 μM respectively) (Table 4, Figure 9, Appendix Table 2). Dissolved oxygen at L07 was significantly lower than sites L03, L04, and L10 which are closest to the oceanic mākāhā (Figure 9, Appendix Table 2). In addition, silicic acid concentrations at sites L06, L07, L08, L09 (region 5) were higher than concentrations at L04/L05 (region 3). Sites L06, L07, L08, L09 correspond to region 5 (Figure 5) which is closest to the mākāhā that was re-constructed during 2017-2019 and therefore freshwater input. Water that has low salinity, low DO, and high silicic acid are consistent with freshwater with a consistent groundwater signal. These patterns support our hypothesis that environmental parameters vary spatially across HFP, we sought to further characterize the relatedness between sites by multivariate clustering. However no individual pairwise comparisons for DIN and N+N were significantly different.

3.3 Spatial heterogeneity in 2017-2019 HFP biogeochemistry is influenced by temporal factors

We hypothesized that spatial heterogeneity of HFP environmental parameters could be predominantly explained by salinity. PERMANOVA was applied using a number of models (Table 6) to determine whether variation was explained by date, site, or season in addition to salinity. Salinity had a moderate (18%) but significant contribution ($p<0.001$) to variation in biogeochemistry (Table 6, Model 2). Next we examined whether variation in biogeochemistry was explained by temporal variation in salinity (Model 2) or by spatial variation in salinity (Model 3). The large decrease in the marginal contribution of salinity down to 3.55% ($p < 0.001$) when site is added as a predictor imply that site and salinity are competing to explain the same variation. Therefore it is likely that some but not all of the spatial variation between sites can be explained by salinity. In contrast, adding date as a predictor (Model 3) does not diminish the variation explained by salinity as dramatically (14.7%) indicating that temporal variation in HFP biogeochemistry cannot be explained by salinity. When salinity was not included (Model 4), more of the 2017-2019 biogeochemistry variation was explained by sampling date (40.7%) than by sample site (23.6%), implying that HFP experienced more temporal variability than spatial variability. Alternatively, spatial variation shows a consistent pattern over time. Finally, in the most conservative model, we asked whether salinity explains biogeochemistry after accounting for any differences between dates and sites (Table 5, Model 5). In this model, temporal variation accounted for 37.65% and site accounted for 9.4% of the variance, and were significant predictors, but salinity was not.

To better understand the temporal dimension of the biogeochemical variability, we then tested how much of the temporal variation can be attributed to interannual, or interseasonal, or other remaining temporal variation. All terms were significant and we found that year explains 9.5%, and season explains 2.2%, while date explains 40.7% (see Model 4). Though ubtropical locations such as the Hawaiian Islands have discernable dry and wet seasons based on precipitation, function in precipitation on shorter timescales than season may contribute to the observed variation in biogeochemical parameters based on date. Taken together, this implies that 29% of the temporal variation is due to other factors or activities at HFP that were temporal, potentially including biocultural restoration.

Previous work by Moehlenkamp *et al.* (2019) demonstrated that biocultural restoration led to increased freshwater input. As salinity in HFP is directly impacted by biocultural restoration, biogeochemical distribution patterns are likewise impacted by restoration. Biogeochemical parameters that varied significantly by sampling date (Kruskal Wallis, $p<0.05$) were plotted to visualize temporal patterns over the course of the sampling campaign (Figure 10). Mean phosphate concentrations increased over between February 18, 2017 to June 11, 2019. However, over the period of time when Egret Island was removed, October 11, 2017 - January 25, 2018, short term increases in pH, and nitrogen species were observed before returning to 2017 levels. In contrast, dissolved oxygen and silica decreased over the Egret Island removal period and then returned.

To differentiate biogeochemistry changes that were influenced by season over the 2017-2019 campaign period, environmental parameters were plotted by season and year (Figure 11).

Salinity was excluded from this analysis as mean interannual/interseasonal salinity was not significantly different by Kruskal Wallis. Though seasonal and annual mean dissolved oxygen and H_4SiO_4 concentrations were significantly different across 2017-2019 (Kruskal Wallis, $p<0.05$), no individual pairwise comparisons were significantly different, indicating that the temporal influence on these parameters may be marginal as compared to spatial influence.

To examine intra-annual seasonality, wet vs. dry seasons for each year during the 2017-2019 sampling campaign were compared (Figure 11, Table 5). We found that 2017 exhibited no seasonality for any of the environmental parameters measured. Only temperature was significantly different between multiple wet and dry seasons (2018, $p = 0.0004$; 2019 $p < 0.001$; Appendix Table 2), with higher temperatures in the dry season (26.25 ± 0.55 C in 2018 and 25.66 ± 1.68 C in 2019) as compared to the wet season (23.20 ± 0.75 C in 2018 and 21.56 ± 2.39 C in 2019), likely corresponding to decreased precipitation and therefore input of colder, fresh water. Overall, mean dry season temperatures did not change over the sampling periods but we documented a trend toward colder mean wet season temperatures decreased from 24.29 ± 1.18 C in 2017 to 21.56 ± 2.39 C in 2019, though trends were not significant. In 2018, DOP concentrations were significantly higher in the dry season, 0.1446 ± 0.04 µM as compared to 0.06091 ± 0.05 µM in the wet season (Dunn's $p = 0.0224$, Appendix Table 2). Overall, we observed a steady and significant increase TDP and PO_4 concentrations from the start (TDP: 0.1710 ± 0.06 µM; PO_4: 0.08141 ± 0.04 µM), to the end (TDP 0.3486 ± 0.11; PO_4: 0.2141 ± 0.09 µM) of the 2017-2019 sampling campaign that is significant between annual seasons (Table 5, Appendix Table 2). In 2019, TDN and DON exhibited seasonality between wet and dry seasons in opposition directions. TDN concentrations decreased from wet to dry season (wet:

7.628 ± 2.72 to dry: 1.24 ± 1.82) where as DON increased from wet to dry season (wet: 6.643 ± 2.58 to 11.10 ± 2.03), Dunn's $p < 0.001$ for both.

We also investigated interannual variation between seasons and noted a pattern where pH and the concentrations of nitrogen species (TDN, DIN, N+N and NH_3) rose between 2017 and 2018 then decreased between 2018 and 2019 (Figure 11 and Table 5). Loko i'a pH significantly increased between the 2017 wet and 2018 wet season (Dunn's $p<0.001$) and between the 2017 dry and 2018 dry season (Dunn's $p = 0.0069$). The pH then decreased significantly between the 2018 and 2019 wet seasons (Dunn's $p<0.001$). Similarly, TDN, DIN, N+N and NH3 exhibited trends of increasing between the 2017 and 2018 wet season then decreasing between the 2018 and 2019 wet seasons (Appendix Table 2).

Next, we visualized water biogeochemistry patterns using an NMDS with a biplot to understand how water column biogeochemistry variable and predictor vary along the axes (Figure 12). We observed a general axis of pH vs. phosphorus and silica while measures of nitrogen and temperature are mostly orthogonal to this axis and opposite to dissolved oxygen. The loko i'a water column environment appears to to moving toward higher nitrogen concentration, lower dissolved oxygen.

3.4 2017-2019 diatom abundance is influenced by temporal factors

As Indigenous resource management practices improve the functioning of the fishpond, we posited that efficacy in constraining nutrient inventories would increase with biocultural restoration, and therefore diatom abundance would increase from 2017 to 2019. We quantified diatom abundance by measuring the gene concentrations of *rbcL,* which encodes the RuBisCo enzyme, using taxon specific primers. Standard curves were generated from synthetic Gblock standards (Appendix Figure 2) in order to convert cycle threshold values to diatom cells mL^{-1}. Diatom concentrations did not pass the Shapiro Wiks normality test so concentrations were log-transformed (Appendix Table 1, Appendix Figure 3) for further analyses.

We examined whether abundance was spatially and then temporally structured. When grouped by sites, L07 had the lowest mean diatom abundance (5.249 ± 5.36 $\log_{10}$diatoms mL^{-1}) and the site with the highest mean diatom abundance was L01 (5.798 ± 6.14 $\log_{10}$diatoms mL^{-1}). However, when grouped by site, diatom concentrations did not vary significantly (Kruskal Wallis p-value = 0.1809, Figure 13A, Table 5). Though there was no spatial difference in diatom concentrations when averaged over 2017-2019, diatom concentrations were significantly higher in the wet season (Figure 13C) as compared to the dry season (Figure 13D), $p < 0.001$. Thus when examining temporal variability, we examined diatom concentration by season and year. In 2017, there was no seasonality in diatom concentration (Appendix Table 4, $p > 0.999$). However, 2018 and 2019 diatom concentrations displayed strong seasonality (with almost 10-fold increase in the wet season (2018: 5.850 ± 5.80 and 2019: 6.001 ± 6.19) as compared to the dry season (2018: 5.057 ± 5.12 and 2019: 5.078 ± 5.16). These seasonal differences were statistically significant (2018: $p = 0.0039$; 2019: $p < 0.001$). We also noted that no significant interannual differences in diatom concentrations were observed between all dry seasons; 2017 to 2018 ($p = 0.5954$) and 2018 and 2019 ($p > 0.999$) or 2017 to 2019 ($p = 0.2704$). Instead, diatom concentrations increased steadily between each wet season during the 2017-2019 campaign, with a significant increase in abundance between 2017 and 2019 ($p = 0.0318$). Because we noted a correlation between diatom concentrations, we hypothesized that diatom distribution patterns would positively correlate with nitrate and silicic acid, which are required for diatom growth.

3.5 Inferring environmental drivers that influence 2017-2019 diatom abundance

To determine which environmental parameters might be strong predictors for diatom abundance, continuous predictors (salinity, phosphate species, nitrogen species and silicic acid) were log_{10}-transformed and we explored the relationship between diatom concentrations and nutrient concentrations (Figure 14). We found that salinity and phosphate species displayed year-dependent patterns: no seasonality in parameter:diatom relationships in 2017; dramatically different (even opposite) correlations between diatoms and parameters in 2018; followed by a return to similar parameter:diatom relationships between seasons but with a higher y-intercept for the wet seasons. Salinity was positively correlated with diatom concentration in 2017 and 2019 but negatively correlated in 2018. TDP and PO4 were negatively correlated with diatom concentrations in 2017, 2019 and the 2018 wet season, but positively correlated in the dry season of 2018. For all nitrogen species (TDN, DIN, N+N, NH3), the relationship between these variables and diatoms shifted from neutral/negative correlation in 2017 to slightly positive correlation in 2019. Similar to the other variables, 2018 marked a strong shift in diatom:parameter relationships. However in 2018, a steeply positive correlation was found between diatoms and nitrogen species, indicating that increased nitrogen concentrations in 2018 increased diatom growth. Since diatoms are utilizing N and P simultaneously, the inverse relationship between N and P indicates that HFP likely has excess P relative to bioavailable nitrogen. In other words, the loko iʻa was N-limited but underwent substantial changes in water chemistry in 2018 which resulted in an increase in diatom abundance. In 2019, our data indicate a re-establishment of diatom:parameter relationships. These changes were consistent with the timeline of removal of Egret Island. Interestingly, silicic acid‘s relationship to diatom concentration was distinct from the other environmental parameters. During dry seasons, there was no correlation to diatoms in 2017, followed by a positive relationship in 2018 and ending in a negative relationship in 2019. In contrast, silica:diatom relationships in the wet seasons exhibited a negative correlation in 2017 and 2018 and a positive correlation in 2019.

We used three sets of models to test our hypotheses about the influence of the environmental parameters we measured on diatom concentration. All models included end members and mākāhā sites. First, we asked whether spatial location or season are predictors of diatom abundance (Table 7). We found that season was a significant predictor of diatom concentrations ($p << 0.001$) but sample site location was not ($p = 0.1296$). Together, these two factors explained 21.88% of the variation in diatoms between 2017-2019. Next we tested a linear model of diatoms that incorporated all nutrients measured during the study: PO_4, TPD, H_4SiO_4, NH_3, $NO_2 + NO_3$, DIN, TDN (Table 7, Appendix Table 5). None of the nutrients were significant predictors of diatom abundance according to marginal hypothesis tests, but some nutrients may be correlated with each other, and therefore we used model selection to identify by Akaike weights which predictors have strongest support. $NO_2 + NO_3$, DIN, and TDP were identified as having the strongest support (Appendix Table 6) and were included as terms in a best predictor model (Table 8). In this combined model, nitrate + nitrite ($p = 0.002348$) and TDP ($p = 0.004191$) have strong relationships with diatom concentrations and accounted for 4.774% of variation but DIN had a marginal relationship. We then combinatorically tested subsets of these best predictors (Appendix Table 7) and a linear model with $NO_2 + NO_3$ and DIN also showed significance (NO_2

+ NO_3: p = 0.004586; DIN: p = 0.009806). Third, we tested whether diatoms varied along the major environmental gradient, salinity, and whether the effect of salinity and the predictor nutrients NO_2 + NO_3, DIN, and TDP differed between wet and dry conditions, using a generalized additive model to allow for nonlinear relationships (Table 9 and Appendix Table 7). We found that salinity and H_4SiO_4 are significant predictors in the wet season, and TDP and NH_3 are significant predictors of diatoms in the dry season (Figure 15, red boxes).

3.6 Retrospective analysis of biogeochemistry across 3 phases of biocultural restoration

Activities conducted over a decade of biocultural restoration dramatically altered the physical and biogeochemical parameters and dynamics of HFP. The ecological influence of biocultural restoration at HFP is linked to two main management practices implemented by POH: mangrove removal and kuapā restoration. Mangrove removal decreases the carbon subsidy in the form of leaf litter and root sloughage delivered to the system in the form of refractory detritus and recalcitrant organic matter in sediment. These changes may be significant leading to altered nutrient cycling, metabolic efficiencies and trophic linkages. From 2007-2019, kuapā and mākāhā restoration increased water volume flux, decreased residence times and improved circulation. As a shift in the balance of allochthonous material input and autochthonous biogeochemical processes was anticipated, we predicted that HFP would become a more stable system with less extreme variability in the aquatic environment.

Given that the region adjacent to the kuapā and mākāhā that had been rebuilt the longest, we hypothesized that biocultural restoration increased stability of HFP water quality parameters. To test whether homogeneity increased concomitant with biocultural restoration, nMDS ordinations of the common environmental parameters (temperature, salinity, pH, % DO) were plotted and the 95% confidence intervals were determined (Figure 16A). To test for homogeneity, the distance to centroid was determined for each sampling phase (Figure 16B). Smaller distances indicate more similar conditions. Though we hypothesized that that homogeneity would be highest in 2017-2019, using the parameters in common across sampling campaigns, we found that 2014-2015 exhibited the highest centroid distance (19.16 ± 14.84) with 2017-2019 having a slightly higher heterogeneity (15.03 ±10.2) than 2007-2008 (12.67 ± 10.18). Interestingly, the majority of samples from 2017-2019 outside of the 95% confidence intervals were taken on just 2 dates, therefore a formal outlier analysis and recalculation may result in a lower centroid distance for 2017-2019 than 2007-2008. These data suggest that the 2007-2008 sampling campaign may have captured an early steady state fishpond condition for the parameters included in this analysis. Long residence times in HFP were the result of non-functional mākāhā and mangrove acting as windbreaks created a stagnant, poorly circulating system. In contrast, the 2014-2015 sampling campaign may reflect dramatic changes to circulation due to repair of the seaward mākāhā when HFP was highly dynamic and a significantly higher centroid distance than 2017-2019. Taken together with our PERMANOVA analysis (Table 12), these data support our hypothesis that biocultural restoration has decreased the variability in water quality conditions across HFP from 2014 to 2019.

Next we investigated how the spatial structure of the fishpond shifted between sampling campaigns. We defined 6 regions to account for differences in sampling effort and site location density between campaigns (Figure 5). To determine whether spatial heterogeneity changed across these regions between 2007-2008, 2014-2015 and 2017-2019, we employed a multivariate distance model for conditions in common: salinity temperature, pH and dissolved oxygen (%). We found that these environmental conditions vary significantly by sampling campaign ($p = 0.0001$). Environmental parameters also varied by region ($p = 0.009$). Non-parametric pairwise multiple comparisons based on rank sums were then performed to determine which environmental parameters changed significantly between campaigns in each region. In general, the most significant differences in mean parameters (Tables 10 and 11) were between 2014-2015 and 2017-2019. The environmental parameter that changed the least between campaigns was pH (Figure 12C) whereas the parameter that changed the most across HFP over the 12 years of sampling and biocultural restoration was dissolved oxygen (Figure 17D). The region that experienced the most significant change in its environmental parameters was Region 5, located in the northeastern corner of HFP followed by Region 2, which is adjacent to Region 5 to the south. Region 2 and 5 displayed significant changes in temperature and dissolved oxygen (Figure 17 A and D) whereas region 5 also changed salinity (Figure 17B) between 2014-2015 and 2017-2019. The region which experienced change was region 1, located in the southernmost region of the fishpond. We surmise that as this region was where biocultural restoration occurred first, this area experienced the least change in subsequent years.

CHAPTER 4. DISCUSSION AND FUTURE IMPLICATIONS

4.1 Quantifiable metrics for restoration derived/driven improvements

Historically, loko iʻa practitioners manipulated input of freshwater and salt water to produce wai momona, abundant waters, that could stimulate primary productivity and ultimately drive the foodweb for production of target food species. Working within an Indigenous resource management framework, Paepae o Heʻeia hypothesized that consistent freshwater input and nutrients, via functional mākāhā would increase primary productivity and subsequently increase the biomass of native herbivores in the loko iʻa.

In this study, we assessed the changes in Heʻeia Fishpond biogeochemistry and resultant diatom abundance over the period of time of extensive biocultural restoration: removal of Egret Island and construction of a new freshwater mākāhā was constructed. We endeavored to determine whether completion of the external kuapā resulted in an increase in diatoms. However, a limitation of the sampling designs included in this study was the lack of direct measurements of primary production. Instead, we employed qPCR of functional genes in the photosynthesis pathway to quantify the potential for primary production based on cell mass. We estimated diatom biomass by amplifying the *rbcL* gene, a key component of the RuBisCo enzyme which catalyzes the first step in carbon fixation. A caveat associated with qPCR was that the *rbcL* primers used were specific to pelagic diatoms (Li et al., 2013), and may not have amplified all estuarine or freshwater diatom species. Major shifts in biogeochemical conditions were most predominate in the wet season and this resulted in an increase in diatom abundance. Though freshwater input to the loko iʻa did occur, increased mixing and a change in the input of nutrients from removal of cattle egrets potentially resulted in a new state in the water column permissive for increased diatom growth. These data support the utilization of diatoms as indicators of water quality as correlated with biogeochemical parameters.

We also examined physical changes to the loko iʻa water column over the course of 3 independent sampling campaigns spanning a decade. As biocultural restoration of the kuapā progressed, we observed a decrease in heterogeneity of loko iʻa conditions, which should enable better management and more predictable yield of diatoms and therefore targeted food species. We hypothesized that some combination of environmental parameters best described the heterogeneity of HFP environmental parameters. Our data indicate freshwater inputs both from surface water inputs (such as near L07 and Region 5, Figure 8 and Figure 17) as well as submarine groundwater discharge (L01, Figure 8). However our comparison was limited to physical parameters collected from the YSI sonde. Because of differences in nutrient processing, we were unable to make a detailed comparison in biogeochemistry and nutrients.

4.2 Historical conditions of Heʻeia Fishpond

Consistent with other tropical embayments, Kāneʻohe Bay tends to be N-limited. The phytoplankton in the bay are dominated by cyanobacteria rather than diatoms, specifically *Prochlorococcus* in the outer bay beyond the barrier reef, and *Synechococcus* residing mostly inside the bay. Because some cyanobacteria are diazotrophs (N-fixing), available nitrogen is quickly depleted. During the wet season, the prevalence of rain increases run off and terrigenous inputs (a.k.a. nutrients), resulting in diatom and dinoflagellate blooms. As a result of the bloom, N is drawn down along with photosynthetically active radiation. Thus the system gets heterotrophic (less photosynthesis). Waters become reduced (because of increased respiration) so P desorbs from particles.

The magnitude and consistency of the trade winds matters here because the wind could keep the upper layer of the water column mixed and more oxic (therefore background climatic conditions such as El Nino years matter). The 2014-2015 sampling campaign overlapped with an El Nino year in which tradewinds were not consistent. These conditions led to more stratification, less mixing, more respiration. In the fishpond, with more steady allochthonous input, the expectation might be that nitrogen might be higher such that the phytoplankton community has more dinoflagellates and diatoms relative to cyanobacteria. This may have been the case historically but with land use change and increase sediment from mangroves, phosphate desorbes from particles. This creates a situation where N:P ratios are low, skewed and though there might be some N inputs into the system, it's still N-limited because of excess P.

Historically the fishpond did not have a sedimented bottom, it was a reef substrate so N:P ratios likely remained within Redfield ratios (~ 15:1). While there are no plans to dredge the fishpond, the increased flushing from functional mākāhā may increase the removal of sediment accumulated in the remnant mangrove root mat. Though sample location was not a significant predictor of diatom abundance, our data show that the lowest diatom abundance during the 2017-2019 dry season were areas with remnant mangrove stands, potentially implicating mangroves as nutrient sinks that draw down nutrients necessary for primary production in the water column.

4.3 Management implications: future studies of resilience

Estuaries are among the most naturally dynamic coastal ecosystems. As constructed estuarine systems, loko iʻa are equally dynamic and when paired with biocultural restoration and climate change impacts, identifying drivers of loko iʻa health can be extremely challenging. A key approach that we employed here was to operationally define baseline conditions in order to distinguish tidal forcing and precipitation-driven events. By decoupling baseline conditions from extreme events, we were able to more accurately assess changes due to biocultural restoration. Incorporating customary knowledge into our sampling scheme, we can now focus on steady state loko iʻa conditions. In addition, establishment of baseline conditions will enable us to examine long term trends such as climate mode (e.g. El Nino, La Nina etc). These climate modes may have a stronger impact on the annual scale that restoration as they can impact precipitation and marine conditions (e.g. sea surface temperature and coral bleaching). We hypothesize that our work will enable assessment of how restoration may increase ecosystem resilience in the future. Continuing to work in partnership with kiaʻi loko will be essential.

LIST OF TABLES

Table 1. He‘eia Fishpond sampling campaign and site locations.

GPS coordinates for sampling locations considered in this study. Mākāhā and end members (shaded grey) were excluded from inter-campaign comparisons.

Site ID	Latitude	Longitude	2007-2008	2014-15	2017-2019	Region
Stk1	21.43445827	-157.8054018	△			6
Stk3	21.43661066	-157.8058873	△			6
Stk6	21.4390881	-157.8078584	△			4
Stk7	21.43919262	-157.8095158	△			4
Stk8	21.43785747	-157.8089375	△			5
Stk9	21.43663555	-157.8083143	△			3
Stk13	21.43275716	-157.8063507	△			1
Stk15	21.43331934	-157.807793	△			1
Stk16	21.43432667	-157.8087142	△			2
Stk18	21.43705817	-157.8102405	△			5
P01	21.43272	-157.807456		□		1
P02	21.4347	-157.80862		□		2
P03	21.43743	-157.81073		□		5
P04	21.43871	-157.81001		□		4
P05	21.43703	-157.80923		□		5
P06	21.43573	-157.80754		□		2
P07	21.439924	-157.80829		□		4
P08	21.43769	-157.80676		□		3
P09	21.43579	-157.80563		□		6
P10	21.43353	-157.80646		□		1
L01	21.43257	-157.807037			○	1
L02	21.43526813	-157.8080256			○	2

L03	21.4366529	-157.8083328			○	3
L04	21.43689497	-157.8073568			○	3
L05	21.438975	-157.809387			○	4
L06	21.43705071	-157.8102603			○	5
L07	21.43732522	-157.8108525			○	5
L08	21.43773065	-157.8097896			○	5
L09	21.436953	-157.809789			○	5
L10	21.43609408	-157.8066134			○	6
L11	21.4379231	-157.8078234			○	3
M01/Wai 2	21.4379231	-157.8078234	△	□	○	
M02/Wai 1	21.43865833	-157.8107722	△		○	
M03/Kahoalāhui	21.43966667	-157.8099278	△		○	
M04/Nui	21.43842222	-157.8067472	△		○	
M05/Kahoʻokele	21.43723333	-157.8058306	△	□	○	
M06/Hīhīmanu	21.43573889	-157.8053056	△		○	
RM1	21.43724416	-157.810922	△			
River	21.43544197	-157.8111223	△			
E01/River	21.43388611	-157.8052778			○	
OCN1	21.43938373	-157.8072713	△			
OCN2	21.4348715	-157.8050476	△			
E02/Ocean	21.44120833	-157.8061611			○	

Table 2. *rbcL* sequences used for quantification of diatoms

Sequence name	Sequence (5‘ > 3‘)	Reference
rbcL forward primer	GATGATGARAAYATTAACTC	(Li et al., 2013)
rbcL reverse primer	GTAAACTDGCCCADKNCATTTC	(Li et al., 2013)
rbcL gBlocks standard Genbank HF675093.1	GAT GAT GAA AAC ATT AAC TCA CAA CCA TTC ATG CGT TGG AGA GAG CGT TTC TTA AAC TGT ATG GAA GGT ATT AAC CGT GCT TCT GCT GCT ACA GGT GAG GTA AAA GGT TCT TAC TTA AAC GTT ACA GCT GCT ACT ATG GAA GAA GTA TAC AAA CGT TGT GAG TAT GCT AAA GAA GTA GGT TCT GTA ATT GTA ATG ATC GAT TTA GTT ATG GGT TAC ACA GCA ATT CAA AGT ACT GCT ATT TGG GCT CGT GAG AAC GAT ATG TTA TTA CAC TTA CAC CGT GCC GGT AAC TCT ACA TAC GCT CGT CAA AAG AAT CAT GGT ATT AAC TTC CGT GTT ATC TGT AAA TGG ATG CGT ATG TCT GGT GTA GAT CAT ATT CAC GCT GGA ACA GTT GTA GGT AAA TTA GAA GGT GAT CCT TTA ATG ATT AAA GGT TTC TAC GAT ATT TTA CGT TTA ACT CAA TTA GAA GTA AAC TTA CCA TAC GGT ATT TTC TTC GAA ATG TCT TGG GCT AGT TTA C	This study

Table 3. Filtering of sampling dates based on rain event criteria and extreme tidal criteria. This study includes data from 119 sampling dates. Based on rain events and extreme tides, dates were removed from further analysis (grey).

Sample Date	% Quickflow	Discharge Max (cfs)	Moon phase
08/11/07	1.24%	1.8	NewMoon
09/15/07	1.81%	1.6	NewMoon
10/13/07	2.68%	2.34	NewMoon
11/04/07	47.50%	74	LastQ
11/05/07	48.12%	126	LastQ
11/06/07	45.35%	126	NewMoon
11/07/07	43.68%	126	NewMoon
11/08/07	43.27%	126	NewMoon
11/11/07	4.58%	3.53	NewMoon
11/17/07	2.26%	2.35	FirstQ
12/09/07	37.11%	113	NewMoon
01/12/08	23.90%	25.3	FirstQ
02/16/08	1.27%	2.14	FirstQ
03/15/08	0.54%	1.57	FirstQ
04/19/08	1.59%	2.03	FullMoon
05/17/08	4.07%	2.47	FullMoon
06/14/08	29.24%	75.6	FullMoon
07/26/08	4.09%	1.74	LastQ
08/30/08	2.77%	2.15	NewMoon
05/27/14	21.86%	41.5	NewMoon
06/05/14	3.78%	2.14	FirstQ
06/19/14	5.11%	1.74	LastQ
06/26/14	5.09%	2.14	NewMoon
06/27/14	5.31%	2.14	NewMoon
07/02/14	13.09%	13.6	FirstQ
07/07/14	5.91%	2.03	FirstQ
07/09/14	5.56%	2.03	FullMoon
07/14/14	14.20%	13.6	FullMoon
07/16/14	16.06%	13.6	LastQ
07/21/14	76.10%	689	LastQ
07/23/14	72.61%	689	NewMoon
07/24/14	70.13%	689	NewMoon
07/29/14	3.87%	2.59	NewMoon
07/30/14	4.32%	2.59	NewMoon
08/06/14	4.84%	2.03	FirstQ
08/11/14	4.97%	2.14	FullMoon
08/13/14	4.68%	2.14	FullMoon
08/19/14	3.28%	1.93	LastQ
08/21/14	3.53%	1.93	NewMoon
08/25/14	4.92%	2.24	NewMoon
08/28/14	4.01%	2.97	NewMoon
09/02/14	9.50%	11.1	FirstQ
09/08/14	5.50%	2.47	FullMoon

09/11/14	4.40%	2.03	FullMoon
09/16/14	4.24%	2.35	LastQ
09/17/14	3.79%	2.35	LastQ
09/22/14	5.16%	2.03	NewMoon
09/25/14	3.84%	1.93	NewMoon
09/30/14	7.29%	9.98	FirstQ
10/02/14	13.89%	27.6	FirstQ
10/07/14	4.35%	3.68	FullMoon
10/09/14	9.14%	14.5	FullMoon
10/13/14	3.04%	1.93	LastQ
10/15/14	3.82%	1.74	LastQ
10/20/14	43.58%	64.5	NewMoon
10/22/14	40.20%	64.5	NewMoon
10/27/14	2.95%	3.53	NewMoon
10/29/14	2.67%	2.71	FirstQ
11/03/14	3.88%	2.59	FullMoon
11/06/14	3.02%	2.59	FullMoon
11/11/14	3.70%	3.38	LastQ
11/12/14	4.54%	3.38	LastQ
11/14/14	3.59%	2.97	LastQ
11/19/14	11.49%	30	NewMoon
11/24/14	3.04%	1.84	NewMoon
11/28/14	3.14%	1.65	FirstQ
12/01/14	2.82%	1.74	FirstQ
12/05/14	4.62%	2.97	FullMoon
12/08/14	3.94%	2.24	FullMoon
12/09/14	4.53%	1.93	FullMoon
12/12/14	3.44%	1.65	LastQ
01/12/15	3.54%	1.65	LastQ
01/13/15	3.48%	1.65	LastQ
01/20/15	4.32%	1.65	NewMoon
01/22/15	3.41%	1.65	NewMoon
01/26/15	6.88%	2.71	FirstQ
01/28/15	5.96%	2.71	FirstQ
02/02/15	3.24%	1.74	FullMoon
02/05/15	4.72%	2.24	FullMoon
02/09/15	4.04%	1.74	LastQ
02/13/15	4.17%	1.84	LastQ
02/24/15	3.65%	1.93	FirstQ
02/28/15	3.13%	1.74	FirstQ
03/02/15	3.19%	1.74	FullMoon
03/03/15	3.31%	1.74	FullMoon
03/12/15	3.60%	1.74	LastQ
03/15/15	2.88%	1.48	LastQ
03/16/15	3.09%	1.48	LastQ
03/22/15	5.35%	1.57	NewMoon
03/30/15	9.88%	7.74	FirstQ
04/11/15	3.83%	1.74	LastQ
04/13/15	3.31%	1.65	LastQ
04/20/15	3.01%	1.57	NewMoon
04/21/15	3.13%	1.57	NewMoon

04/29/15	4.97%	2.47	FirstQ
05/04/15	3.53%	1.74	FullMoon
05/20/15	3.89%	1.48	NewMoon
05/26/15	4.89%	1.84	FirstQ
06/04/15	12.52%	9.29	FullMoon
06/10/15	4.22%	2.03	LastQ
06/17/15	4.55%	1.65	NewMoon
06/23/15	4.31%	1.33	FirstQ
06/25/15	4.14%	1.4	FirstQ
07/01/15	29.39%	56	FullMoon
07/07/15	4.92%	1.33	LastQ
07/23/15	19.21%	38.4	FirstQ
02/18/17	4.67%	2.71	LastQ
03/19/17	3.37%	2.35	LastQ
04/02/17	0.21%	2.24	FirstQ
06/02/17	1.70%	3.08	FirstQ
10/11/17	3.59%	1.53	LastQ
12/09/17	0.24%	1.75	LastQ
01/26/18	0.09%	2.08	FirstQ
06/07/18	2.12%	2.74	LastQ
01/28/19	0.74%	2.43	LastQ
02/25/19	2.23%	3.11	LastQ
03/25/19	1.98%	2.16	LastQ
04/25/19	2.40%	2.01	LastQ
06/11/19	2.11%	1.79	FirstQ

Table 4. Environmental characteristics of HFP during 2017-2019 campaign by site

Physical parameters were measured using a YSI Sonde and chemical concentrations were determined using an autoanalyzer from each site from February 18, 20217 - June 11, 2019. Shown is the mean ± standard deviation and sample number for each site.

Site	Temperature, C	Salinity, ppt	pH	DO, %
L01	23.67 ± 2.53, 13	21.43 ± 8.36, 13	7.885 ± 0.2399, 13	75.78 ± 17.57, 13
L02	24.12 ± 2.42, 13	26.04 ± 4.25, 13	7.942 ± 0.1667, 13	74.44 ± 16.97, 13
L03	24.39 ± 2.50, 13	27.37 ± 2.49, 13	7.949 ± 0.1441, 13	81.28 ± 12.81, 13
L04	24.57 ± 2.37, 13	28.71 ± 2.28, 13	7.966 ± 0.1486, 13	87.32 ± 17.48, 13
L05	24.78 ± 2.50, 13	25.88 ± 3.70, 11	7.912 ± 0.1380, 13	80.35 ± 11.29, 13
L06	24.12 ± 2.29, 13	13.53 ± 8.83, 13	7.698 ± 0.2061, 13	72.79 ± 6.194, 13
L07	23.63 ± 2.11, 13	6.276 ± 6.40, 13	7.358 ± 0.2492, 13	59.05 ± 8.416, 13
L08	24.28 ± 2.39, 13	20.82 ± 6.211, 13	7.847 ± 0.1552, 13	80.23 ± 11.47, 13
L09	24.05 ± 2.36, 13	14.67 ± 8.561, 13	7.808 ± 0.1470, 13	68.32 ± 21.11, 13
L10	24.38 ± 2.40, 12	29.55 ± 2.989, 13	7.957 ± 0.1372, 12	82.88 ± 12.22, 12
L11	24.73 ± 2.15, 12	28.15 ± 2.598, 13	7.968 ± 0.1263, 12	84.14 ± 10.48, 12

Site	TDN, µM	DON, µM	DIN, µM	N+N, µM	NH_3 (µM)
L01	9.049 ±3.748, 13	7.543 ± 3.342, 13	1.506 ± 1.664, 13	0.7475 ± 0.4326, 13	0.7585 ± 1.409, 13
L02	9.632 ± 3.246, 13	8.564 ± 2.988, 13	1.067 ± 0.8292, 13	0.6036 ± 0.4351, 13	0.4626 ± 0.4732, 13
L03	8.987 ± 2.749, 13	7.438 ± 2.958, 12	1.548 ± 1.770, 12	0.6518 ± 0.3724, 12	0.8974 ± 1.545, 12
L04	8.520 ± 3.515, 13	7.580 ± 3.377, 13	0.9415 ± 0.5777, 13	0.5533 ± 0.3576, 13	0.3874 ± 1.3658 ± 13
L05	8.989 ± 3.841, 13	7.668 ± 2.903, 12	1.320 ± 1.390, 12	0.5862 ± 0.2990,12	0.7341 ± 1.188, 12
L06	9.068 ± 3.158, 13	7.036 ± 2.167, 13	2.033 ± 1.310, 13	1.183 ± 0.6482, 13	1.8495 ± 0.9129, 13
L07	10.63 ± 4.079, 13	8.574 ± 3.418, 13	2.051 ± 1.104, 13	1.212 ± 0.7581, 13	0.8390 ± 0.7515, 13
L08	9.152 ± 3.442, 13	7.935 ± 3.247, 13	1.216 ± 1.147, 13	0.6801 ± 0.6372, 13	0.5355 ± 0.6029, 13
L09	8.928 ± 3.205, 13	7.595 ± 3.003, 13	1.332 ± 0.7799, 13	0.6615 ± 0.3975, 13	0.6704 ± 0.5561, 13
L10	8.807 ± 3.357, 12	7.907 ± 3.076, 12	0.9002 ± 0.6569, 12	0.5251 ± 0.4281, 12	0.3760 ± 0.2965, 12
L11	9.135 ± 4.112, 12	8.205 ± 3.732, 11	1.270 ± 0.8529, 12	0.6571 ± 0.4733, 12	0.6143 ± 0.4990, 12

Site	TDP (µM)	PO_4 (µM)	DOP (µM)	H_4SiO_4 (µM)	Log_{10}(diatoms mL^{-1})
L01	0.2440 ± 0.03978, 13	0.1402 ± 0.01687, 13	0.1038 ± 0.07294, 13	83.23 ± 43.27, 13	5.798 ± 6.140, 12
L02	0.2194 ± 0.08652, 13	0.12448 ± 0.06724, 13	0.09462 ± 0.06826, 13	79.51 ± 56.95, 13	5.646 ± 6.029, 13
L03	0.2516 ± 0.1166, 12	0.1206 ± 0.07887, 12	0.1302 ± 0.07882, 12	56.14 ± 23.13, 12	5.704 ± 6.018, 12
L04	0.2296 ± 0.1292, 13	0.09790 ± 0.07713, 13	0.1309 ± 00.8863, 13	48.81 ± 29.22, 13	5.532 ± 5.790, 13
L05	0.2332 ± 0.09457, 12	0.1349 ± 0.08979, 12	0.09832 ± 0.07652, 12	83.69 ± 58.79, 12	5.526 ± 5.557, 12
L06	0.2799 ± 0.1425, 13	0.1836 ± 0.07698, 13	0.09630 ± 0.08010, 13	180.3 ± 106.1, 13	5.632 ± 5.811, 13
L07	0.3185 ± 0.1180, 13	0.2140 ± 0.09200, 13	0.1060 ± 0.6481, 13	222.7 ± 117.8, 13	5.249 ± 5.355, 12
L08	0.2556 ± 0.1305, 13	0.1599 ± 0.09520, 13	0.09648 ± 0.06105, 13	119.4 ± 82.66, 13	5.730 ± 6.115, 13
L09	0.2537 ± 0.1401, 13	0.1594 ± 0.09213, 13	0.9815 ± 0.08834, 13	139.5 ± 99.16, 13	5.751 ± 6.069, 13
L10	0.2265 ± 0.08196, 12	0.1057 ± 0.07187, 12	0.1200 ± 0.07115, 12	40.94 ± 30.76, 12	5.512 ± 5.765, 11
L11	0.2303 ± 0.07256, 12	0.1377 ± 0.08283, 12	0.1076 ± 0.06843, 11	53.56 ± 25.70, 12	5.455 ± 5.598, 10

Table 5. Environmental characteristics of HFP during 2017-2019 campaign by season and year.

Shown is the mean ± standard deviation and sample number for each season and year.

Year	Season	Temperature, C	Salinity, ppt	pH	DO, %
2017	Wet	24.29 ± 1.175, 23	21.10 ± 10.62, 31	7.843 ± 0.11, 31	69.23 ± 13.81, 34
	Dry	25.48 ± 1.485, 33	23.13 ± 9.12, 33	7.733 ± 0.20, 33	76.23 ± 16.51, 33
2018	Wet	23.20 ± 0.7510, 11	23.23 ± 3.51, 11	8.177 ± 0.10, 11	79.04 ± 5.39, 11
	Dry	26.25 ± 0.5538, 11	20.76 ± 9.13, 11	8.009 ± 0.24, 10	87.30 ± 21.51, 11
2019	Wet	21.56 ± 2.387, 32	22.76 ± 8.35, 32	7.818 ± 0.16, 32	77.75 ± 16.16, 32
	Dry	25.66 ± 1.682, 22	19.55 ± 10.29, 22	7.904 ± 0.20, 22	79.37 ± 12.65, 22

Year	Season	TDN, µM	DON, µM	DIN, µM	N+N, µM	NH_3 (µM)
2017	Wet	8.081 ± 2.89, 31	6.740 ± 2.24, 31	1.340 ± 0.80, 31	0.8252 ± 0.32, 31	0.5150 ± 0.5679, 31
	Dry	8.497 ± 2.75, 33	7.273 ± 2.14, 33	1.224 ± 1.01, 33	0.6042 ± 0.47, 33	0.6195 ± 0.5982, 31
2018	Wet	13.09 ± 3.96, 11	9.882 ± 3.97, 11	3.207 ± 2.22, 11	1.073 ± 0.35, 11	2.135 ± 2.01, 11
	Dry	9.195 ± 4.69, 10	7.138 ± 4.12, 10	2.057 ± 1.04, 10	1.244 ± 0.71, 10	0.8130 ± 0.48, 10
2019	Wet	7.628 ± 2.72, 32	6.643 ± 2.58, 31	0.336 ± 0.72, 22	0.6029 ± 0.68, 32	0.4619 ± 0.48, 32
	Dry	1.24 ± 1.82, 22	11.10 ± 2.03, 22	1.064 ± 0.80, 32	0.6059 ± 0.38, 22	0.3273 ± 0.41, 22

Year	Season	TDP (µM)	PO_4 (µM)	DOP (µM)	H_4SiO_4 (µM)
2017	Wet	0.1710 ± 0.06, 31	0.08141 ± 0.04, 31	0.09954 ± 0.05, 31	63.39 ± 41.20, 31
	Dry	0.2142 ± 0.07, 33	0.1002 ± 0.06, 33	0.1140 ± 0.06, 33	101.2 ± 92.41, 33
2018	Wet	0.1791 ± 0.07, 11	0.1182 ± 0.08, 11	0.06091 ± 0.05, 11	83.77 ± 57.30, 11
	Dry	0.2950 ± 0.11, 10	0.1504 ± 0.10, 10	0.1446 ± 0.06, 10	82.05 ± 81.10, 10
2019	Wet	0.3047 ± 0.12, 32	0.2078 ± 0.06, 32	0.09719 ± 0.10, 32	96.45 ± 74.84, 21
	Dry	0.3486 ± 0.11, 22	0.2141 ± 0.09, 22	0.1448 ± 0.08, 21	174.9 ± 124.9, 22

Year	Season	Log_{10}(diatoms mL^{-1})
2017	Wet	5.209 ± 5.00, 52
	Dry	5.246 ± 5.10, 57
2018	Wet	5.850 ± 5.80, 12
	Dry	5.057 ± 5.12, 18
2019	Wet	6.001 ± 6.19, 58
	Dry	5.078 ± 5.16, 39

Table 6. Summary of PERMANOVA results for the analysis of differences in 2017-2019 HFP biogeochemistry cross different factors

Euclidean distance-based multivariate analysis on log-transformed parameters. df: degrees of freedom; SS: sum of squares; significance indicated in bold with P-values *** p<0.001, **p<0.01,* p<0.05

Model 1: Salinity

Source	df	SS	R^2	F	*Pr* (>F)
Salinity	1	6.935	0.187	31.052	**0.001** ***
Residual	135	30.150	0.813		
Total	136	37.085	1.00000		

Model 2: Date + Salinity

Source	df	SS	R^2	F	*Pr* (>F)
Date	12	13.612	0.36705	8.4365	**0.001** ***
Salinity	1	5.449	0.14693	40.5268	**0.001** ***
Residual	123	16.538	0.44595		
Total	136	37.085	1.00000		

Model 3: Site + Salinity

Source	df	SS	R^2	F	*Pr* (>F)
Site	10	3.142	0.08471	1.454	0.052
Salinity	1	1.318	0.03555	6.101	**0.002** **
Residual	125	27.008	0.72828		
Total	136	37.085	1.00000		

Model 4: Date + Site

Source	df	SS	R^2	F	*Pr* (>F)
Date	12	15.092	0.40696	10.8337	**0.001** ***
Site	10	8.753	0.23602	7.5396	**0.001** ***
Residual	113	13.234	0.35686		
Total	136	37.085	1.00000		

Model 5: Date + Site + Salinity

Source	df	SS	R^2	F	*Pr* (>F)
Date	12	13.963	0.37652	10.0794	**0.001** ***
Site	10	3.493	0.09419	3.0257	**0.001** ***
Salinity	1	0.189	0.00510	1.6388	0.165
Residual	113	13.045	0.35176		
Total	136	37.085	1.00000		

Model 6: Year + Season + Site

Source	df	SS	R^2	F	*Pr* (>F)
Year	2	3.539	0.09542	9.0138	**0.001** ***
Season	1	0.819	0.02209	4.1724	**0.008** **
Site	10	8.781	0.23679	4.4735	**0.001** ***
Residual	123	24.145	0.65106		

Total	136	37.085	1.00000

Table 7. Summary of distance-based linear models of diatoms, season, site, and biogeochemical predicator variables, 2017-2019

Distance-based modeling of log-transformed parameters. Analysis includes end members (E sites) and mākāhā (M sites). df: degrees of freedom; SS: sum of squares; significance indicated in bold with P-values *** p<0.001, **p<0.01,* p<0.05

Model 1: Season + Site: lm(formula = log10(diatom) ~ Season * Site)

Predictor	df	SS	F	*P*r (>F)
Season	1	6.843	17.2184	**4.964e-05** ***
Site	19	10.579	1.4010	0.1296
Season + Site	19	3.956	0.5239	0.9498
Residuals	196	77.894		

Residual standard error: 0.6304 on 196 degrees of freedom
Multiple R-squared: 0.2188, Adjusted R-squared: 0.06332
F-statistic: 1.407 on 39 and 196 DF, p-value: 0.06923

Model 2: Season + Site: lm(formula = log_{10}(diatoms) ~ log_{10}(DIN) + log_{10}(PO_4) + log_{10}(TDP) + log_{10}(H_4SiO_4) + log_{10}(NH_3) + log_{10}(NO_2NO_3) + log_{10}(TDN))

Predictor	df	SS	F	*P*r (>F)
DIN	1	0.441	1.0644	0.30330
PO_4	1	0.000	0.0011	0.97403
TDP	1	0.840	2.0278	0.15581
H_4SiO_4	1	0.204	0.4932	0.48322
NH_3	1	0.074	0.1778	0.67369
NO_2NO_3	1	1.400	3.3793	0.06732
TDN	1	0.006	0.0156	0.90060
Residuals	228	94.483		

Residual standard error: 0.6437 on 228 degrees of freedom
Multiple R-squared: 0.05239, Adjusted R-squared: 0.0233
F-statistic: 1.801 on 7 and 228 DF, p-value: 0.08806

Table 8. Linear model of diatoms with the best predictors from model selection

Distance-based modeling of log-transformed parameters. Analysis includes end members (E sites) and mākāhā (M sites). df: degrees of freedom; SS: sum of squares; significance indicated in bold with P-values *** p<0.001, **p<0.01,* p<0.05

Best predictor model: NO_2NO_3 + DIN + TDP: lm(formula = $\log_{10}$(diatoms) ~ $\log_{10}(NO_2NO_3)$+ $\log_{10}$(DIN) + $\log_{10}$(TDP)

Predictor	df	SS	F	*P*r (>F)
NO_2NO_3	1	3.867	9.4651	**0.002348 ****
DIN	1	1.268	3.1027	0.079493
TDP	1	3.418	8.3653	**0.004191 ****
Residuals	230	93.966		

Residual standard error: 0.6392 on 230 degrees of freedom
Multiple R-squared: 0.04774, Adjusted R-squared: 0.03532
F-statistic: 3.844 on 3 and 230 DF, p-value: 0.01032

Model 3: NO_2 + NO_3: lm(formula = log10(diatom) ~ $\log_{10}(NO_2NO_3)$)

Predictor	df	SS	F	*P*r (>F)
NO_2+NO_3	1	0.648	1.5324	0.217
Residuals	232	98.030		

Residual standard error: 0.65 on 232 degrees of freedom
Multiple R-squared: 0.006562, Adjusted R-squared: 0.00228
F-statistic: 1.532 on 1 and 232 DF, p-value: 0.217

Model 4: TDP: lm(formula = log10(diatom) ~ $\log_{10}$(TDP))

Predictor	df	SS	F	*P*r (>F)
TDP	1	0.704	1.6677	0.1978
Residuals	232	97.973		

Residual standard error: 0.6498 on 232 degrees of freedom
Multiple R-squared: 0.007137, Adjusted R-squared: 0.002858
F-statistic: 1.668 on 1 and 232 DF, p-value: 0.1978

Model 5: DIN: lm(formula = log10(diatom) ~ $\log_{10}$(DIN))

Predictor	df	SS	F	*P*r (>F)
DIN	1	0.704	1.6677	0.1978
Residuals	232	97.973		

Residual standard error: 0.652 on 232 degrees of freedom
Multiple R-squared: 0.000657, Adjusted R-squared: -0.003651
F-statistic: 0.1525 on 1 and 232 DF, p-value: 0.6965

Model 6: TDP+ (NO_2 + NO_3): lm(formula = log10(diatom) ~ $\log_{10}$(TDP) + $\log_{10}(NO_2NO_3)$)

Predictor	df	SS	F	*P*r (>F)

TDP	1	0.646	1.5321	0.2170
NO_2NO_3	1	0.589	1.3975	0.2384
Residuals	232	97.384		

Residual standard error: 0.6493 on 231 degrees of freedom
Multiple R-squared: 0.01311, Adjusted R-squared: 0.004563
F-statistic: 1.534 on 2 and 231 DF, p-value: 0.2179

Model 7: TDP + DIN lm(formula = log10(diatom) ~ $\log_{10}$(TDP) + $\log_{10}$(DIN))

Predictor	**df**	**SS**	**F**	***P*r (>F)**
TDP	1	0.779	1.8400	0.1763
DIN	1	0.140	0.3302	0.5661
Residuals	231	97.833		

Residual standard error: 0.6508 on 231 degrees of freedom
Multiple R-squared: 0.008554, Adjusted R-squared: -2.976e-05
F-statistic: 0.9965 on 2 and 231 DF, p-value: 0.3707

Model 8: NO_2 + NO_3: lm(formula = log10(diatom) ~ $\log_{10}$(NO_2NO_3) +$\log_{10}$(DIN))

Predictor	**df**	**SS**	**F**	***P*r (>F)**
NO_2NO_3	1	3.379	8.1952	**0.004586 ****
DIN	1	2.796	6.7819	**0.009806 ****
Residuals	231	95.234		

Residual standard error: 0.6421 on 231 degrees of freedom
Multiple R-squared: 0.0349, Adjusted R-squared: 0.02654
F-statistic: 4.176 on 2 and 231 DF, p-value: 0.01653

Table 9. General additive model of 2017-2019 diatom abundance and seasonality of environmental parameters.

Predictor	Season	edf	Ref df	F	p-value
Salinity	Dry	3.279	4.035	1.652	0.159242
	Wet	3.107	3.820	6.485	**0.000121 *** **
H_4SiO_4	Dry	2.361	2.975	1.798	0.13250
	Wet	8.157	8.774	3.671	**0.00023 *** **
TDP	Dry	1.000	1.000	4.154	**0.0427***
	Wet	1.011	1.022	0.004	0.9771
PO_4	Dry	1	1	1.021	0.313
	Wet	1	1	0.235	0.628
DIN	Dry	1	1	0.168	0.683
	Wet	1	1	0.009	0.923
$NO_2 + NO_3$	Dry	1	1	0.108	0.743
	Wet	1	1	1.990	0.160
NH3	Dry	6.128	6.858	3.215	**0.00328 ** **
	Wet	1.000	1.000	3.165	0.07658

Table 10. Physical characteristics of HFP across 2007-2008, 2014-2015, and 2017-2019 sampling campaigns

Physical parameters were measured using a YSI Sonde. Shown is the mean ± standard deviation and sample number for each region (Figure 5).

Parameter	Campaign	Grand mean	Region 1	Region 2	Region 3	Region 4	Region 5	Region 6
Temperature	2007-2008	**24.95 ± 1.41, 82**	25.08 ± 1.35, 17	25.24 ± 0.96, 4	25.34 ± 1.03, 9	25.50 ± 1.14, 12	24.33 ± 1.91, 16	24.98 ± 1.44, 14
	2014-2015	**25.96 ± 2.47, 410**	25.94 ± 2.59, 82	25.85 ± 2.35, 82	26.20 ± 2.54, 41	26.16 ± 2.53, 82	25.67 ± 2.41, 82	26.22 ± 2.4, 41
	2017-2019	**24.73 ± 2.56, 241**	25.13 ± 3.2, 26	24.12 ± 2.42, 13	24.81 ± 2.4,63	25.11 ± 2.51, 25	23.94 ± 2.19, 65	26.19 ± 2.77, 26
Salinity	2007-2008	**27.45 ± 9.58, 86**	30.14 ± 3.87, 17	27.47 ± 1.39, 4	30.95 ± 2.78, 9	30.09 ± 2.22, 12	20.25 ± 13.06, 16	32.39 ± 2.225, 14
	2014-2015	**27.11 ± 5.78, 410**	27.06 ± 4.57, 82	27.26 ± 5.72, 82	30.17 ± 3.38, 41	26.85 ± 4.76, 82	23.94 ± 7.72, 82	30.77 ± 3.34, 41
	2017-2019	**22.19 ± 1.42, 241**	24.98 ± 7.36, 26	26.04 ± 4.25, 13	28.64 ± 2.65, 63	24.12 ± 5.78, 25	12.26 ± 9.36, 65	30.10 ± 2.62, 26
DO%	2007-2008	**88.87 ± 15.75, 63**	92.96 ± 16.44, 13	95.47 ± 7.74, 3	95.38 ± 16.63, 7	84.28 ± 7.23, 9	74.89 ± 21.02, 12	94.74 ± 10.69, 11
	2014-2015	**93.62 ± 23.4, 410**	95.8 ± 24.59, 82	94.64 ± 24.47, 82	100.63 ± 22.14, 41	91.33 ± 23.6, 82	84.58 ± 21.47, 8	102.87 ± 16.82, 41
	2017-2019	**80.08 ± 22.38, 241**	90.41 ± 21.79, 26	74.44 ± 16.97, 13	86.19 ± 13.51, 63	77.44 ± 17.04, 25	66.20 ± 15.93, 65	105.74 ± 17.09, 26
pH	2007-2008	**7.87 ± 0.17, 82**	7.9 ± 0.13, 17	7.87 ± 0.11, 4	7.93 ± 0.06, 9	7.86 ± 0.07, 12	7.69 ± 0.32, 16	7.97 ± 0.05, 14
	2014-2015	**7.96 ± 0.97, 410**	7.92 ± 0.24, 82	7.94 ± 0.21, 82	7.97 ± 0.22, 41	7.9 ± 0.21, 82	8.05 ± 2.13, 82	8.01 ± 0.19, 41
	2017-2019	**7.83 ± 0.30, 241**	7.95 ± 0.22, 26	7.94 ± 0.17, 14	7.96 ± 0.13, 63	7.85 ± 0.16, 25	7.66 ± 0.29, 65	8.02 ± 0.11, 26

Table 11. Chemical characteristics of HFP across 2007-2008, 2014-2015, and 2017-2019 sampling campaigns

Chemical concentrations were determined using an autoanalyzer from each site. Shown is the mean ± standard deviation and sample number for each region (Figure 5).

Parameter	Campaign	Grand mean	Region 1	Region 2	Region 3	Region 4	Region 5	Region 6
TDN, µM	2007-2008	**8.09 ± 1.51, 6**	9.27 ± 0.84	n/a	8.25 ± 0.58, 2	8.50 ± 1.45, 4	8.33 ± 1.03, 2	n/a
	2017-2019	**9.37 ± 5.43, 240**	9.19 ± 3.72, 26	9.63 ± 3.25, 13	8.64 ± 3.40, 62	9.93 ± 3.30, 25	9.52 ± 3.60, 65	8.27 ± 2.67, 26
N+N, µM	2007-2008	**0.20 ± 0.15, 91**	0.18 ± 0.15, 16	0.16 ± 0.26, 4	0.17 ± 0.09, 9	0.14 ± 0.09, 14	0.17 ± 0.14, 18	0.25 ± 0.18, 15
	2017-2019	**0.77 ± 0.55, 240**	0.67 ± 0.36, 26	0.60 ± 0.44, 13	0.63 ± 0.44, 62	0.66 ± 0.34, 25	0.96 ± 0.67, 65	0.782 ± 0.59, 26
NH_4, µM	2007-2008	**5.22 ± 3.86, 92**	4.32 ± 2.47, 17	6.22 ± 1.9, 4	4.49 ± 6.59, 9	4.99 ± 1.83, 14	7.83 ± 3.39, 18	4.07 ± 5.06, 15
	2017-2019	**0.64 ± 0.79, 240**	0.69 ± 1.03, 26	0.46 ± 0.47, 13	0.54 ± 0.75, 62	0.78 ± 0.92, 25	0.72 ± 0.70, 65	0.55 ± 0.62, 26
DIN, µM	2007-2008	**5.45 ± 3.9, 91**	4.61 ± 2.57, 16	6.38 ± 2.14, 4	4.66 ± 6.59, 9	5.13 ± 1.86, 14	8.00 ± 3.46, 18	4.32 ± 5.07, 15
	2017-2019	**1.41 ± 1.12, 240**	1.36 ± 1.24, 26	1.07 ± 0.83, 13	1.17 ± 0.99, 62	1.44 ± 1.13, 25	1.68 ± 1.15, 65	1.33 ± 1.13, 26
DON, µM	2007-2008	**4.23 ± 1.84, 13**	4.80 ± 0.56, 3	n/a	5.00 ± 2.43, 2	3.91 ± 2.30, 4	1.92 ± 0.04, 2	n/a
	2017-2019	**7.78 ± 4.95, 239**	7.83 ± 3.31, 26	8.56 ± 2.99, 13	7.53 ± 3.22, 61	7.5 ± 2.68, 25	7.85 ± 3.08, 65	6.94 ± 2.29, 26
TDP, µM	2007-2008	**0.58 ± 0.11, 20**	0.58 ± 0.04, 4	0.51, 1	0.63 ± 0.02, 2	0.61 ± 0.06, 3	0.46 ± 0.21, 4	0.65 ± 0.05, 3
	2017-2019	**0.27 ± 0.15, 240**	0.24 ± 0.10, 26	0.22 ± 0.09, 13	0.23 ± 0.10, 62	0.28 ± 0.12, 25	0.28 ± 0.13, 65	0.24 ± 0.09, 26
PO_4, µM	2007-2008	**0.48 ± 0.33, 91**	0.49 ± 0.41, 16	0.086 ± 0.44, 4	0.23 ± 0.07, 9	0.49 ± 0.27, 14	0.70 ± 0.28, 18	0.27 ± 0.11, 15
	2017-2019	**0.16 ± 0.1281, 240**	0.12 ± 0.07, 26	0.12 ± 0.07, 13	0.11 ± 0.08, 62	0.18 ± 0.11, 25	0.19 ± 0.09, 65	0.11 ± 0.07, 26
DOP, µM	2007-2008	**0.38 ± 0.13, 14**	0.38 ± 0.23, 4	n/a	0.40 ± 0.01, 2	0.24 ± 0.08, 2	0.33, 1	0.44 ± 0.05, 3
	2017-2019	**0.11 ± 0.08, 239**	0.12 ± 0.09, 26	0.09 ± 0.07, 13	0.12 ± 0.08, 61	0.10 ± 0.08, 25	0.09 ± 0.07, 65	0.13 ± 0.07, 26
H_4SiO_4, µM	2007-2008	**104.65 ± 117.47, 92**	71.06 ± 83.63, 17	163.04 ± 102.49, 4	42.39 ± 18.9, 9	80.60 ± 44.75, 14	201.03 ± 138.62, 18	30.95 ± 19.82, 15
	2017-2019	**102.52 ± 100.17, 240**	66.29 ± 38.91, 26	79.51 ± 56.95, 13	47.96 ± 26.25, 62	104.94 ± 79.34, 25	180.15 ± 113.07, 65	38.86 ± 25.83, 26

Table 12. Summary of PERMANOVA results for the analysis of differences in 2007-2008, 2014-2015, 2017-2019 sampling campaigns and regions

P < 0.001, ***; P<0.01, **, P <0.05, *

*Model: Regions*Campaign + Season*					
Source	**df**	**SS**	**R^2**	**F**	***P*r (>F)**
Regions	1	5612	0.29240	11.555	**0.002** ***
Sampling campaign	2	31283	0.43227	32.206	**0.001*** **
Season	1	13462	0.03471	27.719	**0.001*** **
Regions:Campaign	2	981	0.24062	1.009	0.374
Residuals	573	278285	0.84426		
Total	579	329622	1.00000		

LIST OF FIGURES

Figure 1. Loko iʻa foodweb

Hawaiian fishponds were focused on maximizing primary production of phytoplankton and macroalgae, which served as the base of the foodweb for herbivorous target species. This simplified foodweb provided more efficient conversion to protein than the natural foodweb system and supported a large populace. Source: (Kleven, 2014)

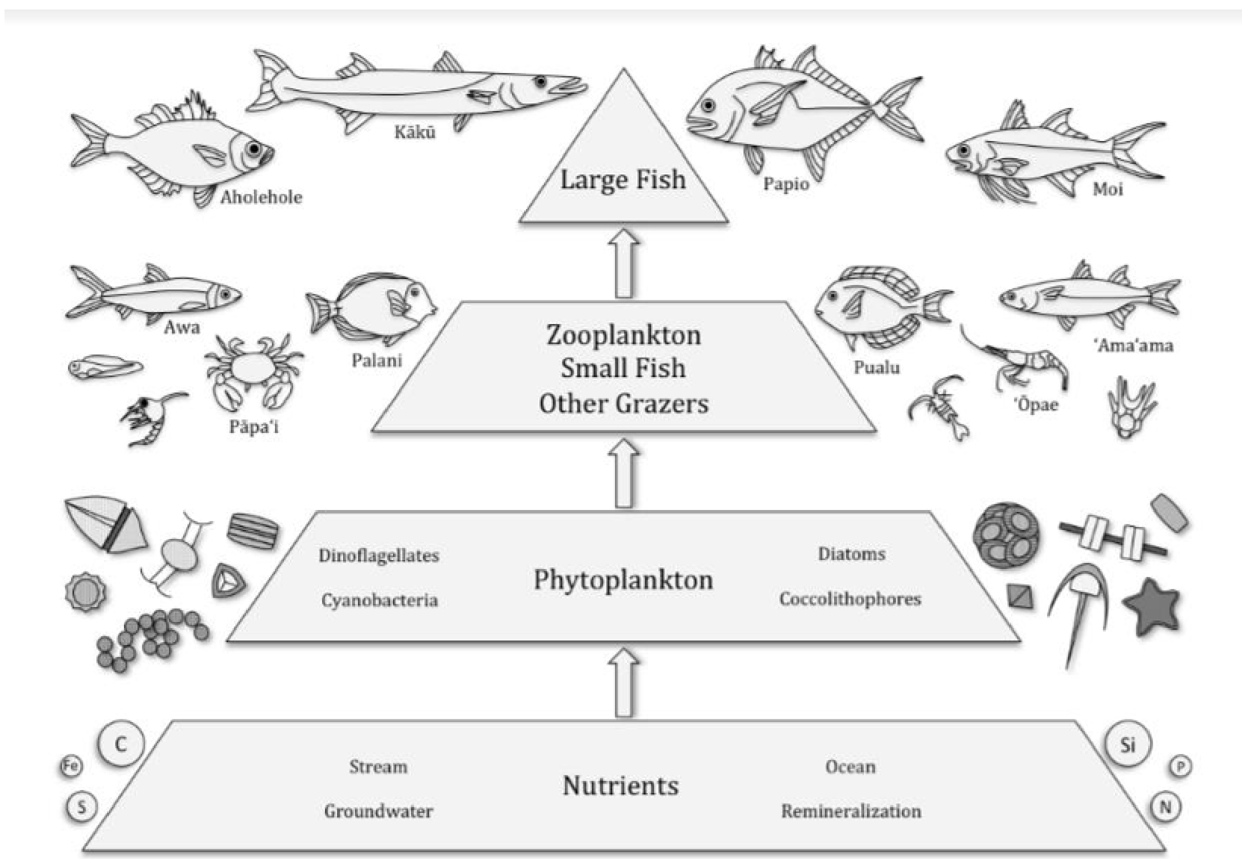

Figure 2. Loko iʻa of Kawahaokamanō and Heʻeia ahupuaʻa

(A) Government survey map of Kāneʻohe and Heʻeia ahupuaʻa , show the location of fishponds along the coast (source: F.W. Thrum, 1892 Hawaiʻi Government Survey). (B) The Heʻeia ahupuaʻa (pink line) encompasses the Heʻeia watershed, adjacent areas of Kāneʻohe Bay and extends to the Mokapu Peninsula. The Heʻeia NERR (yellow line) was established in 2017 within the ahupuaʻa and includes the Heʻeia Wetland (green), Heʻeia Fishpond (light blue) and the Malaukaʻa Reef. source: Heʻeia National Estuarine Research Reserve.

A

B

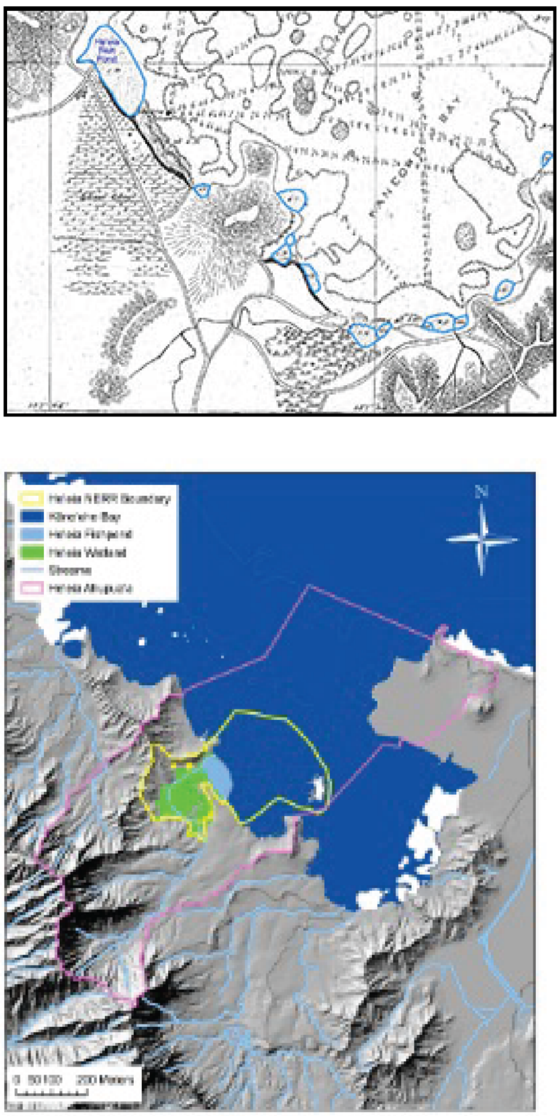

Figure 3. Chronosequence of biocultural restoration at HPF, 2007-2020

Dates of successive biocultural restoration involving removal of mangrove and rebuilding kuapā: Phase I (purple), Phase II (orange), Phase III (blue). Mākāhā (double white lines) and kuapā (red) are shown for reference.

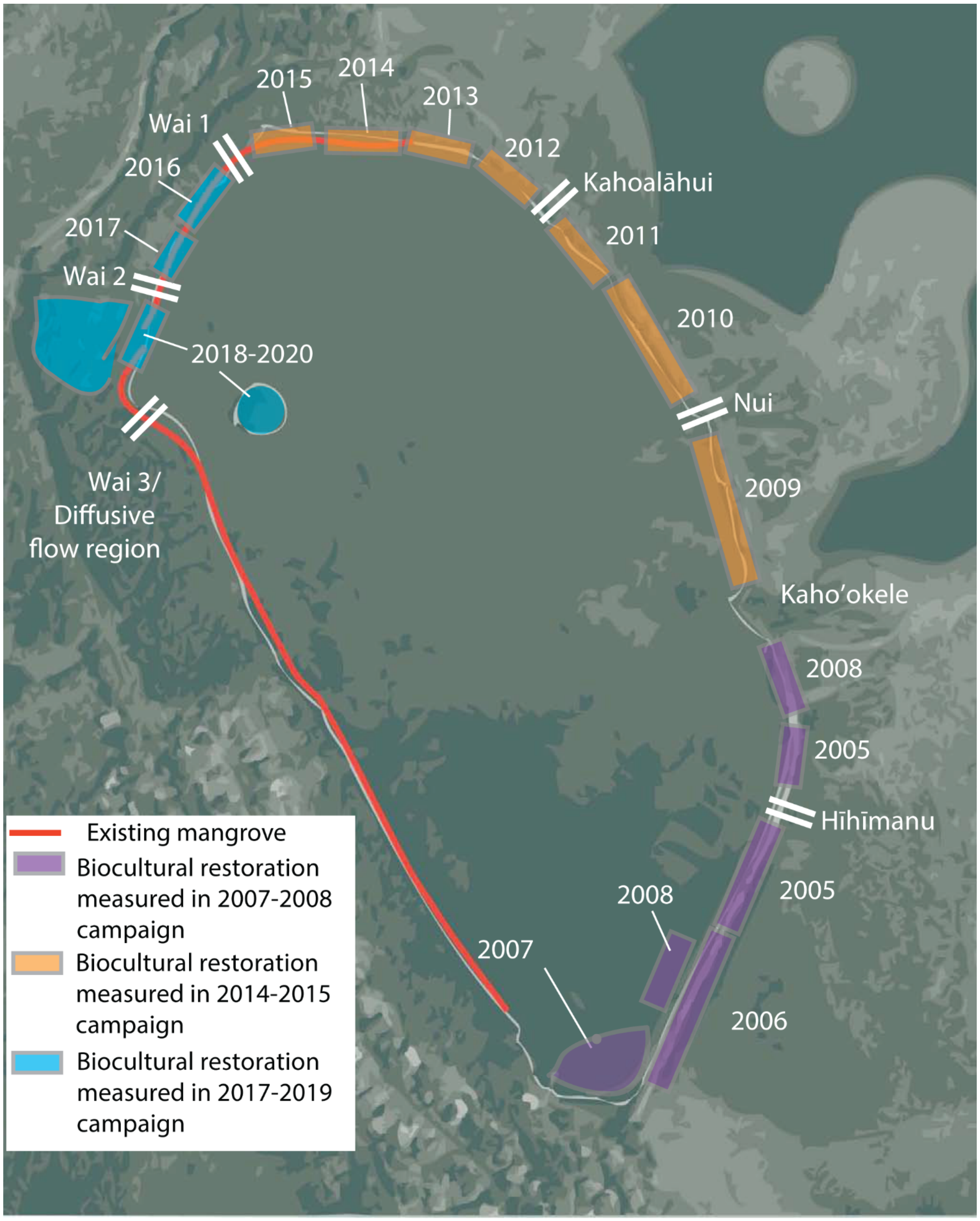

Figure 4. Discrete sample processing methods over the course of this study

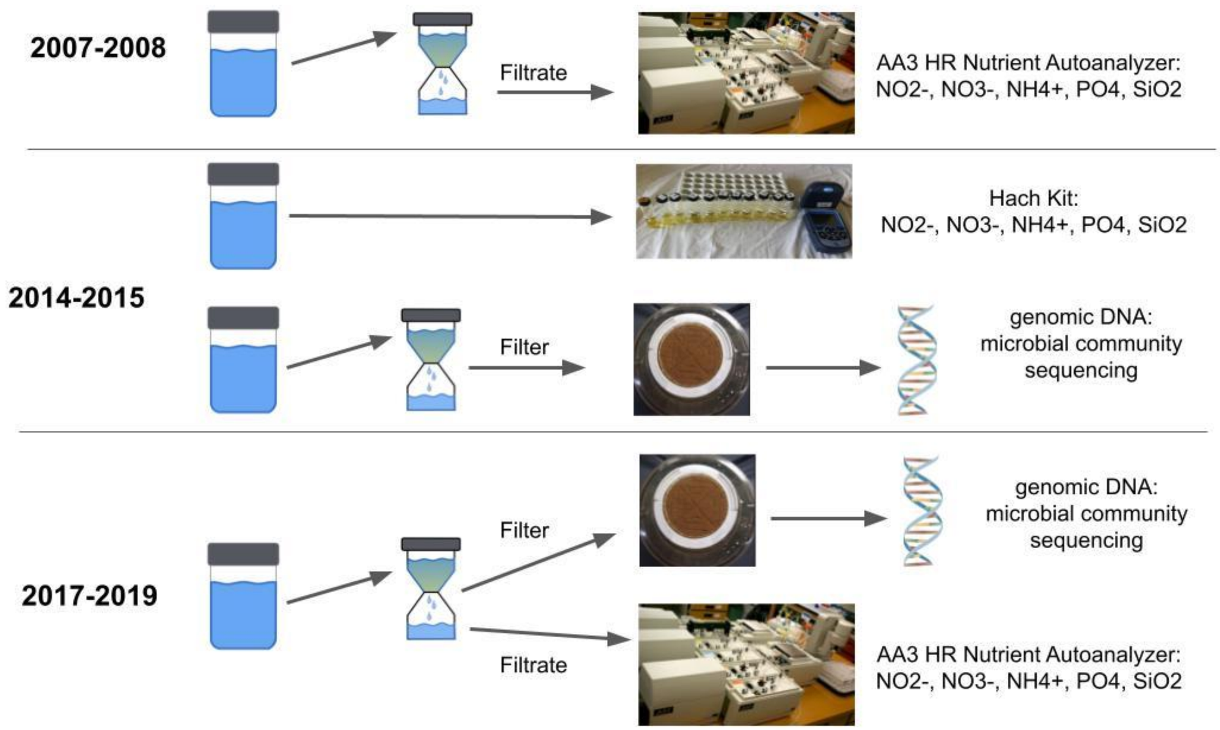

Figure 5. Standardization of sampling effort for inter-campaign comparison

Sample sites distribution of sites differed between campaigns. To standardize geospatial analysis and sampling effort, the loko iʻa was divided into 6 polygon regions such that sites from each of the sampling campaigns (2007-2008, 2014-2015, 2017-2019) were represented in each of the 6 regions by at least 1 site. Colors represent regions and symbols differentiate sampling campaign (triangle: 2007-2008; square: 2014-2015; circle: 2017-2019)

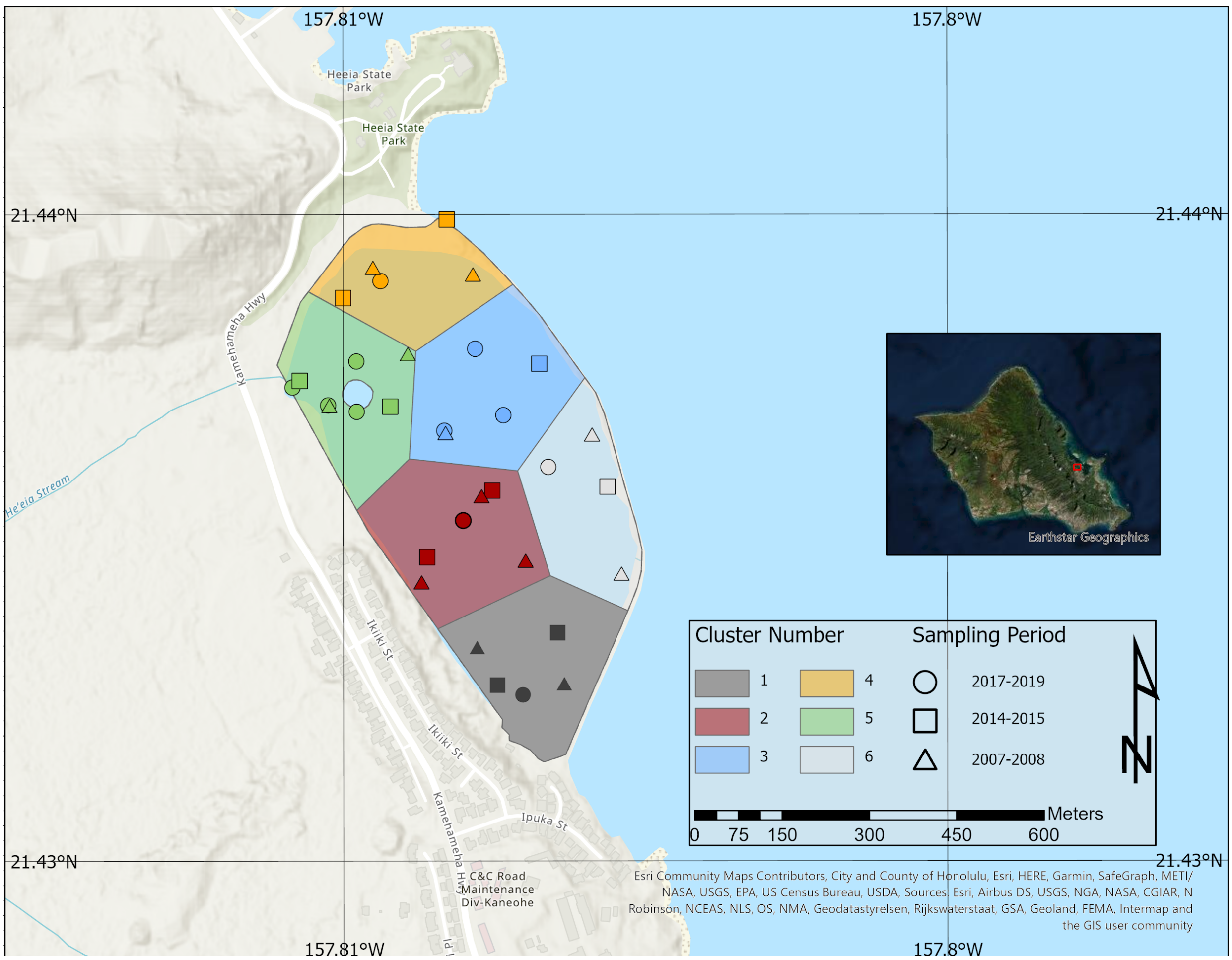

Figure 6: Establishing baseline sampling dates using He‘eia Stream discharge

Top: Example of applying quickflow criteria to sample dates. The percentage of He‘eia stream discharge attributed to quickflow (red) and base flow (purple) due to effects of subtropical storm Wali (7/19/14 - 7/23/14). Bottom: Hydrograph of He‘eia Stream plotting discharge (ft^3s^{-1}) from 7/19/14 - 7/23/14. Vertical line on the bottom axis shows a sampling date that was excluded based on the criteria for selecting baseline sample dates. The rapid increase in discharge due to intense precipitation of the storm displays the dynamics of the baseflow separation technique employed with quick flow quickly becoming the dominant component of stream discharge.

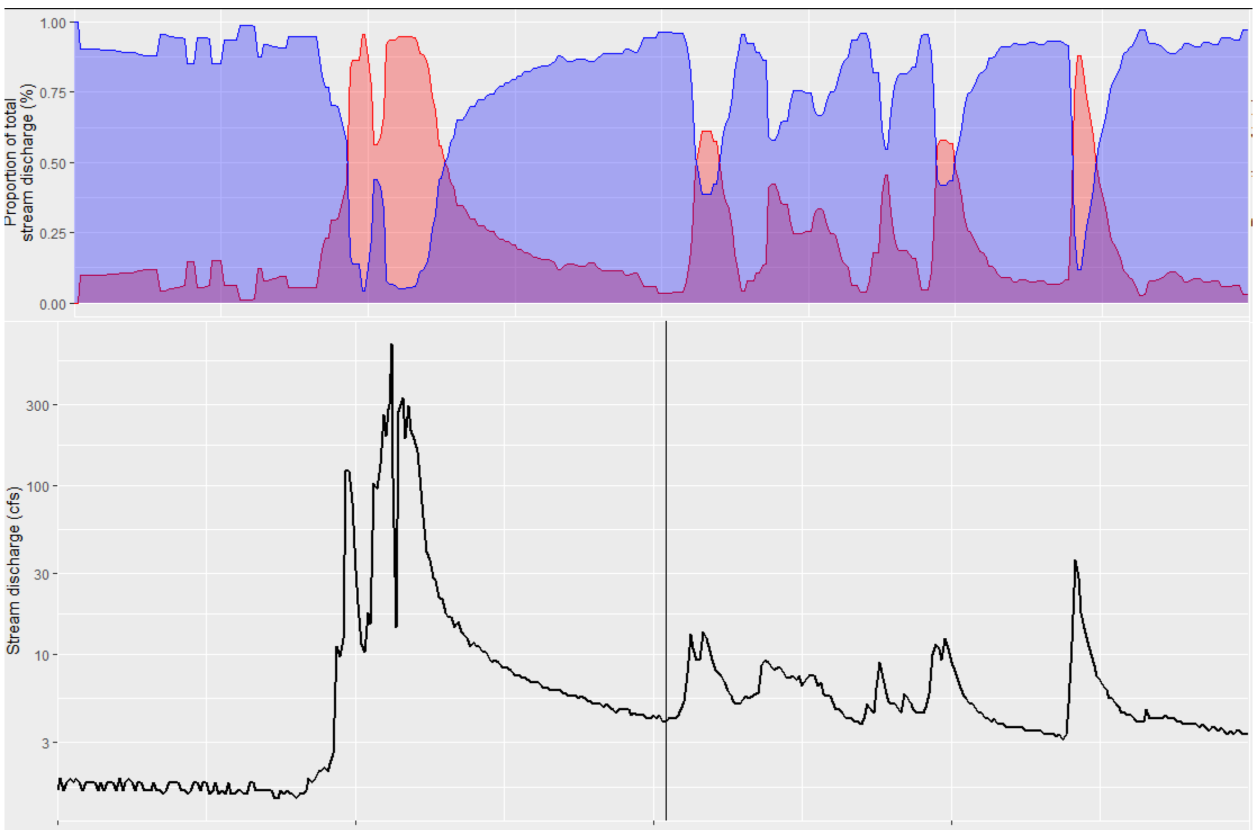

Figure 7. Progress of Egret Island removal, October 2017-2018

Biocultural-based removal of Egret Island was documented at designated photo points from October 2017-October 2018. Above water plant material was removed, but root mass was left in place.

Figure 8. Spatial distribution of biogeochemical parameters, 2017-2019

Mean values of physical parameters (temperature, salinity, pH, DO%) and nutrients (TN, DIN, NO_2+NO_3, NH_3, TDP, PO_4, H_4SiO_4) for each site were calculated and values were interpolated.

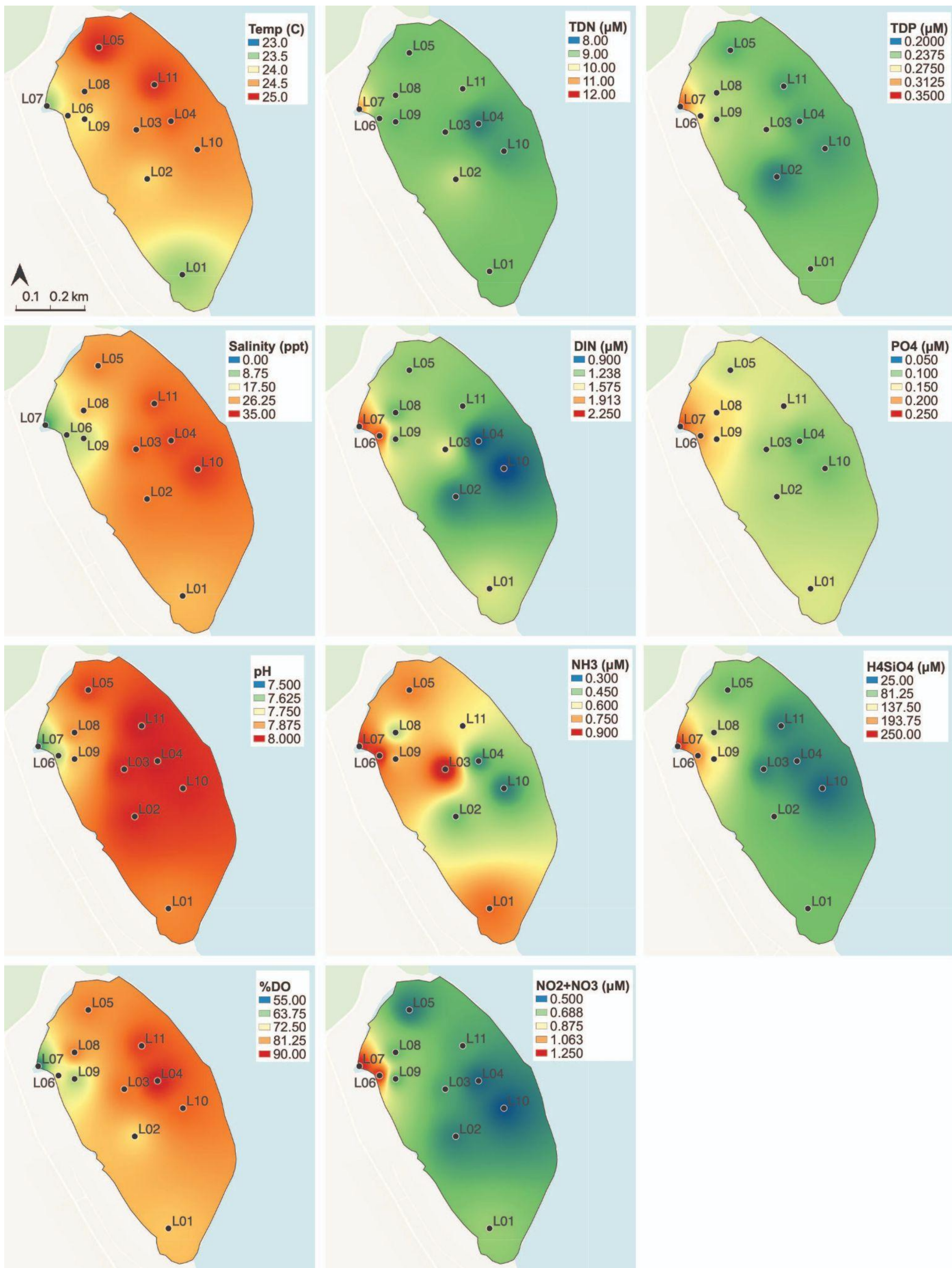

Figure 9. Comparison of 2017-2019 biogeochemical parameters between sites.

Boxplot of all discrete environmental measurements for sites for measurements with distributions that varied significantly by site (Kruskal Wallis, p ≤ 0.05). Dunn's post hoc comparisons for significance are plotted, * p<0.05; ** p<0.01; ***p <0.001.

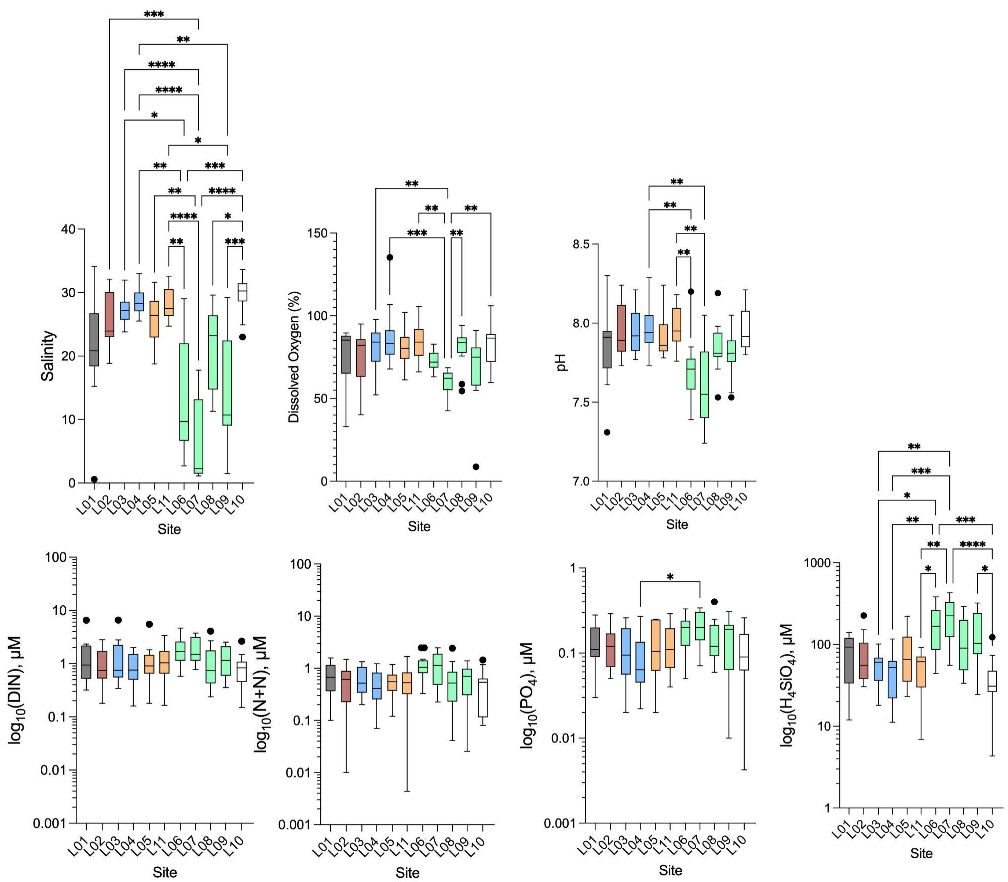

Figure 10. 2017-2019 biogeochemical parameters that vary significantly by date

Distribution significance was assessed by (Kruskal Wallis, $p \leq 0.05$. Grey box indicates sample dates coinciding with Egret Island removal.

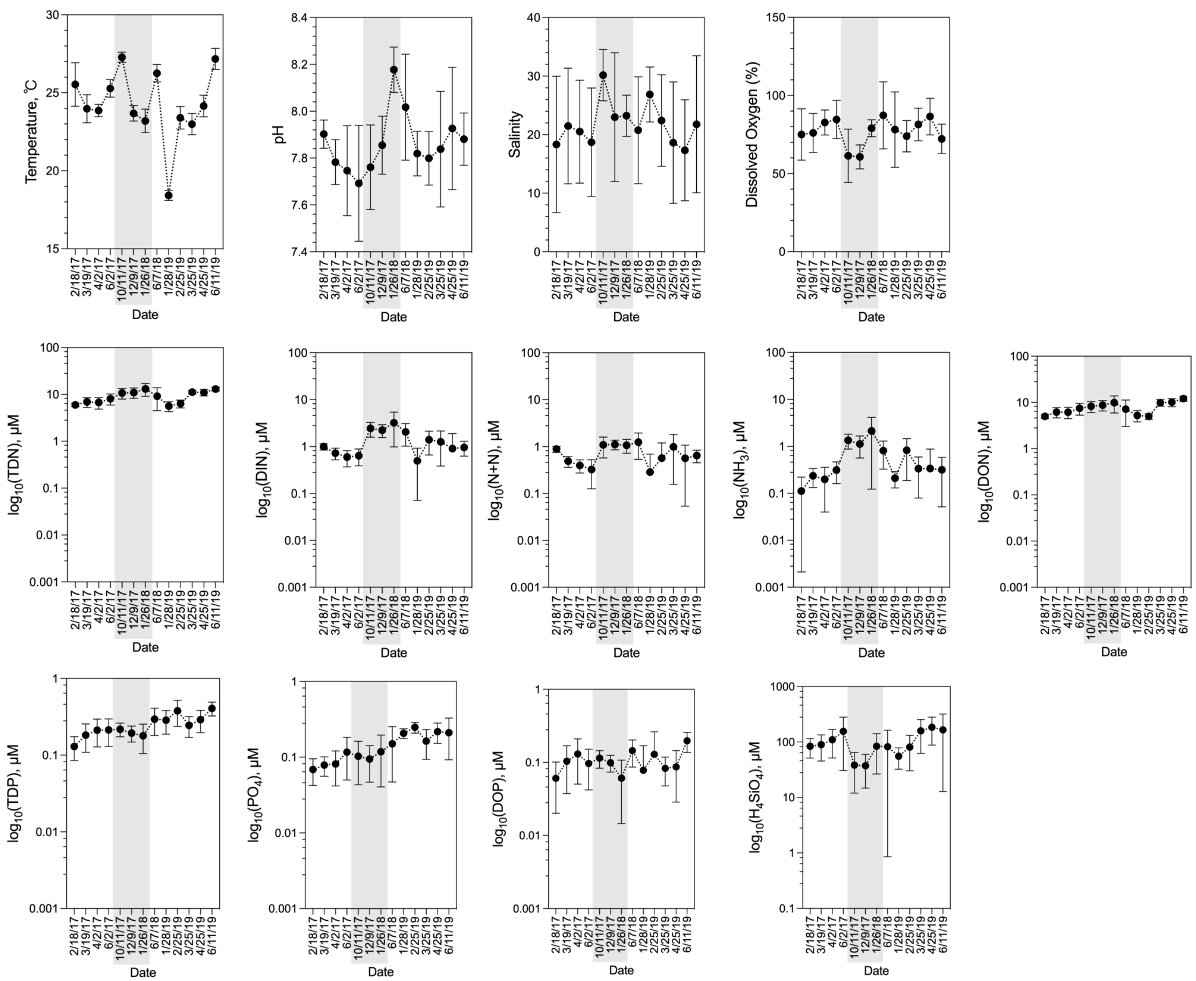

Figure 11. Comparisons of 2017-2019 biogeochemical parameters between year and season.

Boxplot of all discrete environmental measurements for wet (grey) and dry (white) seasons. For measurements with distributions that varied significantly by year-season (Kruskal Wallis, p ≤ 0.05), significant Dunn's post-hoc pairwise comparisons between seasons or years are plotted, * p<0.05; ** p<0.01; ***p <0.001.

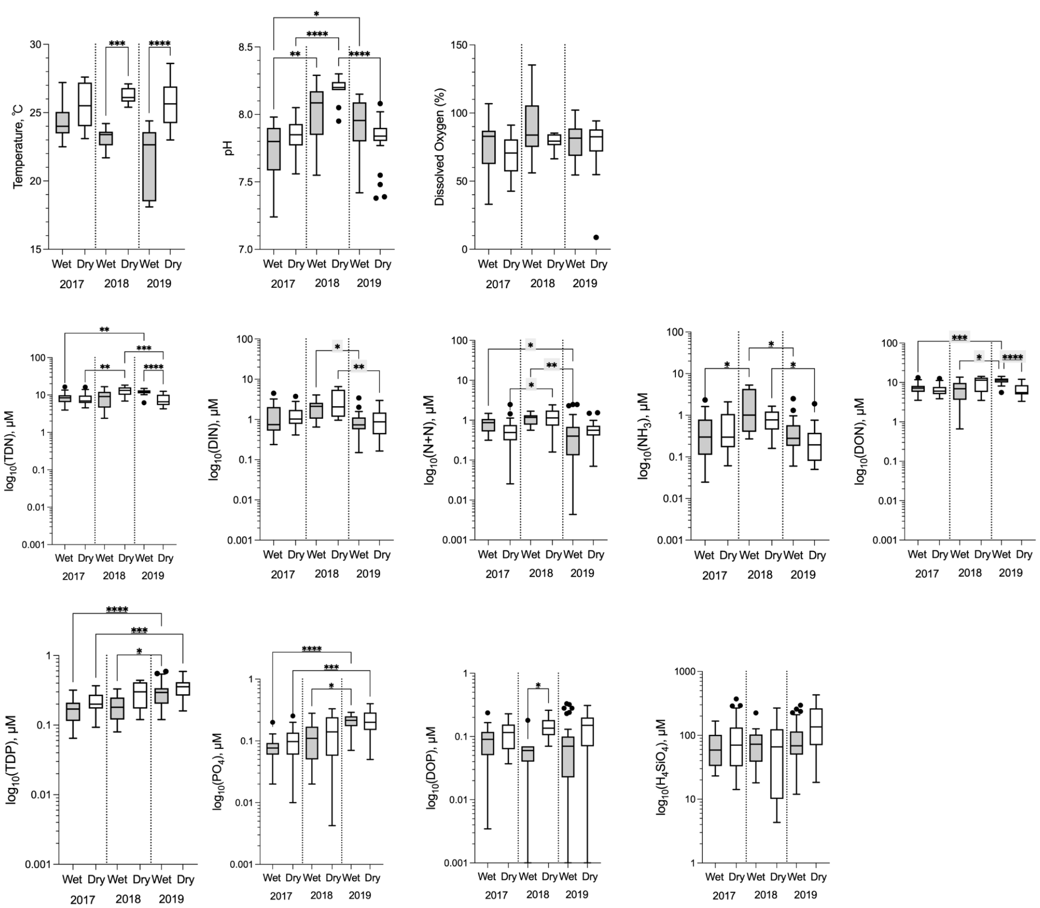

Figure 12. Relationships between biogeochemical parameter and site location, 2017-2019.

Non-metric multidimensional (nMDS) ordination of Euclidian distances colored by region. The biplot vectors show the direction and magnitude of significant surface water environmental vectors within the ordination space. Ellipses represent 95% confidence intervals.

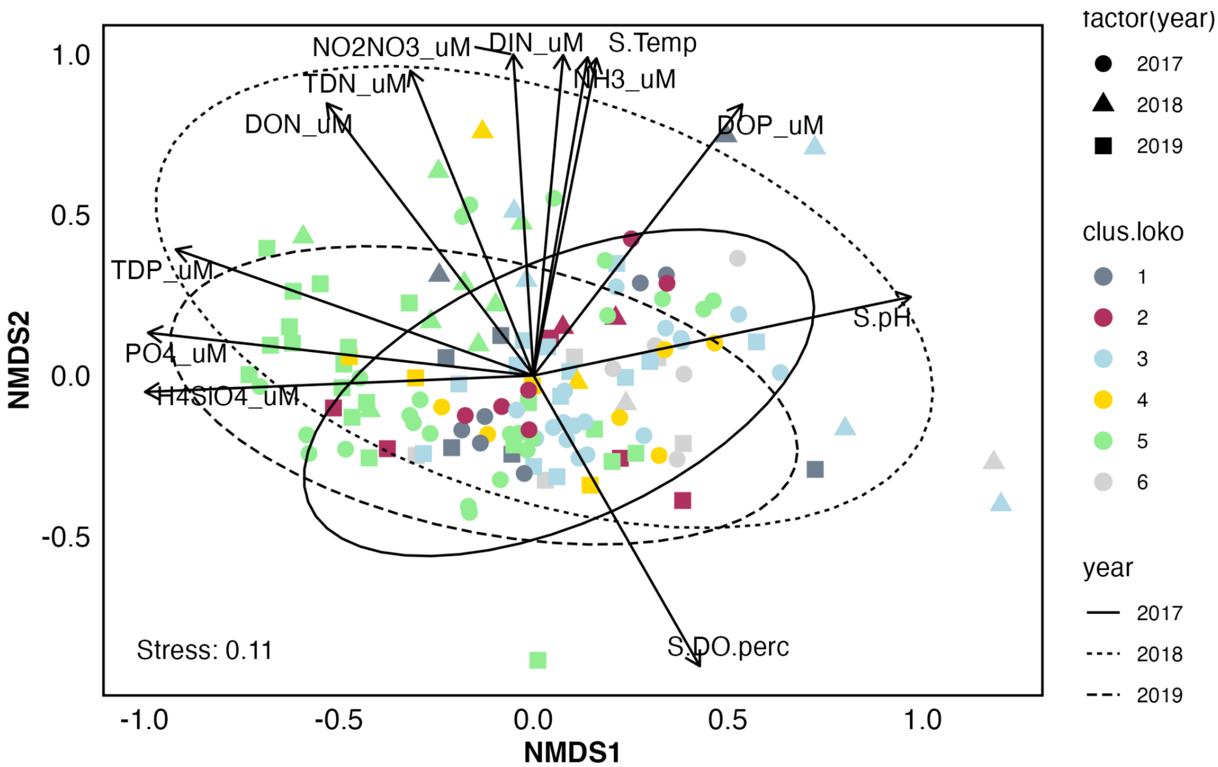

Figure 13. Seasonal shifts in diatom abundance and spatial distribution, 2017-2019

Boxplots of diatom abundance from the 2017-2019 campaign sample sites (A) and mean concentrations during wet and dry season (B). For each site, the line inside the box is the median. The top and bottom lines of the box are the first and third quartiles, respectively. The top and bottom whiskers are the 5th and 95th percentiles, respectively. Box plots demonstrate a trend of higher diatom abundance during the wet season. Heatmaps illustrate spatial distribution of mean diatom abundance in the 2017-2019 wet (C) and dry (D) seasons.

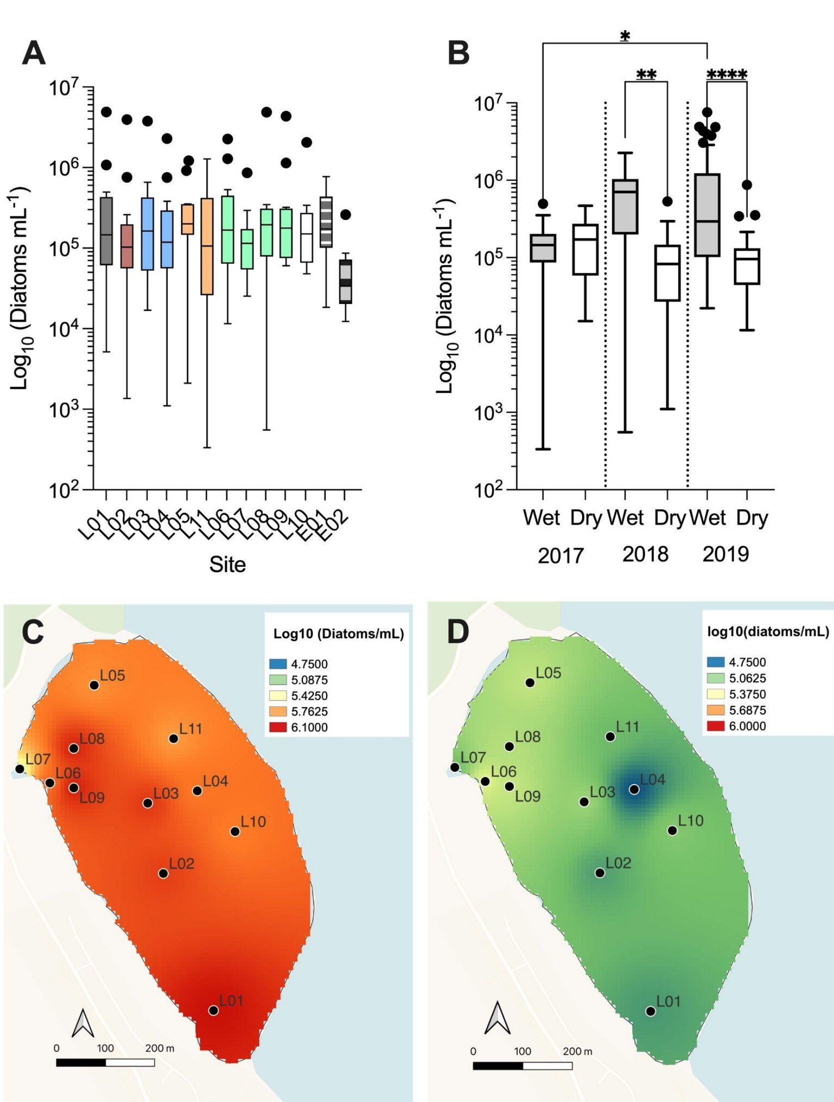

Figure 14. Seasonal and interannual relationships between diatom abundance and environmental parameters, 2017-2019.

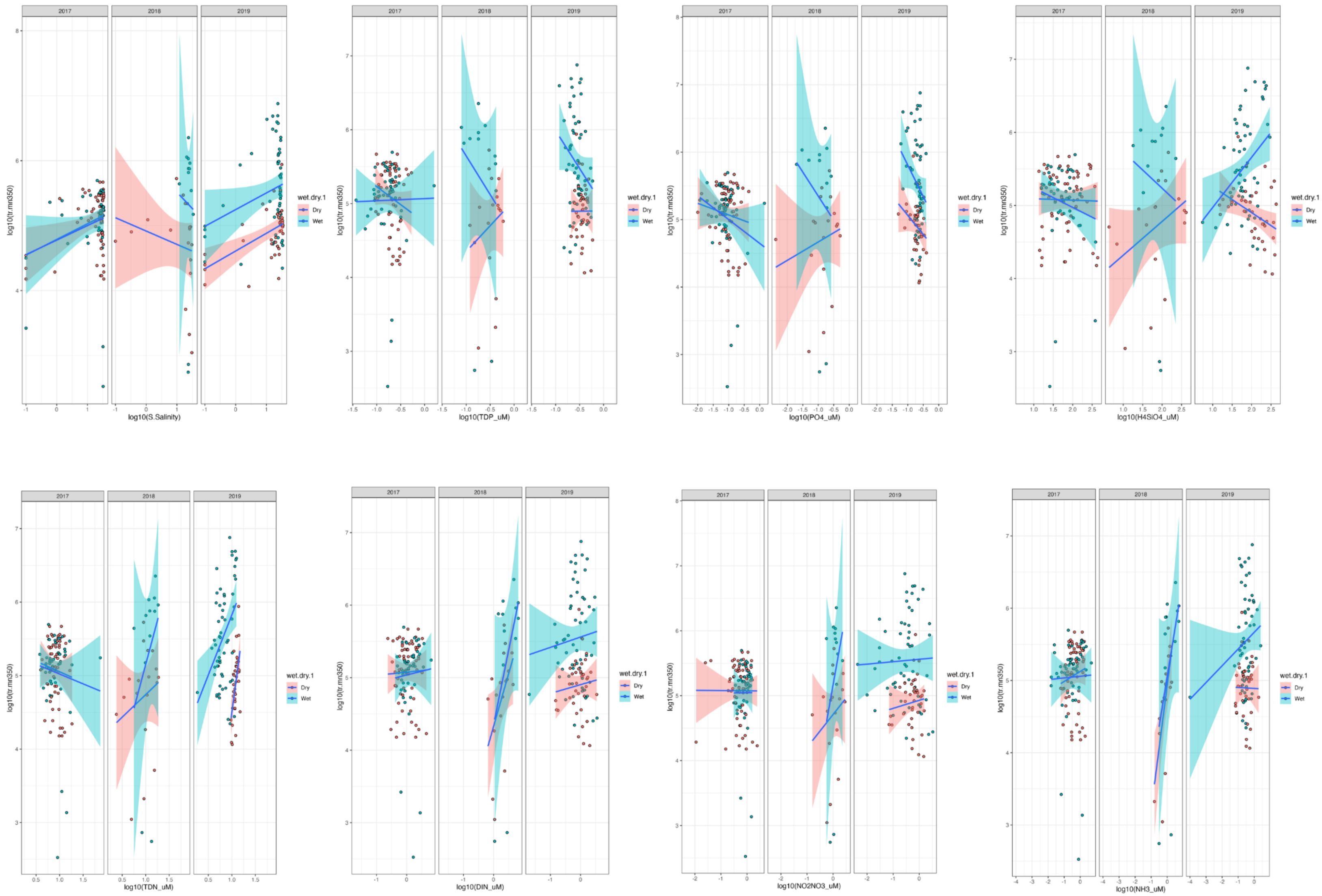

Figure 15. General additive models of seasonal environmental parameter predictors of 2017-2019 diatom abundance.

Environmental factors were tested as predictors of diatom abundance by season. Shown are plots of model fitted effects plots for salinity, silicic acid, TPD and NH_3, the significant predicators during specific seasons (red box).

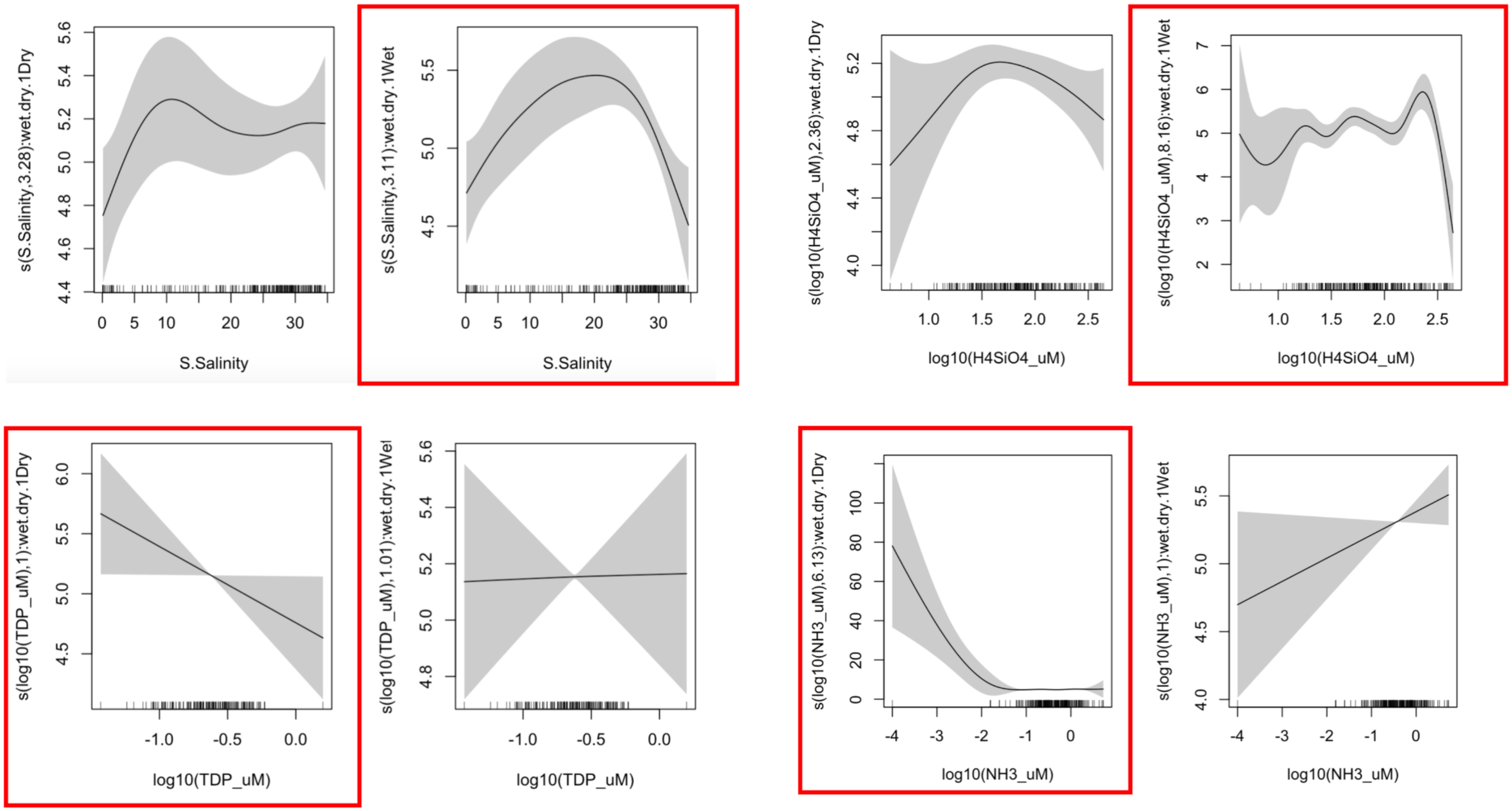

Figure 16. In-pond variation decreased from 2007-2008 to 2017-2019

(A) Non-metric multidimensional scaling (nMDS) ordinations were generated from the Euclidean distance metrics between temperature, salinity, pH and dissolved oxygen from filtered data using "ordiplot" in two-dimensions. Ellipses represent 95% confidence intervals. (B) Dispersion, or level of variability was determined by measuring distance to centroid for each sampling date, * $p<0.05$

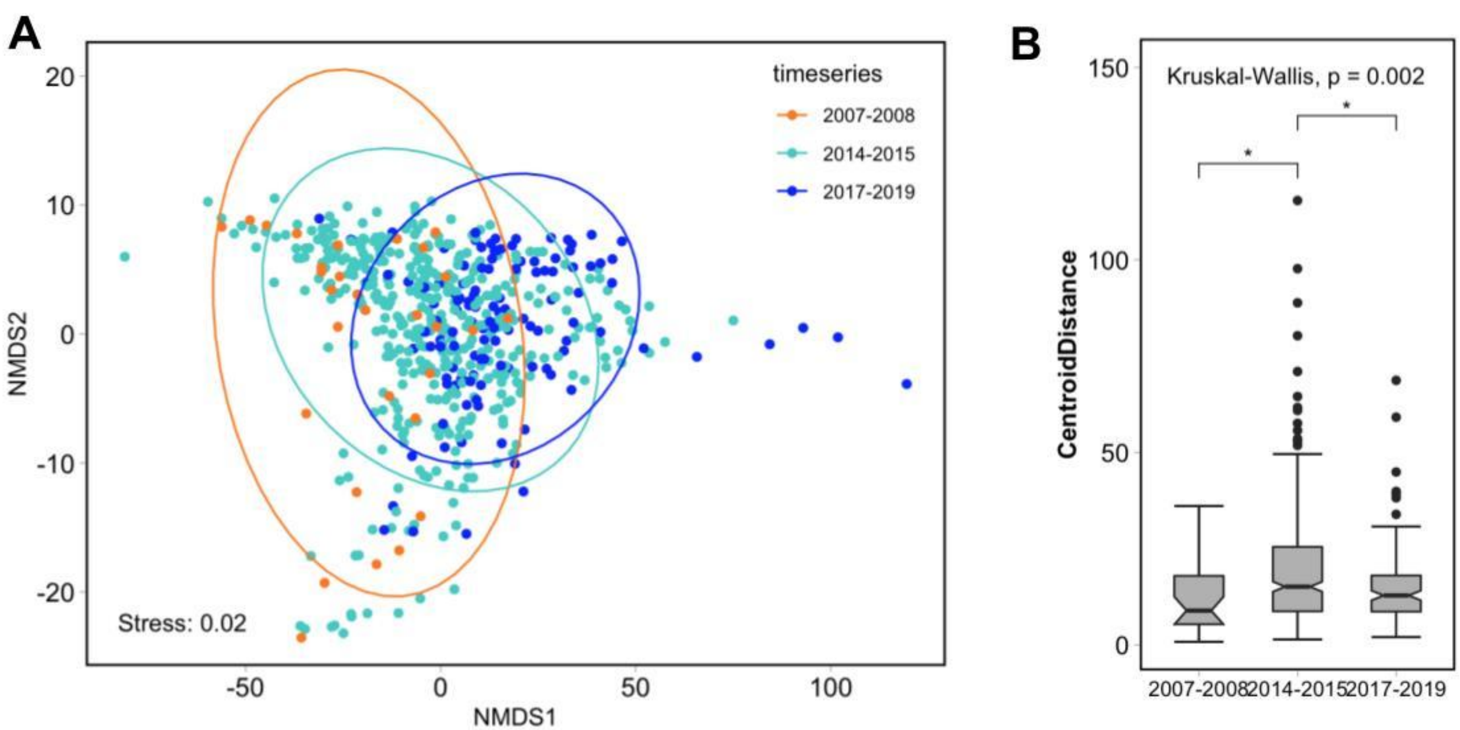

Figure 17. Retrospective comparison of physical parameters between sampling campaigns.

Each parameter shows the mean and standard deviation and indicates results of Dunn's post hoc comparisons for significance, p-value < 0.05 (*), < 0.001 (***), < 0.0001 (****).

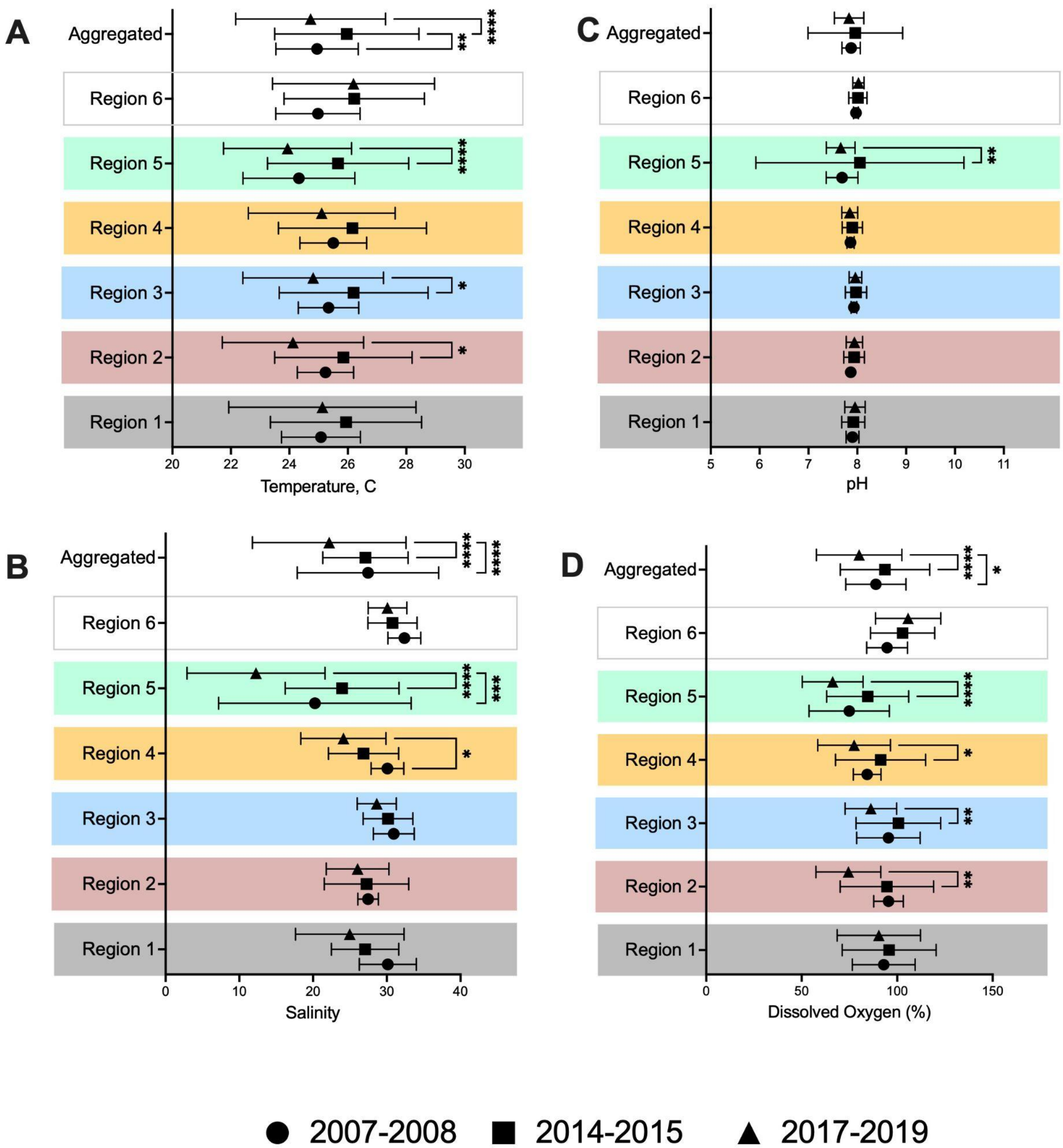

APPENDICES

Appendix Table 1. 2017-2019 biogeochemistry parameter normality determination by Shapiro-Wiks Test.

All environmental parameters measure do not have normal distribution.

Parameter	W	P value	Passed normality test (alpha=0.05)?	P value summary
Temperature	0.9639	<0.0001	No	****
DO, %	0.9582	<0.0001	No	****
Salinity	0.8056	<0.0001	No	****
pH	0.7196	<0.0001	No	****
TDN, µM	0.8192	<0.0001	No	****
TDP, µM	0.8003	<0.0001	No	****
PO_4, µM	0.7176	<0.0001	No	****
H_4SiO_4, µM	0.7792	<0.0001	No	****
NO_2NO_3, µM	0.9026	<0.0001	No	****
NH_3, µM	0.6531	<0.0001	No	****
DIN, µM	0.8148	<0.0001	No	****
TDN: TDP	0.8571	<0.0001	No	****
DIN:DIP	0.3772	<0.0001	No	****
DON, µM	0.5788	<0.0001	No	****
DOP, µMM	0.9415	<0.0001	No	****
DON DOP	0.06985	<0.0001	No	****
Diatoms mL^{-1}	0.3344	<0.0001	No	****

Appendix Table 2. Pairwise comparisons of biogeochemical parameters of HFP sites, 2017-2019

For parameter that were significant by Kruskal Wallis (* p<0.05; ** p<0.01; ***p <0.001), Dunn's post hoc comparisons were performed. Shown are Dunn's p-values with shaded and bold values indicating significant comparisons.

	Sal***	DO (%)***	pH***	DIN (µM)*	N+N (µM)*	PO_4 (µM)*	H_4SiO_4 (µM)***
L01 vs. L02	>0.9999	>0.9999	>0.9999	>0.9999	>0.9999	>0.9999	>0.9999
L01 vs. L03	>0.9999	>0.9999	>0.9999	>0.9999	>0.9999	>0.9999	>0.9999
L01 vs. L04	0.5155	>0.9999	>0.9999	>0.9999	>0.9999	>0.9999	>0.9999
L01 vs. L05	>0.9999	>0.9999	>0.9999	>0.9999	>0.9999	>0.9999	>0.9999
L01 vs. L06	>0.9999	>0.9999	0.7548	>0.9999	>0.9999	>0.9999	>0.9999
L01 vs. L07	0.1473	**0.0311**	0.5351	>0.9999	>0.9999	>0.9999	0.245
L01 vs. L08	>0.9999	>0.9999	>0.9999	>0.9999	>0.9999	>0.9999	>0.9999
L01 vs. L09	>0.9999	>0.9999	>0.9999	>0.9999	>0.9999	>0.9999	>0.9999
L01 vs. L10	0.1184	>0.9999	>0.9999	>0.9999	>0.9999	>0.9999	>0.9999
L01 vs. L11	>0.9999	>0.9999	>0.9999	>0.9999	>0.9999	>0.9999	>0.9999
L02 vs. L03	>0.9999	>0.9999	>0.9999	>0.9999	>0.9999	>0.9999	>0.9999
L02 vs. L04	>0.9999	>0.9999	>0.9999	>0.9999	>0.9999	>0.9999	>0.9999
L02 vs. L05	>0.9999	>0.9999	>0.9999	>0.9999	>0.9999	>0.9999	>0.9999
L02 vs. L06	0.145	>0.9999	0.0995	0.9866	0.7916	>0.9999	0.4699
L02 vs. L07	**0.0008**	0.1519	0.0656	0.4126	>0.9999	>0.9999	0.0501
L02 vs. L08	>0.9999	>0.9999	>0.9999	>0.9999	>0.9999	>0.9999	>0.9999
L02 vs. L09	0.336	>0.9999	>0.9999	>0.9999	>0.9999	>0.9999	>0.9999
L02 vs. L10	>0.9999	>0.9999	>0.9999	>0.9999	>0.9999	>0.9999	>0.9999
L02 vs. L11	>0.9999	>0.9999	>0.9999	>0.9999	>0.9999	>0.9999	>0.9999
L03 vs. L04	>0.9999	>0.9999	>0.9999	>0.9999	>0.9999	>0.9999	>0.9999
L03 vs. L05	>0.9999	>0.9999	>0.9999	>0.9999	>0.9999	>0.9999	>0.9999
L03 vs. L06	**0.0257**	>0.9999	**0.0256**	>0.9999	>0.9999	>0.9999	**0.0396**
L03 vs. L07	<0.0001	**0.0032**	**0.0162**	>0.9999	>0.9999	0.5468	**0.0028**
L03 vs. L08	>0.9999	>0.9999	>0.9999	>0.9999	>0.9999	>0.9999	>0.9999
L03 vs. L09	0.0672	>0.9999	>0.9999	>0.9999	>0.9999	>0.9999	0.9282
L03 vs. L10	>0.9999	>0.9999	>0.9999	>0.9999	>0.9999	>0.9999	>0.9999
L03 vs. L11	>0.9999	>0.9999	>0.9999	>0.9999	>0.9999	>0.9999	>0.9999
L04 vs. L05	>0.9999	>0.9999	>0.9999	>0.9999	>0.9999	>0.9999	>0.9999
L04 vs. L06	**0.0011**	0.5671	**0.0071**	0.5531	0.2981	0.2424	**0.0035**
L04 vs. L07	**<0.0001**	**0.0006**	**0.0043**	0.2183	0.6767	**0.0247**	**0.0002**
L04 vs. L08	0.22	>0.9999	>0.9999	>0.9999	>0.9999	>0.9999	0.5571
L04 vs. L09	**0.0034**	>0.9999	0.9039	>0.9999	>0.9999	>0.9999	0.1558
L04 vs. L10	>0.9999	>0.9999	>0.9999	>0.9999	>0.9999	>0.9999	>0.9999
L04 vs. L11	>0.9999	>0.9999	>0.9999	>0.9999	>0.9999	>0.9999	>0.9999
L05 vs. L06	0.2952	>0.9999	0.3687	>0.9999	0.8239	>0.9999	0.7939
L05 vs. L07	**0.0027**	**0.0219**	0.2563	>0.9999	>0.9999	>0.9999	0.0998
L05 vs. L08	>0.9999	>0.9999	>0.9999	>0.9999	>0.9999	>0.9999	>0.9999
L05 vs. L09	0.6274	>0.9999	>0.9999	>0.9999	>0.9999	>0.9999	>0.9999
L05 vs. L10	>0.9999	>0.9999	>0.9999	>0.9999	>0.9999	>0.9999	>0.9999
L05 vs. L11	>0.9999	>0.9999	>0.9999	>0.9999	>0.9999	>0.9999	>0.9999
L06 vs. L07	>0.9999	>0.9999	>0.9999	>0.9999	>0.9999	>0.9999	>0.9999
L06 vs. L08	>0.9999	>0.9999	>0.9999	>0.9999	0.6721	>0.9999	>0.9999
L06 vs. L09	>0.9999	>0.9999	>0.9999	>0.9999	>0.9999	>0.9999	>0.9999
L06 vs. L10	**0.0001**	0.8605	**0.0226**	0.4014	0.1917	>0.9999	**0.0004**
L06 vs. L11	**0.0072**	0.6946	**0.007**	>0.9999	>0.9999	>0.9999	**0.026**
L07 vs. L08	0.3565	**0.0057**	>0.9999	0.5302	>0.9999	>0.9999	>0.9999

L07 vs. L09	>0.9999	>0.9999	>0.9999	>0.9999	>0.9999	>0.9999	>0.9999
L07 vs. L10	**<0.0001**	**0.0014**	**0.0144**	0.1567	0.4435	0.1806	<0.0001
L07 vs. L11	**<0.0001**	**0.001**	**0.0043**	>0.9999	>0.9999	>0.9999	**0.0017**
L08 vs. L09	>0.9999	>0.9999	>0.9999	>0.9999	>0.9999	>0.9999	>0.9999
L08 vs. L10	**0.0457**	>0.9999	>0.9999	>0.9999	>0.9999	>0.9999	0.116
L08 vs. L11	0.7671	>0.9999	>0.9999	>0.9999	>0.9999	>0.9999	>0.9999
L09 vs. L10	**0.0005**	>0.9999	>0.9999	>0.9999	>0.9999	>0.9999	**0.0276**
L09 vs. L11	**0.0201**	>0.9999	0.8304	>0.9999	>0.9999	>0.9999	0.6771
L10 vs. L11	>0.9999	>0.9999	>0.9999	>0.9999	>0.9999	>0.9999	>0.9999

Appendix Table 3. Pairwise comparisons of biogeochemical parameters of HFP year and season, 2017-2019

For parameter that were significant by Kruskal Wallis (* p<0.05; ** p<0.01; ***p <0.001), Dunn‘s post hoc comparisons were performed. Shown are Dunn‘s p-values with shaded and bold values indicating significant comparisons.

	Temp***	DO%*	pH***	TDN***	DON**	DIN**	N+N***	NH3***	TDP***	PO4***	DOP**	H4SiO4*
2017- Dry vs. 2017 - Wet	0.0834	0.3378	>0.9999	>0.9999	>0.9999	>0.9999	0.1533	>0.9999	0.7461	>0.9999	>0.9999	>0.9999
2017- Dry vs. 2018 - Dry	>0.9999	>0.9999	**0.0069**	>0.9999	>0.9999	0.136	>0.9999	**0.012**	>0.9999	>0.9999	>0.9999	>0.9999
2017- Dry vs. 2019 - Dry	>0.9999	>0.9999	**0.032**	**0.001**	**0.0007**	>0.9999	**0.0156**	>0.9999	**<0.0001**	**<0.0001**	>0.9999	>0.9999
2017 - Wet vs. 2018 - Wet	0.639	>0.9999	**<0.0001**	**0.0036**	0.1422	0.2347	**0.037**	>0.9999	0.8923	>0.9999	>0.9999	>0.9999
2017 - Wet vs. 2019 - Wet	**0.0008**	0.0626	>0.9999	>0.9999	>0.9999	>0.9999	>0.9999	0.3614	**0.0005**	**0.0002**	>0.9999	0.1365
2018 - Dry vs. 2018 - Wet	**0.0004**	>0.9999	>0.9999	0.334	>0.9999	>0.9999	>0.9999	>0.9999	0.1615	>0.9999	**0.0224**	>0.9999
2018 - Dry vs. 2019 - Dry	>0.9999	>0.9999	>0.9999	0.1755	**0.0348**	**0.04**	**0.0022**	**0.0324**	**0.01**	**0.0271**	>0.9999	>0.9999
2018 - Wet vs. 2019 - Wet	>0.9999	>0.9999	**<0.0001**	**0.0006**	0.0811	**0.0035**	0.1461	**0.0255**	>0.9999	>0.9999	>0.9999	0.2498
2019 - Dry vs. 2019 - Wet	**<0.0001**	>0.9999	>0.9999	**<0.0001**	**<0.0001**	>0.9999	>0.9999	>0.9999	>0.9999	>0.9999	0.0616	0.2794

Appendix Table 4. Pairwise comparisons of diatom concentrations, of HFP year and season, 2017-2019

Shown are Dunn's p-values with shaded and bold values indicating significant comparisons.

	Adjusted P Value
2017 - wet vs. 2017 - dry	>0.9999
2017 - wet vs. 2018 - wet	0.1829
2017 - wet vs. 2018 - dry	0.6202
2017 - wet vs. 2019 - wet	**0.0318**
2017 - wet vs. 2019 - dry	0.2984
2017 - dry vs. 2018 - wet	0.1697
2017 - dry vs. 2018 - dry	0.5954
2017 - dry vs. 2019 - wet	**0.0240**
2017 - dry vs. 2019 - dry	0.2704
2018 - wet vs. 2018 - dry	**0.0039**
2018 - wet vs. 2019 - wet	>0.9999
2018 - wet vs. 2019 - dry	**0.0013**
2018 - dry vs. 2019 - wet	**0.0003**
2018 - dry vs. 2019 - dry	>0.9999
2019 - wet vs. 2019 - dry	**<0.0001**

Appendix Table 5. Residuals Coefficients from distance-based linear models of diatoms and biogeochemical predicator variables, 2017-2019

(1) *Model 1: Season + Site:* lm(formula = log10(diatom) ~ Season * Site, data = hfp)

	Min	1Q	Median	3Q	Max
Residuals	-2.46738	-0.27941	0.00313	0.34829	1.54375

Coefficients	Estimate Std.	Error	t value	Pr(>|t|)
(Intercept)	5.125622	0.257364	19.916	<2e-16 ***
Season	0.226151	0.363968	0.621	0.535
SiteE02	-0.568268	0.363968	-1.561	0.120
SiteL01	-0.421190	0.381732	-1.103	0.271
SiteL02	-0.227750	0.363968	-0.626	0.532
SiteL03	-0.241135	0.381732	-0.632	0.528
SiteL04	-0.622148	0.363968	-1.709	0.089
SiteL05	-0.174662	0.363968	-0.480	0.632
SiteL06	-0.120958	0.363968	-0.332	0.740
SiteL07	-0.083192	0.363968	-0.229	0.819
SiteL08	-0.023001	0.363968	-0.063	0.950
SiteL09	0.073377	0.363968	0.202	0.840
SiteL10	-0.104178	0.363968	-0.286	0.775
SiteL11	-0.288320	0.363968	-0.792	0.429
SiteM01	-0.507356	0.363968	-1.394	0.165
SiteM02	0.023209	0.363968	0.064	0.949
SiteM03	0.125668	0.363968	0.345	0.730
SiteM04	-0.064407	0.363968	-0.177	0.860
SiteM05	-0.266249	0.381732	-0.697	0.486
SiteM06	-0.113843	0.363968	-0.313	0.755
Season:SiteE02	-0.106486	0.545951	-0.195	0.846
Season:SiteL01	0.612419	0.518392	1.181	0.239
SeasonWet:SiteL02	-0.006293	0.505453	-0.012	0.990
SeasonWet:SiteL03	0.388005	0.518392	0.748	0.455
SeasonWet:SiteL04	0.777298	0.505453	1.538	0.126
SeasonWet:SiteL05	0.351344	0.514728	0.683	0.496
SeasonWet:SiteL06	0.185519	0.505453	0.367	0.714
SeasonWet:SiteL07	-0.199826	0.514728	-0.388	0.698
SeasonWet:SiteL08	-0.185687	0.505453	-0.367	0.714
SeasonWet:SiteL09	0.016014	0.505453	0.032	0.975
SeasonWet:SiteL10	0.179016	0.527439	0.339	0.735
SeasonWet:SiteL11	-0.071627	0.527439	-0.136	0.892
SeasonWet:SiteM01	0.100305	0.505453	0.198	0.843
SeasonWet:SiteM02	-0.204204	0.505453	-0.404	0.687
SeasonWet:SiteM03	0.045073	0.514728	0.088	0.930
SeasonWet:SiteM04	0.139803	0.505453	0.277	0.782
SeasonWet:SiteM05	0.008319	0.539851	0.015	0.988
Season:SiteM06	0.012937	0.514728	0.025	0.980

(2) *Model 2: All nutrients:* lm(formula = $\log_{10}$(diatoms) ~ $\log_{10}$(DIN) + $\log_{10}$(PO_4) + $\log_{10}$(TDP) + $\log_{10}$(H_4SiO_4) + $\log_{10}$(NH_3) + $\log_{10}$(NO_2NO_3) + $\log_{10}$(TDN)

	Min	1Q	Median	3Q	Max
Residuals	-2.66142	-0.24671	0.05307	0.30502	1.70581

Coefficients	Estimate Std.	Error	t value	Pr(>|t|)
(Intercept)	4.577213	0.481799	9.500	<2e-16 ***
log10(DIN	0.481503	0.466704	1.032	0.3033
log10(PO4)	0.006955	0.213433	0.033	0.9740
log10(TDP)	-0.425735	0.298966	-1.424	0.1558
log10(H4SiO4)	0.090135	0.128345	0.702	0.4832
log10(NH3)	0.081100	0.192351	0.422	0.6737
log10(NO2NO3)	-0.466975	0.254027	-1.838	0.0673
log10(TDN)	0.036696	0.293464	0.125	0.9006

Appendix Table 6. Model selection of nutrient predictors for linear models of diatom abundance and all nutrients

The Akaike weights were summed over all models for each predictor. A predictor with sum of weights > 0.6 indicated support from the data and was selected for the best predictor model (Table 8, Appendix Table 7)

	log_{10}(NO2NO3)	**log_{10}(TDP)**	**log_{10}(DIN)**	log_{10}(NH_3)	log_{10}(PO_4)	log,(H_4SiO_4)	log_{10}(TDN)
Sum of weights	**0.80**	**0.64**	**0.63**	0.54	0.32	0.31	0.27
N containing models	64	64	64	64	64	64	64

Models

	(Intercept)	**log_{10}(DIN)**	**log_{10}(H_4SiO_4)**	**log_{10}(NH_3)**	**log_{10}(N+N)**	**log_{10}(PO_4)**	**log_{10}(TDN)**	**log_{10}(TDP)**	**df**	**logLik**	**AICc**	**delta**	**weight**
52	5.008296	0.06660451	0.060816126	*NA*	*NA*	-0.07166492	-0.0490165574	*NA*	6	-230.7531	473.8763	13.0482597	0.0001227175
116	4.887933	0.06817298	0.024933284	*NA*	*NA*	0.15434312	0.0565403587	-0.4720684	7	-229.4897	473.4750	12.6468997	0.0001499894
50	5.138728	0.05943843	*NA*	*NA*	*NA*	-0.03565634	-0.0338381052	*NA*	5	-230.8698	472.0028	11.1747312	0.0003131395
36	5.155647	0.07139801	0.032802201	*NA*	*NA*	*NA*	-0.0821731266	*NA*	5	-230.8601	471.9834	11.1553155	0.0003161942
51	4.952658	*NA*	0.054934854	*NA*	*NA*	-0.07672171	0.0191003106	*NA*	5	-230.8580	471.9792	11.1511316	0.0003168564
59	4.694389	*NA*	0.056499322	*NA*	-0.1635457	-0.12280457	0.2014980633	*NA*	6	-229.7720	471.9140	11.0859346	0.0003273556
100	4.753810	0.06209237	0.068836051	*NA*	*NA*	*NA*	0.0621448814	-0.3242305	6	-229.7611	471.8922	11.0640864	0.0003309513
20	4.961293	0.05378583	0.058471866	*NA*	*NA*	-0.07824725	*NA*	*NA*	5	-230.7677	471.7985	10.9704348	0.0003468169
123	4.580811	*NA*	0.021186790	*NA*	-0.1600081	0.09942408	0.3025042713	-0.4623358	7	-228.5506	471.5967	10.7686341	0.0003836372
115	4.831230	*NA*	0.018986006	*NA*	*NA*	0.14871265	0.1260456521	-0.4711183	6	-229.6008	471.5716	10.7434918	0.0003884904

114	4.937112	0.06536122	NA	NA	NA	0.17356294	0.0648659261	-0.4823439	6	-229.5089	471.3879	10.5597916	0.0004258634
84	4.942672	0.08216391	0.028478010	NA	NA	0.15538776	NA	-0.4591985	6	-229.5082	471.3865	10.5584657	0.0004261458
91	4.911903	NA	0.033989848	NA	-0.1085506	0.11463032	NA	-0.3892123	6	-229.1307	470.6315	9.8033970	0.0006216119
56	5.087566	-0.26446980	0.089468968	0.30669377	NA	-0.12990735	-0.0968812143	NA	7	-228.0374	470.5703	9.7422427	0.0006409126
43	4.958708	NA	0.009290052	NA	-0.1463374	NA	0.1355641866	NA	5	-230.0775	470.4182	9.5901321	0.0006915590
27	4.914592	NA	0.061575288	NA	-0.1269654	-0.08739363	NA	NA	5	-230.0413	470.3457	9.5176321	0.0007170879
55	5.168842	NA	0.090104085	0.18633116	NA	-0.09683543	-0.2156905473	NA	6	-228.8956	470.1612	9.3331066	0.0007863965
98	4.868656	0.04947189	NA	NA	NA	NA	0.0940535183	-0.2954666	5	-229.9480	470.1592	9.3311762	0.0007871559
35	5.106903	NA	0.024335690	NA	NA	NA	-0.0113019640	NA	4	-230.9811	470.1369	9.3088592	0.0007959886
49	5.077179	NA	NA	NA	NA	-0.04335676	0.0262654110	NA	4	-230.9541	470.0830	9.2548985	0.0008177570
57	4.823120	NA	NA	NA	-0.1631196	-0.08837185	0.2083914693	NA	5	-229.8746	470.0124	9.1842828	0.0008471460
34	5.195224	0.06467858	NA	NA	NA	NA	-0.0598291684	NA	4	-230.9043	469.9832	9.1551086	0.0008595940
4	5.095822	0.04927171	0.024012556	NA	NA	NA	NA	NA	4	-230.9036	469.9819	9.1538251	0.0008601458
99	4.706467	NA	0.061938058	NA	NA	NA	0.1254705620	-0.3282905	5	-229.8533	469.9697	9.1416547	0.0008653959
18	5.102375	0.05067527	NA	NA	NA	-0.04122506	NA	NA	4	-230.8768	469.9283	9.1002493	0.0008834987
19	4.971964	NA	0.055579754	NA	NA	-0.07373800	NA	NA	4	-230.8610	469.8967	9.0686649	0.0008975618
68	4.813017	0.07743520	0.073061580	NA	NA	NA	NA	-0.3089748	5	-229.7834	469.8300	9.0019418	0.0009280110
83	4.959739	NA	0.025915547	NA	NA	0.14838204	NA	-0.4321655	5	-229.7239	469.7109	8.8828339	0.0009849565

107	4.486487	NA	0.049274893	NA	-0.1683593	NA	0.3113395359	-0.3688584	6	-228.6616	469.6932	8.8651254	0.0009937163
121	4.625365	NA	NA	NA	-0.1597856	0.11618360	0.3069429175	-0.4711986	6	-228.5647	469.4994	8.6713445	0.0010948167
113	4.870849	NA	NA	NA	NA	0.16367202	0.1302437207	-0.4790508	5	-229.6120	469.4872	8.6590856	0.0011015479
82	5.009447	0.08128711	NA	NA	NA	0.17798886	NA	-0.4689751	5	-229.5338	469.3308	8.5027665	0.0011910984
40	5.343281	-0.23705831	0.038351183	0.28914370	NA	NA	-0.1527033384	NA	6	-228.3875	469.1451	8.3170241	0.0013070166
120	4.952411	-0.29358668	0.049645898	0.33538752	NA	0.13235361	0.0236744532	-0.5591723	8	-226.2432	469.1263	8.2982335	0.0013193543
119	5.050054	NA	0.052687585	0.20086587	NA	0.15343716	-0.1145325117	-0.5263047	7	-227.3098	469.1153	8.2872031	0.0013266509
54	5.275249	-0.26502802	NA	0.29753829	NA	-0.07570151	-0.0733362158	NA	6	-228.2932	468.9564	8.1283696	0.0014363057
75	4.813863	NA	0.066952212	NA	-0.1164817	NA	NA	-0.2784811	5	-229.2782	468.8195	7.9914525	0.0015380770
23	4.954501	NA	0.078081429	0.15390927	NA	-0.12064734	NA	NA	5	-229.2115	468.6861	7.8580406	0.0016441752
64	4.636181	0.59704577	0.117610754	0.02563028	-0.5350551	-0.18492346	-0.0270671598	NA	8	-226.0151	468.6702	7.8421429	0.0016572966
11	5.065672	NA	0.023173532	NA	-0.1228490	NA	NA	NA	4	-230.2118	468.5983	7.7702797	0.0017179287
89	4.991883	NA	NA	NA	-0.1069683	0.14211921	NA	-0.4018214	5	-229.1672	468.5975	7.7694786	0.0017186170
53	5.358033	NA	NA	0.17685469	NA	-0.04217368	-0.1922306074	NA	5	-229.1531	468.5694	7.7413799	0.0017429328
24	4.994318	-0.28623464	0.084561516	0.30350601	NA	-0.14224516	NA	NA	6	-228.0952	468.5604	7.7322887	0.0017508735
25	5.063557	NA	NA	NA	-0.1251316	-0.04842739	NA	NA	4	-230.1632	468.5012	7.6730839	0.0018034784
39	5.358174	NA	0.050916822	0.18244574	NA	NA	-0.2490011170	NA	5	-229.0941	468.4513	7.6232314	0.0018489972
41	4.970437	NA	NA	NA	-0.1472820	NA	0.1410142867	NA	4	-230.0811	468.3369	7.5088774	0.0019577982

128	4.579666	0.46067870	0.080085286	0.08644920	-0.4657474	0.04532596	0.0664543466	-0.4757253	9	-224.7311	468.2657	7.4376786	0.0020287500
97	4.820791	NA	NA	NA	NA	NA	0.1429564733	-0.3011129	4	-230.0077	468.1901	7.3620438	0.0021069413
66	4.972196	0.07223764	NA	NA	NA	NA	NA	-0.2688672	4	-230.0009	468.1764	7.3483261	0.0021214421
63	4.859719	NA	0.101358417	0.23425286	-0.2309560	-0.16708567	-0.0184969953	NA	7	-226.8158	468.1272	7.2991201	0.0021742833
67	4.834666	NA	0.068740998	NA	NA	NA	NA	-0.2898311	4	-229.9750	468.1247	7.2966336	0.0021769882
33	5.140484	NA	NA	NA	NA	NA	0.0006160350	NA	3	-231.0060	468.1164	7.2882857	0.0021860939
3	5.098509	NA	0.023178303	NA	NA	NA	NA	NA	3	-230.9822	468.0688	7.2407786	0.0022386430
17	5.105865	NA	NA	NA	NA	-0.03869462	NA	NA	3	-230.9599	468.0241	7.1959961	0.0022893344
2	5.139915	0.04871665	NA	NA	NA	NA	NA	NA	3	-230.9291	467.9626	7.1345103	0.0023608082
48	5.035271	0.54679770	0.044180577	0.03014359	-0.4803510	NA	-0.1112508629	NA	7	-226.7140	467.9236	7.0955409	0.0024072589
105	4.572307	NA	NA	NA	-0.1719091	NA	0.3290941272	-0.3482098	5	-228.7598	467.7828	6.9547048	0.0025828844
81	5.020398	NA	NA	NA	NA	0.16903735	NA	-0.4413337	4	-229.7450	467.6648	6.8367016	0.0027398642
103	4.920542	NA	0.096876128	0.20013227	NA	NA	-0.1142471717	-0.3787544	6	-227.5839	467.5379	6.7098398	0.0029192866
62	4.903364	0.55138479	NA	0.02840539	-0.5071468	-0.11168729	-0.0001440248	NA	7	-226.4589	467.4134	6.5853483	0.0031067744
104	4.838261	-0.30253560	0.087484773	0.33885820	NA	NA	0.0281321227	-0.4335164	7	-226.4480	467.3916	6.5635391	0.0031408379
8	5.228293	-0.26900887	0.022073135	0.28104901	NA	NA	NA	NA	5	-228.5389	467.3409	6.5128694	0.0032214272
7	5.156832	NA	0.024926035	0.14239268	NA	NA	NA	NA	4	-229.5307	467.2362	6.4080932	0.0033946904
117	5.153052	NA	NA	0.19603869	NA	0.19419883	-0.0972800978	-0.5466532	6	-227.3967	467.1635	6.3354444	0.0035202674

87	4.935363	NA	0.044781272	0.18507435	NA	0.15331654	NA	-0.5515160	6	-227.3964	467.1629	6.3347836	0.0035214308
38	5.388861	-0.24381012	NA	0.28811233	NA	NA	-0.1263414703	NA	5	-228.4491	467.1614	6.3333146	0.0035240182
47	5.206126	NA	0.035714307	0.22237007	-0.2044379	NA	-0.0958398909	NA	6	-227.3874	467.1449	6.3168644	0.0035531232
118	5.049001	-0.29489360	NA	0.33143909	NA	0.17065775	0.0405416774	-0.5784871	7	-226.3210	467.1375	6.3094730	0.0035662786
73	4.958802	NA	NA	NA	-0.1173022	NA	NA	-0.2426898	4	-229.4623	467.0992	6.2711755	0.0036352264
127	4.740598	NA	0.063914900	0.24883553	-0.2311215	0.08337124	0.0828971804	-0.5267982	8	-225.1984	467.0368	6.2087404	0.0037504994
21	5.141363	NA	NA	0.14867721	NA	-0.07030416	NA	NA	4	-229.4073	466.9892	6.1611522	0.0038408093
88	4.975377	-0.28824899	0.051162016	0.33585952	NA	0.13275922	NA	-0.5539165	7	-226.2465	466.9886	6.1604831	0.0038420943
22	5.195812	-0.28170245	NA	0.29547792	NA	-0.08744810	NA	NA	5	-228.3267	466.9165	6.0884648	0.0039829661
61	5.077549	NA	NA	0.22277287	-0.2269046	-0.10448391	0.0043826400	NA	6	-227.1468	466.6637	5.8356669	0.0045196101
37	5.419826	NA	NA	0.17699092	NA	NA	-0.2173478489	NA	4	-229.2030	466.5806	5.7525444	0.0047114089
9	5.108212	NA	NA	NA	-0.1228498	NA	NA	NA	3	-230.2357	466.5758	5.7477633	0.0047226852
60	4.611076	0.65194633	0.117870690	NA	-0.5611630	-0.18534510	-0.0218009323	NA	7	-226.0242	466.5439	5.7158705	0.0047985987
32	4.607932	0.59598161	0.116420850	0.02314543	-0.5381150	-0.18863425	NA	NA	7	-226.0196	466.5348	5.7067636	0.0048204986
126	4.751242	0.42068770	NA	0.09271774	-0.4423305	0.11031031	0.0909925124	-0.5104828	8	-224.9322	466.5045	5.6763903	0.0048942644
65	4.983656	NA	NA	NA	NA	NA	NA	-0.2531587	3	-230.1680	466.4403	5.6122085	0.0050538732
124	4.501338	0.64618780	0.082980896	NA	-0.5542099	0.03136416	0.0784179110	-0.4497037	8	-224.8314	466.3029	5.4747858	0.0054133398
101	5.082817	NA	NA	0.18825107	NA	NA	-0.0732520922	-0.3341607	5	-227.9605	466.1842	5.3561569	0.0057441429

96	4.647837	0.46711628	0.083969890	0.09054927	-0.4605374	0.04742982	NA	-0.4620122	8	-224.7575	466.1551	5.3269921	0.0058285202
112	4.531935	0.47967446	0.093204953	0.08034707	-0.4792639	NA	0.0691373829	-0.4326692	8	-224.7541	466.1482	5.3201086	0.0058486150
1	5.141058	NA	NA	NA	NA	NA	NA	NA	2	-231.0060	466.0640	5.2358929	0.0061001461
31	4.840131	NA	0.100564615	0.23229957	-0.2334188	-0.16964469	NA	NA	6	-226.8179	466.0059	5.1777868	0.0062799736
46	5.089731	0.53394175	NA	0.03063649	-0.4772352	NA	-0.0811768553	NA	6	-226.7969	465.9637	5.1356760	0.0064136026
16	4.946540	0.53771249	0.032504847	0.01964760	-0.4889528	NA	NA	NA	6	-226.7950	465.9600	5.1319677	0.0064255055
102	4.981950	-0.31134579	NA	0.33220219	NA	NA	0.0691835839	-0.3949664	6	-226.7573	465.8846	5.0564875	0.0066726391
44	5.006804	0.61125699	0.044289425	NA	-0.5109219	NA	-0.1052806341	NA	6	-226.7265	465.8230	4.9949781	0.0068810423
71	4.806239	NA	0.088954846	0.18438064	NA	NA	NA	-0.4040185	5	-227.6699	465.6029	4.7748016	0.0076818344
58	4.876188	0.61213238	NA	NA	-0.5360201	-0.11197525	0.0057597604	NA	6	-226.4700	465.3101	4.4820338	0.0088928026
6	5.268929	-0.26977653	NA	0.28127636	NA	NA	NA	NA	4	-228.5609	465.2964	4.4683644	0.0089537907
30	4.903197	0.55138156	NA	0.02839188	-0.5071648	-0.11171122	NA	NA	6	-226.4589	465.2879	4.4598174	0.0089921364
72	4.865151	-0.29622181	0.089425275	0.33943204	NA	NA	NA	-0.4268096	6	-226.4527	465.2755	4.4474213	0.0090480430
5	5.202507	NA	NA	0.14220252	NA	NA	NA	NA	3	-229.5586	465.2215	4.3933980	0.0092957765
85	5.039953	NA	NA	0.18294519	NA	0.18877853	NA	-0.5659085	5	-227.4606	465.1843	4.3562509	0.0094700455
15	5.127059	NA	0.025754211	0.21054936	-0.2158237	NA	NA	NA	5	-227.4473	465.1578	4.3297704	0.0095962653
125	4.868625	NA	NA	0.24247663	-0.2286444	0.13347673	0.1016706190	-0.5514310	7	-225.3283	465.1522	4.3241568	0.0096232379
45	5.247088	NA	NA	0.21910035	-0.2071755	NA	-0.0717131259	NA	5	-227.4415	465.1462	4.3181143	0.0096523560

111	4.662299	NA	0.087641583	0.24996682	-0.2384415	NA	0.0893010295	-0.4487752	7	-225.2787	465.0529	4.2248492	0.0101131300
86	5.094368	-0.28561955	NA	0.33205427	NA	0.17341551	NA	-0.5703193	6	-226.3310	465.0320	4.2039363	0.0102194321
95	4.828747	NA	0.068494629	0.25680833	-0.2204957	0.08667026	NA	-0.5105260	7	-225.2395	464.9746	4.1465600	0.0105168546
110	4.688825	0.46027069	NA	0.07657454	-0.4731216	NA	0.1123130599	-0.3916417	7	-225.1099	464.7153	3.8872216	0.0119729314
122	4.673685	0.61861643	NA	NA	-0.5365465	0.09782336	0.1048113478	-0.4838523	7	-225.0477	464.5911	3.7629965	0.0127401817
29	5.082644	NA	NA	0.22321870	-0.2263077	-0.10375435	NA	NA	5	-227.1470	464.5571	3.7290180	0.0129584770
94	4.857891	0.42695861	NA	0.09885806	-0.4334829	0.11763830	NA	-0.4937142	7	-224.9826	464.4608	3.6327408	0.0135975382
28	4.589884	0.64670330	0.116873182	NA	-0.5615971	-0.18835781	NA	NA	6	-226.0272	464.4244	3.5963197	0.0138474251
92	4.578054	0.66432131	0.087767759	NA	-0.5530025	0.03308004	NA	-0.4319135	7	-224.8685	464.2326	3.4045684	0.0152407835
108	4.471486	0.65036212	0.092116500	NA	-0.5593539	NA	0.0797184226	-0.4205472	7	-224.8427	464.1809	3.3528589	0.0156399686
69	4.998549	NA	NA	0.17848801	NA	NA	NA	-0.3532576	4	-227.9968	464.1683	3.3402354	0.0157389960
80	4.600682	0.48730356	0.097888724	0.08432546	-0.4744873	NA	NA	-0.4162925	7	-224.7828	464.0611	3.2330209	0.0166057451
14	5.008696	0.52947227	NA	0.02228625	-0.4846416	NA	NA	NA	5	-226.8433	463.9497	3.1216024	0.0175570919
42	5.060934	0.59942551	NA	NA	-0.5082994	NA	-0.0750334511	NA	5	-226.8097	463.8826	3.0545641	0.0181555647
12	4.930795	0.58085095	0.032993322	NA	-0.5089517	NA	NA	NA	5	-226.8004	463.8640	3.0358840	0.0183259330
70	5.058392	-0.29579597	NA	0.33328539	NA	NA	NA	-0.3757479	5	-226.7866	463.8363	3.0082750	0.0185806680
109	4.805210	NA	NA	0.23994338	-0.2418342	NA	0.1292290021	-0.4094892	6	-225.5926	463.5553	2.7272617	0.0213836865
26	4.882447	0.61344258	NA	NA	-0.5358473	-0.11100488	NA	NA	5	-226.4702	463.2036	2.3755680	0.0254948166

93	4.989957	NA	NA	0.25184825	-0.2151760	0.14206555	NA	-0.5333450	6	-225.3911	463.1523	2.3242287	0.0261577313
13	5.174265	NA	NA	0.21032136	-0.2157239	NA	NA	NA	4	-227.4776	463.1298	2.3017379	0.0264535457
79	4.754201	NA	0.093604728	0.25863023	-0.2272727	NA	NA	-0.4278561	6	-225.3265	463.0231	2.1949843	0.0279039149
106	4.629436	0.62324940	NA	NA	-0.5495615	NA	0.1219220239	-0.3805395	6	-225.1901	462.7503	1.9222235	0.0319811749
78	4.817346	0.47143030	NA	0.08292884	-0.4645930	NA	NA	-0.3607182	6	-225.1877	462.7455	1.9173966	0.0320584522
90	4.791802	0.64116520	NA	NA	-0.5335119	0.10538777	NA	-0.4622887	6	-225.1152	462.6005	1.7723892	0.0344691446
76	4.547883	0.66904546	0.097495713	NA	-0.5584118	NA	NA	-0.4008226	6	-224.8811	462.1321	1.3040787	0.0435635078
10	4.991861	0.57836238	NA	NA	-0.5072987	NA	NA	NA	4	-226.8502	461.8751	1.0470381	0.0495380039
77	4.956890	NA	NA	0.25185581	-0.2255092	NA	NA	-0.3742774	5	-225.6957	461.6545	0.8263984	0.0553158758
74	4.764562	0.65023672	NA	NA	-0.5471720	NA	NA	-0.3457229	5	-225.2825	460.8281	0.0000000	0.0836180303

Appendix Table 7. Residuals Coefficients from best predictor linear models of diatoms and biogeochemical predicator variables, 2017-2019

Model 2: N+N, TDP + DIN: lm(formula = log_{10}(diatoms) ~ $log_{10}(NO_2+NO_3)$ + log_{10}(TDP) + log_{10}(DIN)

	Min	1Q	Median	3Q	Max
Residuals	-2.68238	-0.23123	0.04448	0.27861	1.73141

Coefficients	Estimate Std.	Error	t value	Pr(>|t|)
(Intercept)	4.7646	0.1451	32.834	< 2e-16 ***
log10(NO_2+NO_3)	-0.5472	0.1779	-3.077	0.00235 **
log10(TDP)	-0.3457	0.1963	-1.761	0.07949
log10(DIN)	0.6502	0.2248	2.892	0.00419 **

Model 3: NO_2+NO_3, lm(formula = log_{10}(diatoms) ~ $log_{10}(NO_2+NO_3)$)

	Min	1Q	Median	3Q	Max
Residuals	-2.59120	-0.30601	0.01779	0.31278	1.70229

Coefficients	Estimate Std.	Error	t value	Pr(>|t|)
(Intercept)	5.10821	0.05010	101.965	<2e-16 ***
log10(NO_2+NO_3)	-0.12285	0.09924	-1.238	0.217

Model 4 : TDP, lm(formula = log_{10}(diatoms) ~ log_{10}(TDP)

	Min	1Q	Median	3Q	Max
Residuals	-2.65403	-0.29879	0.01402	0.32130	1.75480

Coefficients	Estimate Std.	Error	t value	Pr(>|t|)
(Intercept)	4.9837	0.1291	38.611	<2e-16 ***
log10(TDP)	-0.2532	0.1960	-1.291	0.198

Model 5: DIN, lm(formula = log_{10}(diatoms) ~ log_{10}(DIN)

	Min	1Q	Median	3Q	Max
Residuals	-2.62619	-0.29109	0.01573	0.32470	1.73767

Coefficients	Estimate Std.	Error	t value	Pr(>|t|)
(Intercept)	5.13992	0.04272	120.316	<2e-16 ***
log10(DIN)	0.04872	0.12474	0.391	0.696

Model 6: TDP + NO2NO3, lm(formula = log_{10}(diatoms) ~ log_{10}(TDP) +log_{10}(NO2NO3)

	Min	1Q	Median	3Q	Max
Residuals	-2.62821	-0.29837	0.02505	0.32365	1.72060

Coefficients	Estimate Std.	Error	t value	Pr(>|t|)
(Intercept)	4.95880	0.13067	37.950	<2e-16 ***
log10(TDP)	-0.24269	0.19607	-1.238	0.217
log10(NO2NO3)	-0.11730	0.09923	-1.182	0.238

Model 7: TDP + DIN, lm(formula = $\log_{10}$(diatoms) ~ $\log_{10}$(TDP) +$\log_{10}$(DIN)

	Min	1Q	Median	3Q	Max
Residuals	-2.67056	-0.29625	0.01079	0.32697	1.75635

Coefficients	Estimate Std.	Error	t value	Pr(>|t|)
(Intercept)	4.97220	0.13079	38.016	<2e-16 ***
log10(TDP)	-0.26887	0.19821	-1.356	0.176
log10(NO2NO3)	0.07224	0.12572	0.575	0.566

Model 8: NO2NO3 +DIN, lm(formula = $\log_{10}$(diatoms) ~ $\log_{10}$(NO2NO3) + $\log_{10}$(DIN)

	Min	1Q	Median	3Q	Max
Residuals	-2.62540	-0.26982	0.04526	0.29398	1.66410

Coefficients	Estimate Std.	Error	t value	Pr(>|t|)
(Intercept)	4.99186	0.06667	74.875	<2e-16 ***
log10(NO2NO3)	-0.50730	0.17721	-2.863	0.00459 **
log10(DIN)	0.57836	0.22209	2.604	0.00981 **

Appendix Table 8. General additive models with smoother

Intercept	Est Std	Error	T value	Pr(>|t|)	R-sq.(adj)	Deviance explained	GCV	Scale est.	n
Salinity	5.12051	0.04072	125.7	<2e-16 ***	0.11	13.4%	0.38989	0.37769	236
Silica	5.11628	0.04193	122	<2e-16 ***	0.129	16.8%	0.38861	0.36965	236
TDP	5.1532	0.0432	119.3	<2e-16 ***	0.00913	1.76%	0.42584	0.42041	236
PO_4	5.13963	0.04248	121	<2e-16 ***	-0.00318	0.536%	0.43111	0.42563	236
DIN	5.13826	0.04257	120.7	<2e-16 ***	-0.00782	0.0759%	0.43311	0.4276	236
$NO_2 + NO_3$	5.13702	0.04247	121	<2e-16 ***	0.000423	0.893%	0.42957	0.4241	236
NH_3	5.30946	0.05668	93.68	<2e-16 ***	0.0727	10.1%	0.40749	0.39346	236

Appendix Figure 1. Distribution of 2017-2019 biogeochemical parameters

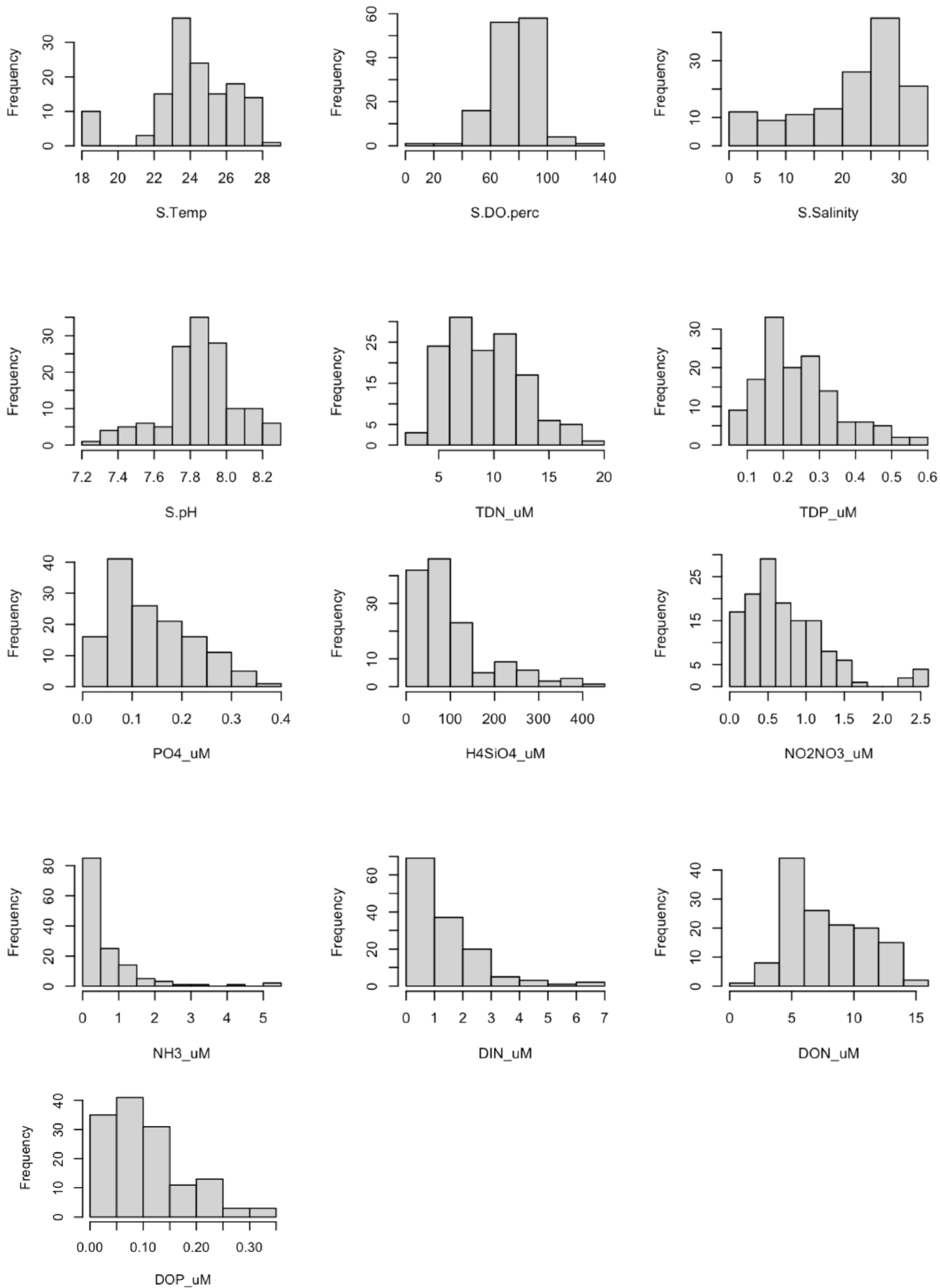

Appendix Figure 2. qPCR amplification standard curve of gBlocks *rbcL*

A standard curve was plotted between mean Ct values obtained from each dilution of gBlocks *rbcL* standard against calculated log copy number (slope = 3.4312, $R^2 = 0.9994$).

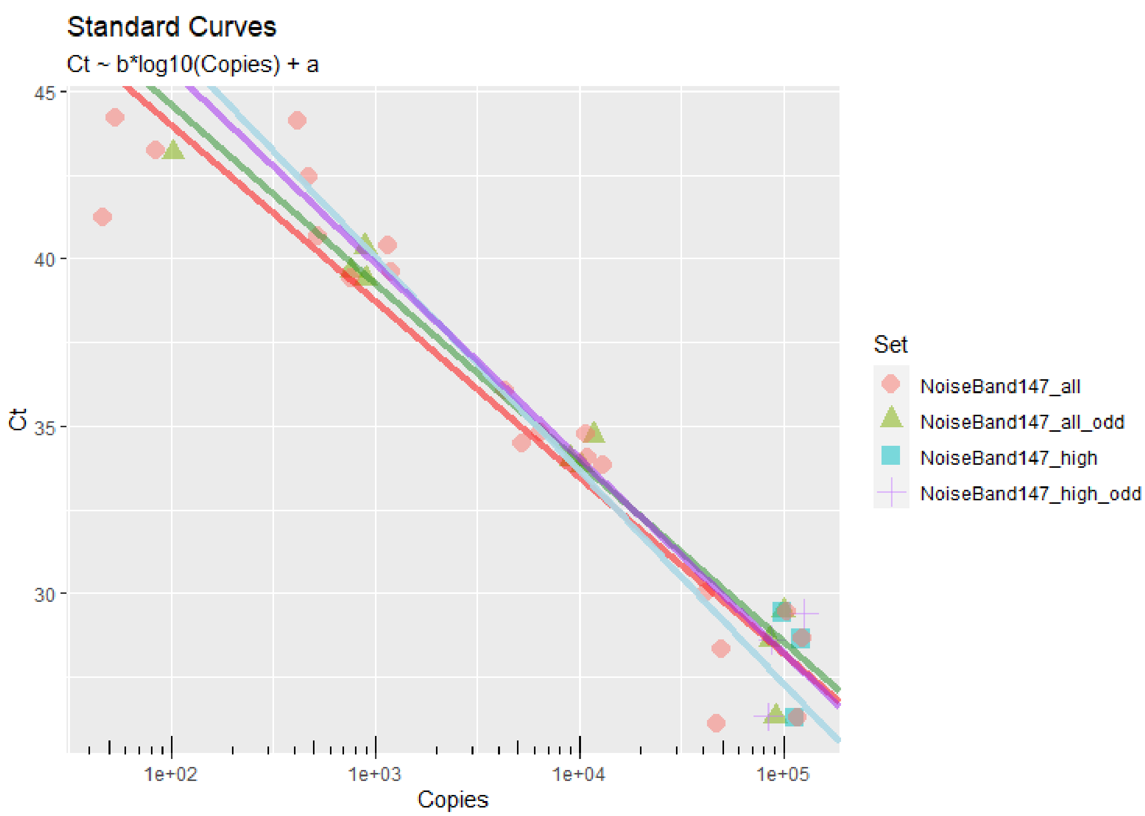

Appendix Figure 3 Distribution of 2017-2019 diatom abundance

(A) Untransformed and (B) Log10-transformed data. (C) Effects plot of log-transformed diatom data.

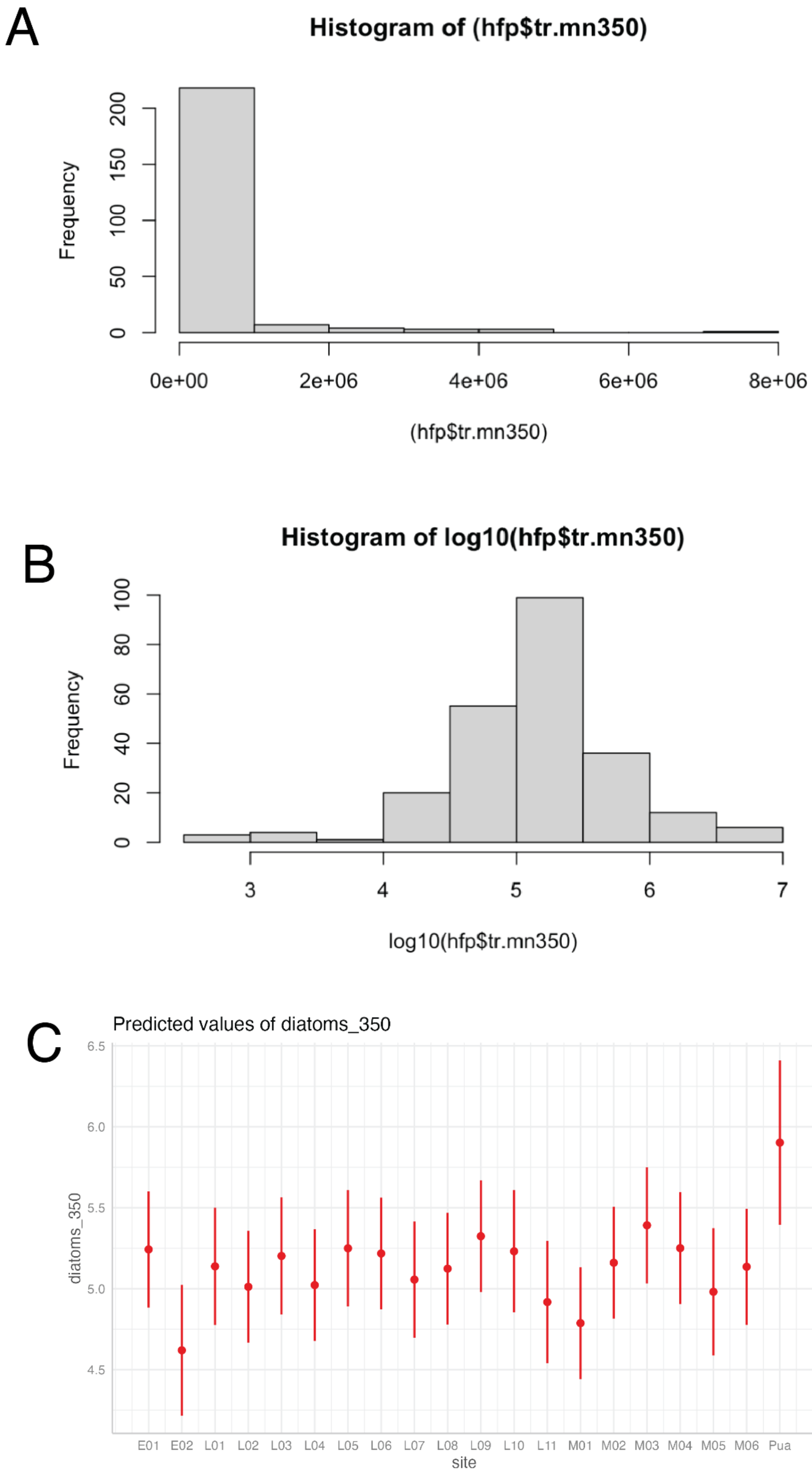

REFERENCES

Allen, J. A. (1998). Mangroves as Alien Species: The Case of Hawaii. *Global Ecology and Biogeography Letters*, *7*(1), 61–71. https://doi.org/10.2307/2997698

Apple, R. K., & Kikuchi, W. K. (1975). *Ancient Hawai'i shore zone fishponds: An evaluation of survivors for historic preservation*.

Banner, A. H. (1968). *A fresh-water" kill" on the coral reefs of Hawaii*. Hawaii Institute of Marine Biology, University of Hawaii. https://scholarspace.manoa.hawaii.edu/bitstream/handle/10125/15011/HIMB-TR15.pdf?sequence=1

Bremer, L. L., Falinski, K., Ching, C., Wada, C. A., Burnett, K. M., Kukea-Shultz, K., Reppun, N., Chun, G., Oleson, K. L. L., & Ticktin, T. (2018). *Biocultural restoration of traditional agriculture: Cultural, environmental, and economic outcomes of lo'i kalo restoration in He'eia, O'ahu. Sustainability 10 (12): 4502*.

Briggs, R. A., Ruttenberg, K. C., Glazer, B. T., & Ricardo, A. E. (2013). Constraining Sources of Organic Matter to Tropical Coastal Sediments: Consideration of Nontraditional End-Members. *Aquatic Geochemistry*, 1–21.

Burke, L. M., & Institute, W. R. (2001). No Title. In *Coastal ecosystems*. World Resources Inst. http://books.google.com/books?id=rGsVAQAAIAAJ&q=Kura+Kassem+Revenga+Burke&dq=Kura+Kassem+Revenga+Burke&hl=&cd=29&source=gbs_api

Cardoso, P. G. (2020). Estuaries: Dynamics, Biodiversity, and Impacts. In W. Leal Filho, A. M. Azul, L. Brandli, A. Lange Salvia, & T. Wall (Eds.), *Life Below Water* (pp. 1–12). Springer International Publishing. https://doi.org/10.1007/978-3-319-71064-8_17-1

Cobb, J. N. (1901). *Commercial Fisheries of the Hawaiian Islands*. U.S. Government Printing Office.

Cox, E. F., Ribes, M., & Kinzie III, R. A. (2006). Temporal and spatial scaling of planktonic responses to nutrient inputs into a subtropical embayment. *Marine Ecology Progress Series*, *324*, 19–35.

Demopoulos, A. W. J., Fry, B., & Smith, C. R. (2007). Food Web Structure in Exotic and Native Mangroves: A Hawaii-Puerto Rico Comparison. *Oecologia*, *153*(3), 675–686.

Dulai, H., Kleven, A., Ruttenberg, K., Briggs, R., & Thomas, F. (2016). Evaluation of submarine groundwater discharge as a coastal nutrient source and its role in coastal groundwater quality and quantity. In *Emerging issues in groundwater resources* (pp. 187–221). Springer.

Flenniken, J. M., Stuglik, S., & Iannone, B. V. (2020). Quantum GIS (QGIS): An introduction to a free alternative to more costly GIS platforms: FOR359/FR428, 2/2020. *EDIS*, *2020*(2), 7–7.

Fuka, D., Walter, M., Archibald, J., Steenhuis, T., & Easton, Z. (2018). *EcoHydRology-package: A community modeling foundation for Eco-Hydrology. in EcoHydRology: A Community Modeling Foundation for Eco-Hydrology* (0.4.12.1) [Computer software]. https://CRAN.R-project.org/package=EcoHydRology

Hiatt, R. W. (1947). Food-Chains and the Food Cycle in Hawaiian Fish Ponds.–Part I. The Food and Feeding Habits of Mullet (Mugil Cephalus), Milkfish (Chanos Chanos), and the Ten-Pounder (Elops Machnata). *Transactions of the American Fisheries Society*, *74*(1), 250–261.

Hoover, D. J., & Mackenzie, F. T. (2009). Fluvial fluxes of water, suspended particulate matter, and nutrients and potential impacts on tropical coastal water biogeochemistry: Oahu, Hawai 'i. *Aquatic Geochemistry*, *15*(4), 547–570.

Hoover, R. S., Hoover, D., Miller, M., Landry, M. R., DeCarlo, E. H., & Mackenzie, F. T. (2006). Zooplankton response to storm runoff in a tropical estuary: Bottom-up and top-down controls. *Marine Ecology Progress Series*, *318*, 187–201.

Hull, D. (2010). *A Quantitative Analysis of Alkaline Phosphatase Activity in Heʻeia Fishpond* [Thesis, University of Hawaiʻi at Mānoa]. http://scholarspace.manoa.hawaii.edu/handle/10125/67754

Jickells, T. D. (1998). Nutrient biogeochemistry of the coastal zone. *Science*, *281*(5374), 217–222.

Julius, M. (2007). Why sweat the small stuff: The Importance of microalgae in Hawaiian stream ecosystems. *Biology of Hawaiian Streams and Estuaries (N.L. Evenhuis and J.M. Fitzsimons, Eds.), 3*, 183–193.

Keala, G., Hollyer, J. R., & Castro, L. (2007). Loko Ia: A manual on Hawaiian fishpond restoration and management. *, University of Hawaii at Mānoa, Honolulu, Hawaii*.

Kelly, M. (1975). *Loko I'a O He'eia: Heeia Fishpond*. Department of Anthropology, Bernice P. Bishop Museum.

Kikuchi, W. K. (1976). Prehistoric hawaiian fishponds. *Science (New York, NY)*, *193*(4250), 295–299.

Kleven, A. (2014). *Coastal Groundwater Discharge as a Source of Nutrients to He'eia Fishpond, O'ahu, HI. Undergraduate thesis, Global Environmental Science Program, University of Hawaii at Manoa*. XB-12-02 Google Scholar.

Kulana Noiʻi Working Group. (2018). *Kūlana Noiʻi* (v1). University of Hawaii Mānoa Sea Grant Program. https://seagrant.soest.hawaii.edu/kulana-noii/

Laws, E. A. (1985). *Nutrient and Energy Cycling Among Phytoplankton, Bacteria, and Zooplankton*.

le Roux, R., Henrico, S., Bezuidenhout, J., & Henrico, I. (2023). Inverse Distance Weighting as an alternative interpolation method to create radiometric maps of natural radionuclide concentrations using QGIS. *Proceedings of the ICA*, *5*, 10.

Li, B., Karl, D. M., Letelier, R. M., Bidigare, R. R., & Church, M. J. (2013). Variability of chromophytic phytoplankton in the North Pacific Subtropical Gyre. *Deep Sea Res. Part 2 Top. Stud. Oceanogr.*, *93*, 84–95. https://doi.org/10.1016/j.dsr2.2013.03.007

Lim, J. H., & Lee, C. W. (2017). Effects of eutrophication on diatom abundance, biovolume and diversity in tropical coastal waters. *Environmental Monitoring and Assessment*, *189*(9), 432. https://doi.org/10.1007/s10661-017-6147-4

McCoy, D. E. (2011). *Improving sample collection and time series analyses of environmental data in Heʻeai Fishpond, Oʻahu, Hawaii=ʻi from 2007-2011*.

McCoy, D., McManus, M. A., Kotubetey, K., Kawelo, A. H., Young, C., D'Andrea, B., Ruttenberg, K. C., & Alegado, R. ʻanolani. (2017). Large-scale climatic effects on traditional Hawaiian fishpond aquaculture. *PLoS One*, *12*(11), e0187951.

Milliman, J. D., & Meade, R. H. (1983). World-wide delivery of river sediment to the oceans. *The Journal of Geology*, *91*(1), 1–21.

Moehlenkamp, P. (2018). *Kū Hou Kuapā: Increase of water exchange rates and changes in microbial source tracking markers resulting from restoration regimes at Heʻeia Fishpond* [Masters Thesis, University of Hawaiʻi Mānoa]. https://www.soest.hawaii.edu/oceanography/masters/2018-Moehlenkamp.pdf

Nathan, R. J., & McMahon, T. A. (1990). Evaluation of automated techniques for base flow and recession analyses. *Water Resources Research*, *26*(7), 1465–1473.

Oksanen, J., Blanchet, G., Friendly, M., Kindt, R., Legendre, P., McGlinn, D., Minchin, P. R., OʻHara, R. B., Simpson, G. L., Solymos, P., Stevens, M. H. H., Szoecs, E., & Wagner, H. (2020). *vegan: Community Ecology Package version 2.5-7 from CRAN* (2.5-7) [Computer software]. https://rdrr.io/cran/vegan/

Phases of the Moon. (n.d.). Retrieved April 22, 2020, from http://astro.ukho.gov.uk/surfbin/showform_beta.cgi?program=Moon_Phase&ticket=0a5a00a061552b82

Pierce, M. (2014). *The Distribution and Abundance of Diatoms in Kaneohe Bay, Oahu, Hawaii*.

http://scholarspace.manoa.hawaii.edu/handle/10125/31988
Ringuet, S., & Mackenzie, F. T. (2005). Controls on nutrient and phytoplankton dynamics during normal flow and storm runoff conditions, southern Kaneohe Bay, Hawaii. *Estuaries*, *28*(3), 327–337.
Schemmel, E., Kamikawa, K., Shimoda, T., & Peyton, K. A. (2019). The life history of the invasive mullet, Osteomugil engeli (Bleeker, 1858) in Hawaiian estuaries. *Environmental Biology of Fishes*, *102*(4), 553–568. https://doi.org/10.1007/s10641-019-00853-y
Selph, K. E., Goetze, E., Jungbluth, M. J., Lenz, P. H., & Kolker, G. (2018). Microbial food web connections and rates in a subtropical embayment. *Marine Ecology Progress Series*, *590*, 19–34.
Tuhiwai, S. L. (1999). *Decolonizing methodologies: Research and indigenous peoples*. Zed Books Limited.
USGS Current Conditions for USGS 16275000 Heeia Stream at Haiku Valley nr Kaneohe, Oahu, HI. (n.d.). Retrieved September 29, 2021, from https://waterdata.usgs.gov/hi/nwis/uv?site_no=16275000
Walsh, G. E. (1963). *An ecological study of the Heeia mangrove swamp*. University of Hawai'i at Manoa.
Water Levels—NOAA Tides & Currents. (n.d.). Retrieved September 24, 2021, from https://tidesandcurrents.noaa.gov/waterlevels.html?id=1612480&units=standard&bdate=19650101&edate=19651201&timezone=GMT&datum=MLLW&interval=m&action=data
Wilson, S. (2001). What is an indigenous research methodology? *Canadian Journal of Native Education*, *25*(2), 175–179.
Wilson, S. (2008). *Research is ceremony: Indigenous research methods*. Fernwood Publishing.
Yeo, S. K., Huggett, M. J., Eiler, A., & Rappé, M. S. (2013). Coastal bacterioplankton community dynamics in response to a natural disturbance. *PloS One*, *8*(2), e56207.
Young, C. W. (2011). *Perturbation of Nutrient Level Inventories and Phytoplankton Community Composition During Storm Events in a Tropical Coastal System: He'eia Fishpond, O'ahu, Hawai'i* [PhD Thesis]. publisher not identified.